Facoltà di Ingegneria

Laurea Magistrale in Ingegneria Meccanica Curriculum Energia

Sviluppo e valutazione di un modello basato su Python per simulare le curve di polarizzazione di elettrolizzatori PEM in diverse condizioni operative

Development and assessment of a Python-based model for resembling the polarisation curves of PEM electrolyzers at different operating conditions

Relatore:
Dr. Mosè Rossi, Ph.D.

Laureando:
Lorenzo Gambadori
Matricola: 1109058

Correlatori:
Prof. Gabriele Comodi, Ph.D.
Dr. Florian Josef Wirkert , Ph.D.

Anno Accademico 2023/2024

Ringraziamenti

Desidero esprimere la mia più sincera gratitudine a tutti coloro che hanno reso possibile il completamento di questo lavoro.

Innanzitutto, ringrazio il Prof. Gabriele Comodi, per la disponibilità con cui ha accolto la mia richiesta di poter svolgere la tesi sotto di lui. La sua collaborazione e i suoi preziosi consigli sono stati fondamentali sia per la riuscita di questo lavoro, sia per la mia crescita personale e professionale.

Un sentito grazie al mio relatore, dott. Mosè Rossi, per la sua costante supervisione, il supporto, la prontezza e la vicinanza durante tutto il periodo di svolgimento del lavoro. La sua competenza e i suoi consigli sono stati fondamentali per portare a termine il tutto nel modo più preciso e completo possibile.

Vorrei esprimere la mia riconoscenza anche ai miei correlatori, Dott.ssa Francesca Mennilli e il Dott. Florian Josef Wirkert. I loro suggerimenti sono stati fondamentali per superare gli ostacoli incontrati durante il lavoro e le loro osservazioni critiche hanno arricchito e migliorato notevolmente questa tesi.

Un ringraziamento speciale va ai miei amici, ai colleghi di studi ma anche e soprattutto ad alcune persone che non fanno parte, in questo momento, della mia vita: grazie per avermi supportato e soprattuto sopportato nei momenti di difficoltà e di stress. Il tempo passato insieme a voi e la vostra vicinanza hanno reso più leggero questo percorso.

Infine voglio ringraziare la mia famiglia. Grazie per aver sempre creduto in me e per avermi offerto il vostro sostegno in ogni momento. Anche se non lo dimostro spesso, la vostra presenza è stata importantissima nel motivarmi ogni giorno.

A tutti voi, il mio più sincero ringraziamento.

Con gratitudine,

Lorenzo.

1 Sunto esteso in italiano

Nel primo capitolo della tesi si è esaminato il quadro delle fonti energetiche utilizzate in Europa con particolare attenzione ai programmi e agli obiettivi di transizione energetica come, ad esempio, il Green Deal. Si è evidenziato il ruolo chiave di iniziative volte a ridurre le emissioni di gas serra e promuovere l'efficienza energetica. Successivamente, il contesto italiano è stato analizzato in relazione agli obiettivi del Piano Nazionale Integrato per l'Energia e il Clima (PNIEC), delineando le strategie adottate per raggiungere gli obiettivi di riduzione delle emissioni e di sviluppo sostenibile.

Si è poi passati ad una analisi dei ruoli e dei settori chiave in cui l'idrogeno può essere sostituito alle fonti fossili, fornendo inoltre indicazioni su come questo possa essere anche un valido sostituto delle batterie a ioni di litio per l'accumulo energetico di periodi di tempo estesi.

Nel secondo capitolo, si è esplorato il potenziale dell'idrogeno come fonte energetica alternativa e sostenibile considerando le sue possibili applicazioni nei settori chiave per la riduzione delle emissioni di carbonio e il miglioramento dell'efficienza energetica.

Si sono esaminati approfonditamente le proprietà dell'idrogeno e le varie tecnologie di produzione, concentrandosi su metodologie come l'elettrolisi dell'acqua alcalina (AWE), la membrana a scambio di anioni (AEM), l'elettrolisi a ossido solido (SOE) e la membrana a scambio di protoni (PEM). Questo approfondimento fornisce una base teorica solida per comprendere il funzionamento e le potenzialità dell'idrogeno come vettore energetico nelle future applicazioni.

Nel terzo capitolo, è stata presentata una descrizione dettagliata del processo di modellazione matematica di un elettrolizzatore a membrana a scambio di protoni (PEM), fornendo un'analisi approfondita dei diversi parametri coinvolti nel suo sviluppo. Sono stati esaminati parametri cruciali come la densità di corrente di scambio di riferimento, l'energia di attivazione, i coefficienti di trasferimento di carica e altri fattori influenti.

Questo approfondimento fornisce una base teorica solida per la comprensione dei meccanismi e dei processi che regolano il funzionamento dell'elettrolizzatore PEM, fondamentale per il successivo sviluppo e ottimizzazione del modello.

Nel quarto capitolo, si è illustrato il processo di adattamento delle equazioni di base per la modellazione di un elettrolizzatore PEM al fine di tener conto delle variazioni delle condizioni operative, in particolare pressioni fino a 100 bar e temperature fino a $70C$.

Sono state apportate modifiche alle equazioni esistenti per integrare gli effetti della pressione e della temperatura sulle reazioni elettrochimiche all'interno della cella PEM.

Questo adattamento è essenziale per garantire la precisione e l'affidabilità del modello in contesti operativi realistici e variegati, consentendo una simulazione accurata delle prestazioni dell'elettrolizzatore in condizioni diverse da quelle atmosferiche.

Nel quinto capitolo, sono stati dettagliati due setup sperimentali adottati per la raccolta dei dati, forniti dall'Istituto Westfalische Hochschule e coordinati dal dott. Florian Wirkert.

I due sistemi differiscono tra loro nel modo in cui consentono di variare i parametri di pressione e temperatura durante i test.

Uno dei setup mantiene costante la temperatura e varia la pressione, mentre l'altro mantiene costante la pressione e varia la temperatura. Questi approcci sperimentali consentono di esaminare in modo esaustivo gli effetti delle variazioni di pressione e temperatura sulle prestazioni dell'elettrolizzatore PEM.

Nel sesto capitolo, sono stati presentati i risultati ottenuti attraverso l'implementazione del modello matematico descritto nel capitolo quattro utilizzando il linguaggio di programmazione Python.

Questo approccio ha permesso di ottenere i parametri cinetici necessari tramite un processo di fitting tra il modello matematico e i dati sperimentali, creando così una baseline. Successivamente, sono state seguite due metodologie per i due setup sperimentali.

Nel caso del setup con pressione variabile e temperatura costante, gli esponenti dei rapporti delle pressioni parziali tra idrogeno, ossigeno e acqua sulla pressione di riferimento sono stati variati al fine di minimizzare il root mean square error (RMSE) tra i dati sperimentali e le previsioni del modello.

Questo approccio ha consentito di ottenere gli esponenti ottimali per ciascun valore di pressione testato.

Dai dati ottenuti si osserva una diminuzione non lineare degli esponenti con l'aumento della pressione: ciò implica una riduzione non lineare delle perdite di attivazione nella curva di polarizzazione dell'elettrolizzatore.

Questo suggerisce un effetto non proporzionale della pressione sulle reazioni stesse con importanti implicazioni sulle prestazioni delle PEM. L'implementazione di tecnologie PEM più efficienti e adatte a una gamma più ampia di condizioni operative, specialmente in ambienti ad alta pressione, potrebbe rivoluzionare l'applicazione di questa tecnologia.

Tuttavia, ulteriori studi e conferme sperimentali sono necessari per confermare

tali conclusioni e comprendere appieno i meccanismi sottostanti.

Per il setup con temperatura variabile e pressione costante, i valori dei coefficienti di trasferimento di carica (alpha) sono stati variati tra zero e uno al fine di minimizzare il RMSE tra i dati sperimentali e il modello.

I valori del coefficiente di trasferimento di carica all'anodo e al catodo aumentano con l'aumentare della temperatura come evidenziato dai dati ottenuti.

Ci si aspettava effettivamente un andamento di questo tipo innanzitutto perchè una temperatura più alta favorisce la mobilità ionica nel materiale elettrolitico della cella PEM, consentendo un trasporto più veloce degli ioni verso gli elettrodi. Di conseguenza, si accelera il trasferimento di cariche attraverso il contatto elettrodo/elettrolita, aumentando il coefficiente di trasferimento di carica.
Le reazioni degli elettrodi più rapide incoraggiano anche lo scambio di elettroni tra l'elettrodo e gli ioni dell'elettrolita.

Inoltre, una migliore conformazione dell'interfaccia elettrodo/elettrolita a temperature più elevate favorisce un miglior contatto elettrico, aumentando i tassi di trasferimento ionico e, di conseguenza, il coefficiente di trasferimento di carica. Questo fenomeno è in linea con le osservazioni riportate in letteratura.

Sebbene sia abbastanza complesso creare una relazione quantitativa esatta tra il coefficiente di trasferimento di carica e la temperatura, l'incremento continuo di tali valori sottolinea il ruolo della temperatura nell'impatto sulle prestazioni della cella. Sulla base dei dati sperimentali raccolti, ulteriori analisi possono rivelare una relazione esatta personalizzata per la specifica cella in studio.

L'uso di Python ha giocato un ruolo cruciale in entrambi i casi, poiché ha permesso di sviluppare algoritmi in grado di determinare sia i parametri cinetici sia i valori ottimali degli esponenti e degli alpha, fondamentali per adattare il modello alle condizioni operative specifiche e ottenere risultati accurati.

In conclusione, il lavoro svolto ha fornito una base solida per la previsione del funzionamento di elettrolizzatori PEM in condizioni di pressione e temperatura elevate, con l'obiettivo di ridurre le perdite interne del sistema.

Si è quindi dimostrato come l'ottimizzazione dei parametri cinetici e la modellazione matematica possano contribuire significativamente a migliorare le prestazioni dell'elettrolizzatore in ambienti operativi più estremi.

I risultati ottenuti forniscono un'importante comprensione delle relazioni complesse tra le variabili operative e le prestazioni del sistema, aprendo la strada allo sviluppo di tecnologie più efficienti e affidabili per la produzione di idrogeno verde.

Abstract

Europe is at the forefront of a massive energy revolution that will lower carbon emissions and increase sustainability. This shift, which includes increasing energy efficiency and modernizing the grid, from fossil fuels to renewable energy sources like wind, solar, and hydropower, is essential to the EU's plan to meet the 2030 climate targets and become carbon neutral by 2050.

Nowadays, the chemical and refining industries in Europe rely heavily on hydrogen, making it an indispensable component of their energy landscape. Future uses for it could include transportation, heating, and power generation, which could greatly aid the EU in meeting its emission reduction goals and improve overall energy security. The most efficient method of producing hydrogen without emitting CO_2 is through the use of electrolyzers, which enable the production of "green hydrogen". Working with electrolyzers that have ever-higher efficiency values is one of the main goals of today's green hydrogen production: getting more hydrogen with the same, or lower, amount of electric energy. Using electrolyzers that run at pressures greater than atmospheric ones is one of the options that are being currently explored; indeed, increasing the electrolytic cell's operating temperature is another method of reducing the input energy consumption.

Therefore, after providing a general overview of the state of hydrogen production worldwide and the global goals associated with the decarbonisation process, this study covers several different hydrogen production techniques.

To analyze and forecast improvements in cell efficiency, a Polymeric Electrolyte Membrane (PEM) electrolyzer in a controlled pressure and temperature environment has been considered a viable option.

To predict the electrolytic cells' behaviour, a mathematical model is developed using Python, tested, and validated with experimental data of a PEM electrolyzer. Experimental data, which have been obtained at the Westfalische Hochschule Institute, are used as a baseline for the current work.

In the end, the developed model showed a strong affinity with the data, mainly thanks to its adaptability and flexibility. In the future, to validate the model for higher operating pressures and subsequently forecast the system's behavior, it is expected to use it with different data from those used in this work.

Contents

1 Sunto esteso in italiano **2**

Abstract **5**

Nomenclature **12**

Glossary **14**

Introduction **15**

2 European energy scenario **19**
2.1 Energy transition in Europe 19
2.2 Current and future hydrogen applications 23

3 Hydrogen properties and production **25**
3.1 Hydrogen properties 25
3.2 Hydrogen production 26
3.3 Alkaline Water Electrolysis (AWE) 29
3.4 Anion Exchange Membrane (AEM) 30
3.5 Solid Oxide Electrolysis (SOE) 31
3.6 Proton Exchange Membrane (PEM) 32

4 Parameters used in the developed numerical model **35**
4.1 Reference exchange current density 36
4.2 Activation energy 37
4.3 Charge transfer coefficients 38
4.4 Reference conductivity of the membrane 38
4.5 Activation protonic energy 39
4.6 Variable parameters 39
4.7 Constants parameters 41

5 Cell voltage model **42**
5.1 Basic cell model 42
5.2 Parameters optimization 43

6 Experimental setup **47**
6.1 Variable pressure and fixed temperature setup 48
6.2 Variable temperature and fixed pressure setup 53

7 Results and comments **56**
7.1 Variable pressure and fixed temperature 56
7.2 Higher pressure values 59
7.3 Optimization results 62
7.4 Variable temperature and fixed pressure 69
7.5 Higher temperatures and optimization results 71

Conclusions **77**

Appendix **79**

Bibliography **100**

List of Figures

1 World's total energy supply [1] . . . 15
2 European total energy supply by source [16] . . . 20
3 Italian total energy supply by source [17] . . . 21
4 Hydrogen final usage as energy vector [24] . . . 23
5 Storage capacity of current technologies [26] . . . 24
6 Hydrogen density vs pressure values [29] . . . 25
7 Different hydrogen production methods [36] . . . 27
8 Hydrogen colors' classification [37] . . . 28
9 Alkaline electrolysis reaction [41] . . . 29
10 AEM electrolysis reaction [41] . . . 30
11 SOE electrolysis reaction [41] . . . 31
12 PEM electrolysis' reaction [41] . . . 32
13 Simple model of a PEM electrolyzer cell [51] . . . 34
14 General layout of the electrolyzer test rig [63] . . . 47
15 Photograph of the PEMEL stack with a reinforced pressure housing [51]. . . . 48
16 Two half cells consisting of plastic cell frames with integrated media channels comprising a monopolar plate[51] . . . 49
17 Modular PEM stack where the number of cells per stack can be easily varied [51] . . . 50
18 Photograph of a prototype electrolyzer stack based on hydraulic compression [63] . . . 51
19 Polarization curves of a prototype PEM electrolysis stack based on hydraulic compression at various gas pressures [63] . . . 52
20 Photograph of the polymer electrolyte membrane water electrolyzer (PEM) test system [64] . . . 54
21 Experimental polarization curves for variable temperature setup [64] . 55
22 Model fitting @40°C and 10 bar . . . 57
23 Comparison between the model and experimental polarization curve without exponents optimization @60 bar and 40°C . . . 59
24 Comparison between the model and experimental polarization curve without exponents optimization @100 bar and 40°C . . . 60
25 Comparison between the model and experimental polarization curve with exponents optimization @60bar and 40°C . . . 62
26 Comparison between the model and experimental polarization curve with exponents optimization @100bar and 40°C . . . 63
27 Comparison between the model and experimental polarization curve at different pressure values and 40°C . . . 66
28 Optimized exponents at different pressures . . . 67
29 Model fitting @40°C and 1 bar . . . 70
30 Comparison between the model and experimental polarization curve with alpha optimization @50°C and 1 bar . . . 72
31 Comparison between the model and experimental polarization curve with alpha optimization @60°C and 1 bar . . . 73

32 Comparison between the model and experimental polarization curves with alpha optimization @70°C and 1 bar 74
33 Alpha's values at different temperatures 75
34 Comparison between the model and experimental polarization curve with alpha optimization 76

List of Tables

1 Antoine's equation parameters 40
2 Electrolyzer's constants 41
3 Kinetic parameters 45
4 Variable pressure cell's setup 52
5 Variable temperature cell's setup 55
6 Baseline kinetic parameters at 40°C and 10 bar 57
7 Comparison of model and experimental voltage values with respective relative percentage errors 58
8 Comparison of model predictions and experimental data at 60 bar with respective relative percentage errors 60
9 Comparison of model predictions and experimental data at 100 bar with respective relative percentage errors 61
10 Comparison of model predictions and experimental data at 60 bar with respective relative percentage errors 64
11 Comparison of model predictions and experimental data at 100 bar with respective relative percentage errors 65
12 RMSE values for different pressure levels used in experimental tests . 66
13 Optimized exponents values at different pressures 67
14 Baseline kinetic parameters at 40°C and 1 bar 70
15 RMSE and optimized alpha values at 50°C 72
16 RMSE and optimized alpha values at 60°C 73
17 RMSE and optimized alpha values at 70°C 74

List of Equations

1 Electrolyzer's voltage equation [10] 17
2 Electrolysis's reaction for PEM electrolyzer/anode side [41] 27
3 Electrolysis's reaction for PEM electrolyzer/cathode side [41] 27
4 Electrolysis's overall reaction for PEM electrolyzer[41] 27
5 Anode current density equation [53] 36
6 cathode current density equation [53] 36
7 Butler-Volmer's anode equation [59] 37
8 Butler-Volmer's cathode equation [59] 37
9 Membrane conductivity's equation [58] 39
10 Ohmic overpotential's equation [59] 39
11 Water pressure equation [60] 40
12 Cell voltage equation model [40] 42
15 Butler-Volmer's anode equation with pressure correction [53] 44
16 Butler-Volmer's cathode equation with pressure correction [53] 44
17 Ohmic Overpotential equation [59] 44
18 model voltage percentual error 58

Nomenclature

Symbol [Unit] Meaning:

V [V]	Voltage
N_c [-]	Number of cells
$V_{\text{Act},c}$ [V]	Cathode activation overpotential
$V_{\text{Act},a}$ [V]	Anode activation overpotential
i [A]	Current
R_{cell} [Ω]	Cell resistance
R [J/(mol·K)]	Gas constant
F [C/mol]	Faraday constant
n [-]	Number of electrons involved in the electrochemical reaction
T_{cell} [K]	Cell temperature
P_a [Pa]	Pressure on the anode side
P_c [Pa]	Pressure on the cathode side
T_{H_2O} [°C]	Water temperature
δ_{Nafion} [cm]	Nafion 115 membrane thickness
T_{ref} [K]	Reference temperature
P_{ref} [Pa]	Reference pressure
A_{Ant} [-]	Antoine equation constant A
B_{Ant} [K]	Antoine equation constant B
C_{Ant} [K]	Antoine equation constant C
p_{H_2O} [Pa]	Partial pressure of water
p_{O_2} [Pa]	Partial pressure of oxygen
p_{H_2} [Pa]	Partial pressure of hydrogen
E_{rev} [V]	Reversible potential
E [V]	Open circuit voltage (OCV)
α_{anode} [-]	Anode charge transfer coefficient
α_{cathode} [-]	Cathode charge transfer coefficient
$i_{0,\text{ref,a}}$ [A/cm^2]	Reference exchange current density at the anode
$i_{0,\text{ref,c}}$ [A/cm^2]	Reference exchange current density at the cathode
E_{aa} [J/mol]	Activation energy at the anode
E_{ac} [J/mol]	Activation energy at the cathode
E_{pro} [V]	Protonic potential

σ_{ref} [S/cm]	Reference conductivity
exponent $p_{O_2}(a)$ [-]	Exponent for partial pressure of oxygen at the anode
exponent $p_{H_2O}(b)$ [-]	Exponent for partial pressure of water
exponent $p_{H_2}(c)$ [-]	Exponent for partial pressure of hydrogen
$i_{0,anode}$ [A/cm^2]	Anode exchange current density
$i_{0,cathode}$ [A/cm^2]	Cathode exchange current density
σ_{mem} [S/m]	Proton conductivity of membrane
V_{trans} [V]	Mass transport overpotential
V_{ohm} [V]	Ohmic overpotential
A_{cell} [cm^2]	Cell active area

Glossary

PEM: Proton Exchange Membrane
IEA: International Energy Agency
RMSE: Root Mean Square Error
EU: European Union
EC: European Commission
PNIEC: Integrated National Energy and Climate Plan
LHV: Lower Heating Value
AWE: Alkaline Water Electrolyzer
AEM: Anion Exchange Membrane
SOE: Solid Oxide Electrolyzer
LCOH: Levelized Cost of Hydrogen
MEA: Membrane Electrode Assembly
PCD: Porous Current Distributors
CCM: Catalyst Coated Membrane
FKM: Flat Gasket
PTL: Porous Transport Layer
HER: Hydrogen Evolution Reaction
OER: Oxygen Evolution Reaction
CTC: Charge Transfer Coefficient
OCV: Open Circuit Voltage
PPs: Pole Plates
GDLs: Gas Diffusion Layers
PEEK: Polyether Ether Ketone
PU: Flexible Polyurethane

Introduction

For more than a century, the main energy sources in the World were fuels such as coal, oil, and gas. The International Energy Agency (IEA) estimated that over 81% of the World's primary energy consumption in 2018 comes from the use of these primary energy sources [1] as shown in figure 1.

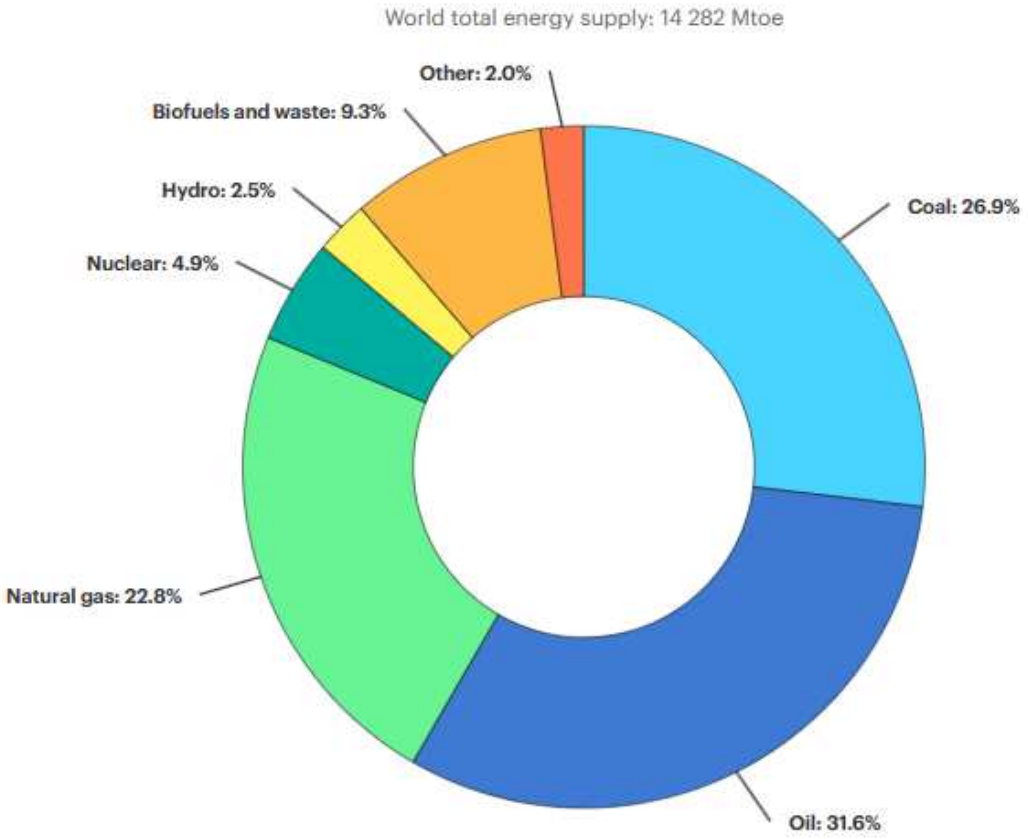

Figure 1: World's total energy supply [1]

The global awareness of the effects on the environment (e.g., climate change) coming from fossil fuels has pushed toward the exploitation and deployment of renewable energy sources through several agreements signed by industrialised countries. In 2021, the IEA reported that renewables satisfied 12.9% of the global final

energy consumption [2]; undoubtedly, renewable energy sources will keep their continuous growth trend until almost all the energy needed all over the World is covered [3].

Although renewables like solar and wind energy have the potential to be a sustainable, affordable, and environmentally friendly power source and lower greenhouse gas emissions, they face energy production variability that affects the reliability of satisfying the end-users' energy demands as well as the physical integrity of transmission grids [4].

To overcome this limitation, energy storage systems like batteries are generally used; however, up to now [5] they partially limit this issue since they are not able to completely satisfy the end-users' energy demand when renewables are not working (e.g., high investment cost and low durability [6]), and are also not able to provide an electrical reserve for longer periods. Besides batteries, as reported by Hassan et al. [7], hydrogen is becoming more and more acknowledged in Europe as a promising solution that helps with the intermittent problems related to renewable energy sources. This process, which is called "power-to-hydrogen", transforms the excess of renewable energy into hydrogen for storage purposes which is used for satisfying future energy consumption.
Furthermore, it offers better exploitation of renewable energy sources, making the transition to a low-carbon energy system more efficient [8]. Indeed, hydrogen is seen as a potential energy vector and interesting fuel in its basic chemical form or, also, in chemical compositions as proposed by Abdin et al. [9]; in particular, water-based electrolysis is seen as a game changer for the "green" energy production while fed by renewable electricity.

The goal of this work is to highlight the potential that hydrogen might offer to the decarbonisation process the World is currently undergoing, with a focus on optimizing hydrogen production through the use of systems and techniques that lower the energy requirements for its production.

Investigating electrolyzer behaviour when operating at high pressures and temperatures causes huge investments. To predict the efficiency reliability in advance would help a lot to decide for many researchers and companies, whether such huge efforts would make sense.

In particular, in the scientific literature, there are several mathematical models capable of resembling the performance curves of water-based electrolyzers, but a few of them employ optimization procedures to fit the numerical results with the experimental data properly.

Indeed, the knowledge of specific parameters, which are mostly unknown due to scarce data availability and manufacturers' copyrights, is required and this is the goal that an optimization procedure might have in further enhancing the prediction capability of a model.

The polarization curves are obtained in many works such as those of Nafeh et al. [10], Dale et al. [11], Myles et al. [12]) that evaluate the cell's voltage in the following way (equation 1):

$$V = N_c \cdot (E + V_{\text{Act},c} + V_{\text{Act},a} + iR_{\text{cell}}) \quad [V] \tag{1}$$

However, this equation is hard to use since the value of the membrane resistance is unknown.

That said, a numerical model capable of fitting the polarisation curve obtained from two different electrolyzers at given operating conditions, installed in the laboratory of the Westfalische Hochschule Institute in Germany, was developed in a Python environment. The main goal is to evaluate those electro-chemical parameters that are difficult to retrieve from electrolyzers' manufacturers. To succeed in this task, known ranges from the scientific literature were used and, through an iterative process, the obtained (and used) values were those showing the lowest Root Mean Square Error (RMSE). After this process, different operating conditions were investigated by the model and compared with additional experimental results.

The document is structured as follows: Section 2 highlights the current energy situation in Europe, focusing mainly on the Italian scenario and how hydrogen can fit into this framework to support the decarbonisation process. Section 3 discusses the chemical-physical characteristics of hydrogen, also providing insights on issues related to its operational security. It explains how hydrogen is classified into different "colours" according to the type of energy source used for its production. Finally, hydrogen production technologies are analysed with a focus on PEM electrolyzers.

Section 4 reports the parameters and the governing equations of the water electrolysis through PEM technologies, explaining why specific parameters and their numerical values are chosen concerning others. The purpose of this section is also to explain how pressure and temperature affect the input power of the water electrolyzers.

Section 5 describes in detail the mathematical model developed in Python. Section 6 provides an overview of the experimental apparatus and its architecture, focusing also on how the electrolysis pressure system works and how pressure values affect energy consumption.

Section 7 shows the main results obtained from the developed model and its validation through experimental data obtained in measurement campaigns performed in the hydrogen labs of Westfalische Hochschule institute.

The model's integration and implementation strategies are finally reported, enabling it to properly resemble the PEM electrolyzer's behavior operating at different conditions, which are aligned with those found in the laboratory, and allow to operate it with different settings.

2 European energy scenario

At present, Europe is leading the way in a significant energy revolution that aims to lower carbon emissions and advance sustainability.

A key component of the European Union's plan to fulfill the 2030 climate targets and become carbon neutral by 2050 is the energy transition taking place in the continent. This transition entails a substantial move away from fossil fuels and toward renewable energy sources including hydroelectric, solar, and wind power in addition to advancements in energy efficiency and grid modernization.

In this scenario, hydrogen is becoming a vital part of the energy landscape in Europe and has potential uses in several industries that could greatly help the EU meet its emission reduction targets. Nowadays, the chemical and refining industries are the main users of hydrogen, but it has a lot of potential for use in the future including power generation, heating, and transportation.

2.1 Energy transition in Europe

When the European Union (EU) unveiled the "Green Deal package", which contained its goals to be achieved by 2020, it became the first to set important energy and climate targets back in 2009. The European Green Deal is a bold action plan intended to make the continent a global leader in the fight against climate change and drastically reduce its environmental impact. The primary objective of this endeavor is to reduce net greenhouse gas emissions down to 55% by 2030 in comparison to 1990 levels. By 2050, this ground-breaking initiative aims to make Europe the first continent in the World to be climate-neutral by establishing a standard for environmentally conscious growth and responsible stewardship on a worldwide basis [13].

To address citizens' concerns and redouble the efforts to tackle climate change, the president of the European Commission (EC) unveiled the European Green Deal, a broad and ambitious policy initiative aimed at bringing the energy transition across the continent. Decoupling the economic growth from resource usage is the primary objective of this new strategy, which aims to make the EU a net-zero greenhouse gas emission society by 2050 and thus transform the society into a resource-efficient and competitive economy [14].

For instance, in 2017 Europe imported from Russia 39% of hard coal, 30% of crude oil, and 39% of European natural gas consumption [15]. European climate policies and targets affected the demand for these resources, lowering the reliance on fossil fuel consumption. That said, the following five points represent a summary of the goals for pursuing successfully the energy transition:

1. decarbonization;
2. import independence and fuel diversity;
3. technology development and research innovation;

4. completion of the internal energy market and effective retail competition;

5. affordability for the European industry.

As a result, the core idea behind the energy transition is to analyse the current energy mix and determine how it might be changed in favor of using cleaner energy sources. Figure 2 shows the current overview of the energy sources used to produce electricity according to the IEA [16].

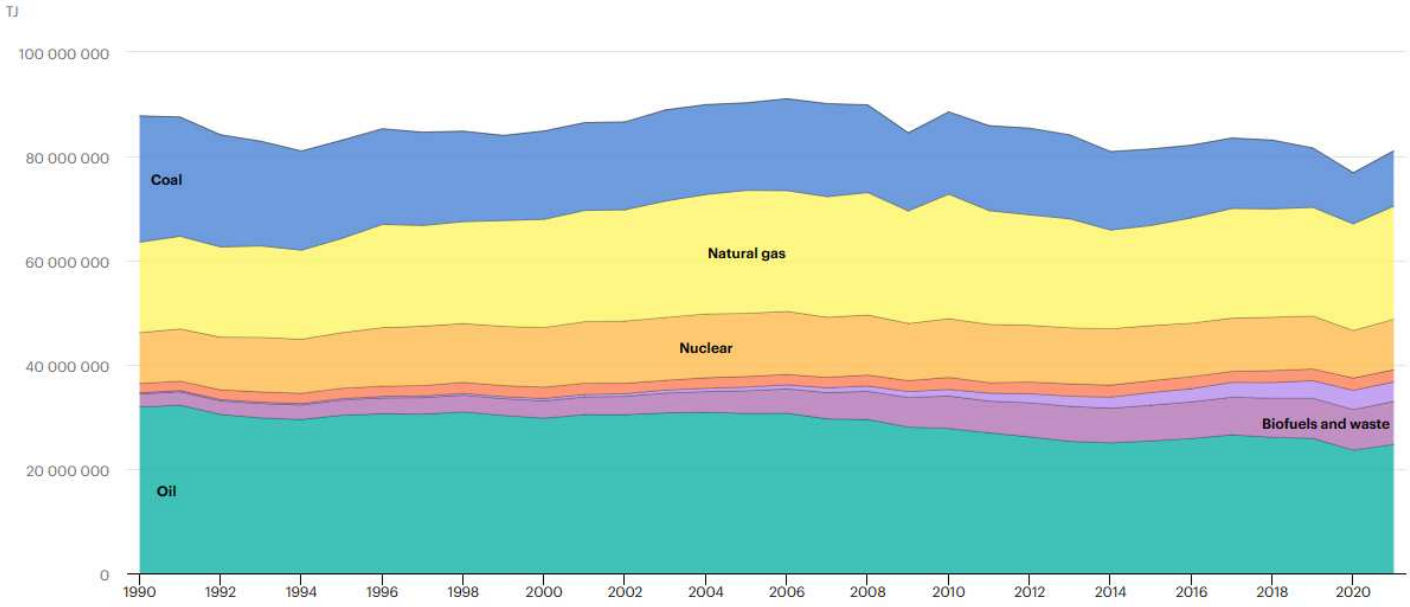

Figure 2: European total energy supply by source [16]

A considerable amount of energy comes from fossil fuels like coal and oil, as well as methane. On the other hand, only a small part of it comes from renewable energy sources, with a huge percentage of this section derived from nuclear sources.

When comparing the Italian scenario with the European one, no appreciable distinctions can be noticed. Figure 3 shows that also in Italy the majority of the energy demand is satisfied by the use of fossil fuels, with renewable energy sources accounting for a negligible amount (notably, the portion of nuclear energy is zero due to the 1989 referendum related to the abolition of nuclear power plants in Italy)[17].

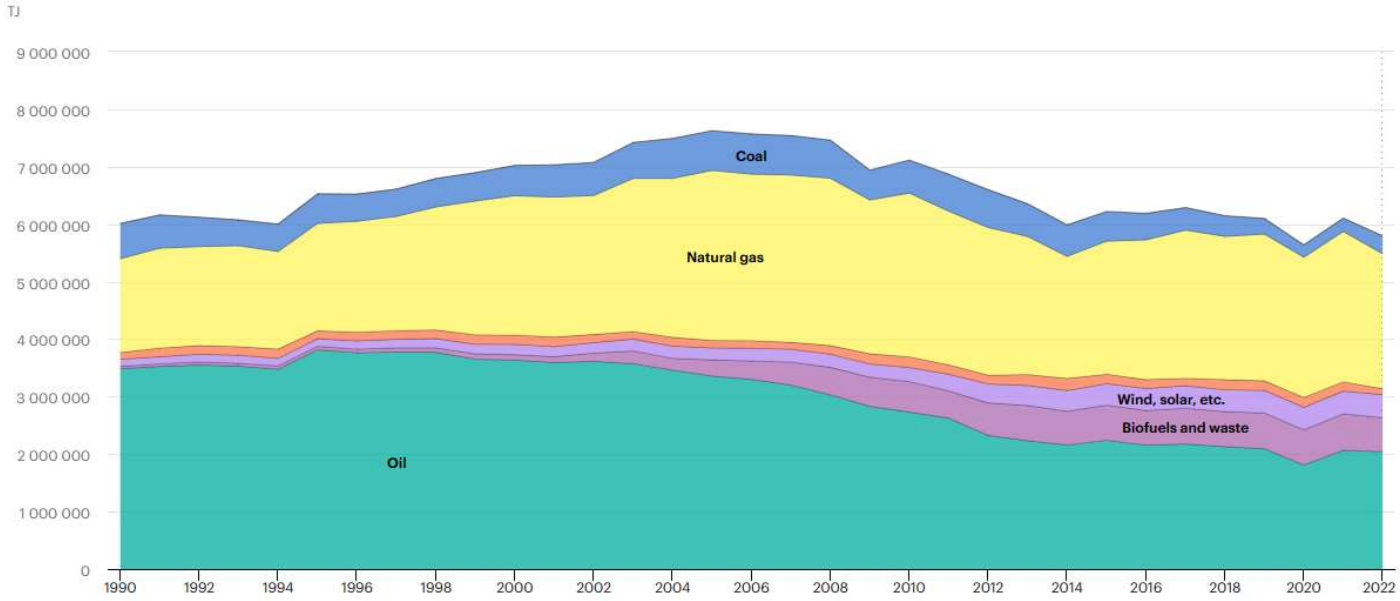

Figure 3: Italian total energy supply by source [17]

In light of this, the goals of Italy and the EU are to gradually decrease the use of fossil fuel-powered systems (e.g., thermal power plants, etc.) and increase the production and consumption of the energy produced by renewables.

In particular, Italy has set emission targets within the National Integrated Plan for Energy and Climate (PNIEC) by achieving specific values:

1. 56% emission reduction from power-intensive industries;
2. 35% emission reduction from commercial, transport, and residential sectors;
3. 30% production from renewables.

Therefore, having an integrated approach to energy generation and consumption is crucial to achieving such achievements; from this point of view, the application of the 'sector coupling' technique is essential. Indeed, 'sector coupling' offers an important added value in the decarbonisation process of the EU energy system, to increase flexibility needs and the reliability of energy systems, as well as reducing the global costs of the energy transition.

When the term "sector coupling" was first used, it mostly referred to the electrification of the end-use sectors (e.g., transportation and heating) to increase the deployment of renewable energy and provide balancing services to the power sector, assuming that the supply of electricity is or can be largely come from renewables. Supply-side "sector coupling" has been also added to the definition of "sector coupling" more recently. The integration of the gas and power industries through

"power-to-hydrogen" technologies is the main goal of supply-side integration [18]. Likewise, the EC uses a wider definition of "sector coupling" since it is considered as a tactic to give the energy system more adaptability so that the decarbonization process might be accomplished more affordably.

Technologies classified as "power-to-hydrogen" should receive special attention [19]. Currently, the use of batteries for energy storage purposes is a valid option for short-term storage, but not for long-term one. Indeed, as presented by Lund et al. [20], this is highly troublesome since there might be a regular mismatch between energy supply and demand given the unpredictable nature of renewable energy sources and the short-term storage capability of such a technology.

When compared to electricity produced by conventional power plants, electricity produced from renewable sources—such as wind and solar power—has a distinctive attribute because it is difficult to control or block in response to demand. This implies that generated energy still needs to be managed in some way even in situations where production exceeds demand.

Green hydrogen offers a workable fix for this issue. Electrolyzers that produce hydrogen by water electrolysis can be powered by excess energy when the production of renewable energy surpasses the demand. Through this process, electrical energy can be transformed into hydrogen, which is easily stored and can be used for a variety of purposes in the future, including heating, producing electricity, and fueling automobiles.

There would have not been many options if this extra energy was not used to create hydrogen, like exporting it (which is not always practical or feasible) or storing it in electric batteries, which have capacity, cost, and lifespan restrictions. Thus, creating green hydrogen from the excess energy not only keeps renewable resources from being wasted but also helps to stabilize the electrical system and encourages the use of clean, sustainable energy.

As a result, hydrogen storage becomes especially useful when there is low demand and high production from renewable sources, as noted by Blanco et al. [21] since it enables the electrical system to fully benefit from the energy produced.

2.2 Current and future hydrogen applications

Hydrogen currently covers a lot of applications that can be divided into three main technological roles according to Ramachandran et al. [22] and Yue et al. [23]):

1. it can be characterized as a new energy vector that is complimentary to electricity and replaces fossil fuels;
2. it can be used as a chemical component for the production of secondary fuels (e.g., e-fuels), derivatives, and commodities;
3. it can represent chemical storage (in various forms) with high energy density to accumulate important amounts of energy that can be subsequently reused for different applications and end uses.

Figure 4 shows a map of hydrogen applications divided by sectors.

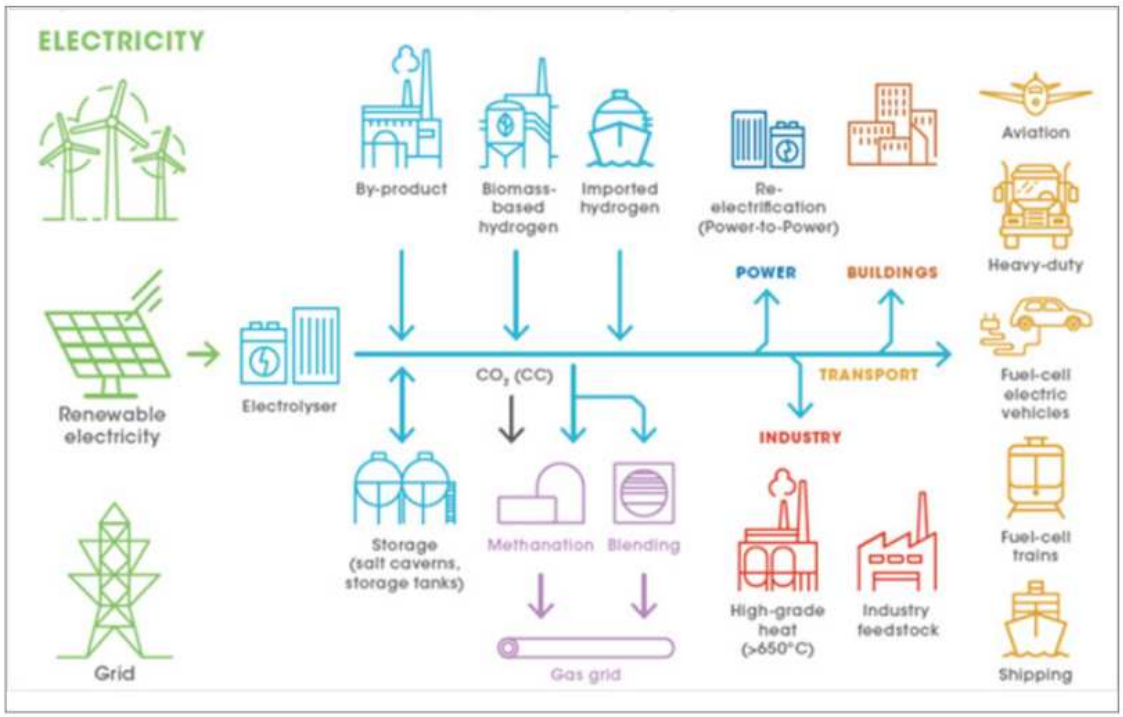

Figure 4: Hydrogen final usage as energy vector [24]

Beside considerably contributing to the decarbonisation of the so-called "hard-to-abate" sectors, hydrogen as an energy vector is highly intriguing for diversifying the production and consumption in other sectors. Simultaneously, the "blending" process of incorporating hydrogen into the natural gas network might result in a decrease of CO_2 emissions that fall under the responsibility of home users (e.g., boilers that operate with a mixed fuel).

On the other end, the redox reaction that occurs in fuel cells does not result in the formation of CO_2, and quite high efficiencies are achieved due to an electro-chemical conversion rather than a thermo-electrical one such as in the case of combustion in conventional power generation systems (e.g., turbogas cycles or steam cycles).

When it comes to storing energy, hydrogen can be used as a vector for large amounts of energy (e.g., GWh). Mostly, this energy can be stored for longer periods (e.g., months) unlike electric batteries that have important rates of self-discharge when operating for this purpose. The storage capacity of the current storage technologies is shown as a function of the withdrawal time in figure 5.

Hydrogen ensures the possibility of balancing energy demand and supply throughout the year; moreover, it allows to provide greater grid flexibility, mitigating the variability of renewables and bridging the gap between energy production and demand [25].

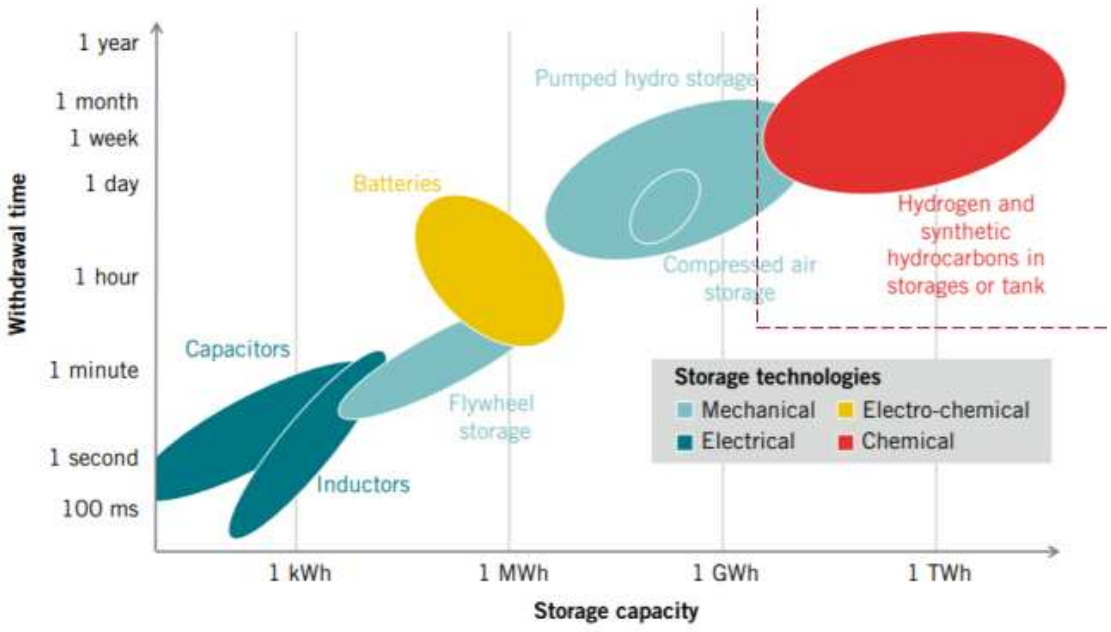

Figure 5: Storage capacity of current technologies [26]

3 Hydrogen properties and production

This section discusses the characteristics of hydrogen taking into account its chemical-physical behavior to emphasize its strengths and weaknesses. To compare the technologies in terms of costs and benefits, it is explained how this molecule can be obtained while considering various electrolysis techniques and production methods. The financial costs of each technology are analysed as well.

3.1 Hydrogen properties

By comparing hydrogen to conventional fossil fuels, some intriguing features arise. In particular, hydrogen's high energy content with a Lower Heating Value (LHV) of 33.33 kWh/kg [27] (coal has 8 kWh/kg) makes it a high energy density carrier. As drawbacks, the hydrogen gas phase has a low mass density which is detrimental to energy density and storage because high pressures are needed for storing a considerable amount of hydrogen (e.g., density of 0.082 kg/m^3 @ $0 - 25$°C and 1 bar [28]). Furthermore, even working at high pressure values (e.g., range of 700–1000 bar which indicates plant complexities and safety issues) does not mean reaching high density values due to the inverse relationship between pressure and the compressible factor "z" of gases as shown in figure 6.

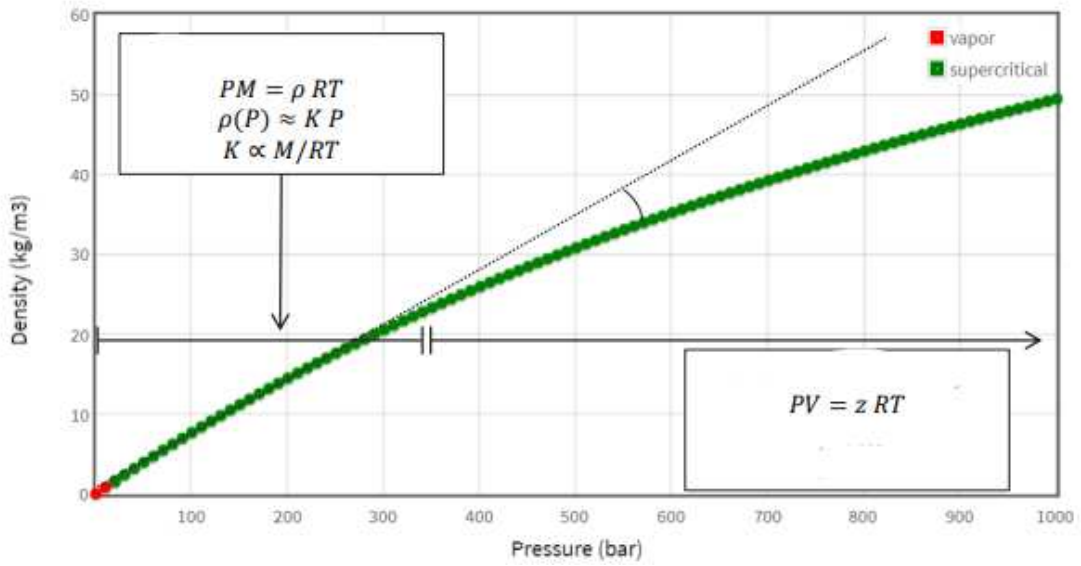

Figure 6: Hydrogen density vs pressure values [29]

To get over this, hydrogen transformation into liquid phase might be thought as a possible solution to increase its energy density; however, extraordinarily low melting temperatures are required (e.g., boiling point of -259.16°C at 1 bar [28]) and thus further cooling energy is needed.

Because of its broad flammability limits (e.g., from 4 to 75% of its volume in air [30]) and extremely low activation energies (e.g, 0.02 mJ [31]), hydrogen poses a significant safety risk. Although storing hydrogen under proper conditions is generally safe, it is important to strictly follow safety procedures and guidelines. The risks related to hydrogen storage must be reduced by proper design, routine maintenance, and adherence to safety regulations.

3.2 Hydrogen production

Hydrogen is the most effective energy vector and it can be obtained from a variety of raw materials, including water. Water electrolysis is one of the main techniques used to produce pure hydrogen but, as presented by Holladay et al. [32], there are plenty of technologies to obtain it. It was thought to be one of the most promising technologies for producing highly pure hydrogen from renewable energy sources while having no carbon emissions and only oxygen as a byproduct. This process has been evaluated in terms of sustainability and environmental impact. The produced oxygen (O_2) and hydrogen (H_2) are directly used for other end-uses along with being reconverted in electricity through fuel cells. However, only 27 million tonnes are produced through electrolysis so far [33].

Global energy consumption has been steadily rising in recent years as a result of better living standards and population growth. Moreover, the development of renewable energy sources has become more and more important as both environmental pollution and global warming increased. One of the most promising clean and sustainable energy sources is hydrogen which does not emit carbon and produces oxygen and pure water as a byproduct.

In 2021 [34], hydrogen demand reached 94 million tonnes, overtaking the pre-pandemic figure of 91 million tonnes in 2019 and accounting for 2.5% of the global final energy consumption. Current governmental policies suggest the hydrogen demand may increase up to 115 million tonnes by 2030, although only a small portion (less than 2 million tonnes) will come from new applications. This projection falls short of the 130 million tonnes required to fulfill the existing global climate commitments, which include 25% from new uses, and it is far from the nearly 200 million tonnes needed by 2030 to align with the net-zero targets to be reached by 2050. The majority of the industrial uses for the produced hydrogen are in the fertilizer, petrochemical, and power sectors [35].

Water electrolysis leads to a high hydrogen yield with high purity (e.g., 99.999%). The reaction occurring in water electrolysis (the overall one is presented by equation 4), which can be divided for the anode (equation 2) and the cathode (equation 3) side, is described by the following equations:

$$\text{Anode side: } H_2O \rightarrow 2H^+ + \frac{1}{2}O_2 + 2e^- \tag{2}$$

$$\text{Cathode side: } 2H^+ + 2e^- \rightarrow H_2 \tag{3}$$

$$\text{Overall cell: } 2H_2O \rightarrow 2H_2 + O_2 \tag{4}$$

As shown in Figure 7, there are numerous ways to produce hydrogen starting from both renewable energy sources and fossil fuels. The section where hydrogen is produced using renewable energy, meaning the splitting of water through "green" electricity, is the one that is currently keeping a lot of attention.

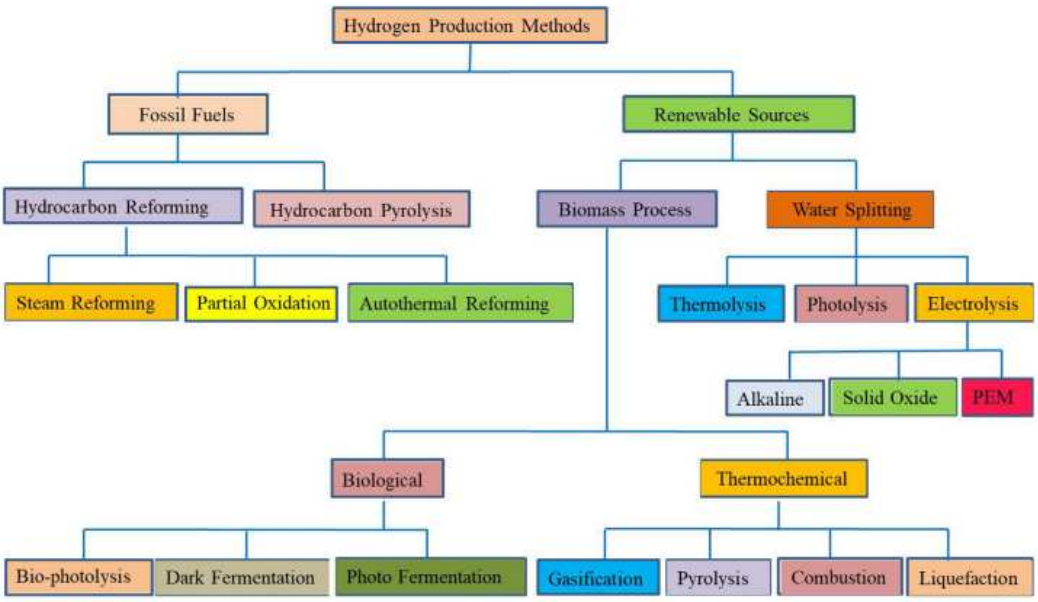

Figure 7: Different hydrogen production methods [36]

Hydrogen can be also classified based on the energy source with which it is produced; thus, the following classifications (indicated through "colors" of hydrogen) are reported (see also figure 8):

1. Grey hydrogen is obtained from fossil sources (either steam methane reforming or gasification);
2. Blue hydrogen is obtained from fossil sources equipped with carbon capture systems (either steam methane reforming or gasification);
3. Turquoise hydrogen is obtained from methane (e.g., pyrolysis process);
4. Green hydrogen is obtained from renewable energy sources (e.g., water-based electrolysis process).

It is evident that "green" hydrogen is the key to the current and future energy transition.

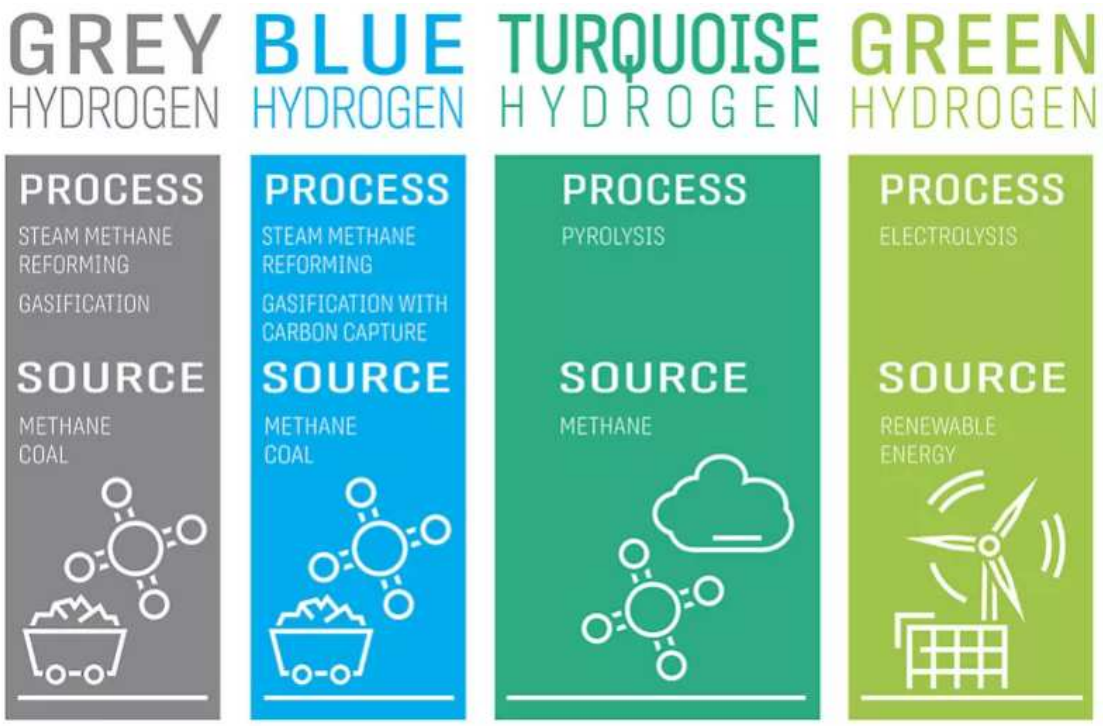

Figure 8: Hydrogen colors' classification [37]

Next paragraphs aim to provide an overview of the current state of several hydrogen generation technologies, including alkaline, anion exchange, polymeric, and solid oxide electrolyzers technologies. Furthermore, it is explained why the use of polymeric materials at high operating pressures further improves hydrogen production.

3.3 Alkaline Water Electrolysis (AWE)

Alkaline water electrolysis is a well-established technology for producing hydrogen up to the MW range for commercial use. Alkaline electrolysis uses an aqueous solution (either KOH or $NaOH$) as electrolyte, and runs at lower temperatures between 30° and 80°C. The electrolyte concentration is between 20% and 30% in volume. Asbestos diaphragm and nickel materials are used as electrodes in the alkaline water electrolysis process [38],[39]. Alkaline water electrolysis has several benefits; among them, it uses inexpensive catalysts based on non-noble metals which can be used to create multi-cell stacks for commercial applications. On the other hand, the system's drawbacks include the use of an electrolyte that is corrosive, low current densities, and low pressure ($> 400\ mA/cm^2$ @ambient pressure)[40]. Figure 9 displays a graphic representation of an alkaline electrolysis's reaction.

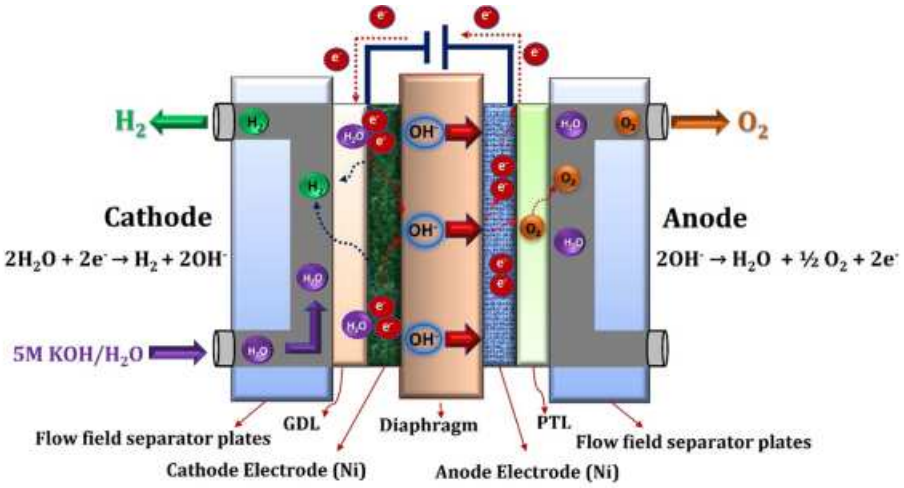

Figure 9: Alkaline electrolysis reaction [41]

3.4 Anion Exchange Membrane (AEM)

AEM water electrolysis is a developing technology for green hydrogen production (see Figure 10). In recent years, many research organizations and institutions have been actively working on the development of AEM water electrolysis due to its low cost and high performance compared to other conventional electrolysis technologies. The first journal publication on AEM water electrolysis was by We and Scott in 2011, and since then many researchers have contributed to its development. AEM water electrolysis technology is similar to conventional alkaline water electrolysis, but it replaces traditional diaphragms (asbestos) with an anion exchange membrane (quaternary ammonium ion exchange membranes). AEM water electrolysis offers several advantages such as the use of cost-effective transition metal catalysts instead of noble metal catalysts, and the ability to use distilled water or low-concentrated alkaline solutions (1M KOH) as the electrolyte instead of highly concentrated solutions (5M KOH). Despite these significant advantages, AEM water electrolysis still requires further improvements in MEA stability and cell efficiency, which are essential for large-scale or commercial applications. Currently, reported stability is 2000 hours with Sustainion, 1000 hours for Fumatech (A201 and FAA3-50), and over $35,000$ hours for the Enapter multicore AEM electrolyzer.

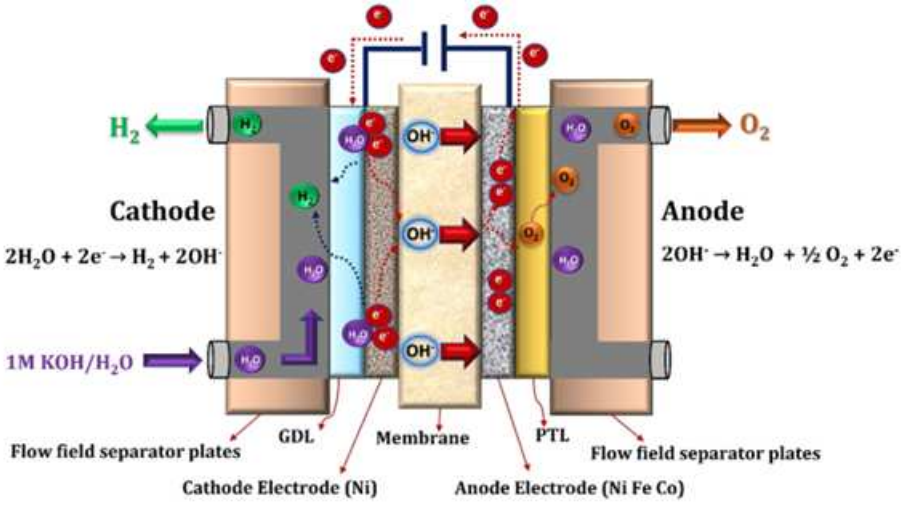

Figure 10: AEM electrolysis reaction [41]

3.5 Solid Oxide Electrolysis (SOE)

Donitz and Erdle initially described SOEs in the 1980s [42]. SOE has gained significant attention due to its ability to transform electrical energy into chemical one and produce ultra-pure hydrogen efficiently. Steam is produced via SOE which uses water at temperatures between 500 and 850°C and high pressures. The primary benefit of the SOE technology over low-temperature electrolysis ones is, indeed, its higher operating temperature. Nevertheless, the SOE technology must address certain problems with instability and deterioration before facing widespread commercialization [43]. Figure 11 shows a graphic representation of SOE's reaction.

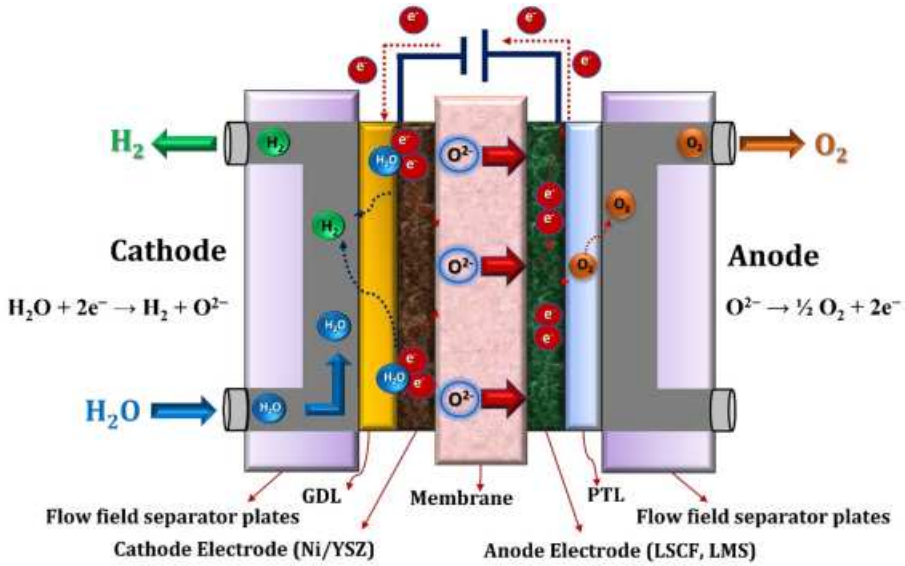

Figure 11: SOE electrolysis reaction [41]

3.6 Proton Exchange Membrane (PEM)

Grubb created the first PEM water electrolysis in the early 1950s, and General Electric Co. was founded in 1966 to address the shortcomings of the alkaline water electrolysis process [44]. The PEM technology employs $Nafion^{®}$, $Fumapem^{®}$ that uses solid polysulfonated membranes as an electrolyte (e.g., proton conductor). The PEM technology offers numerous benefits including reduced gas permeability, elevated proton conductivity (e.g., 0.1 ±, 0.02 S/cm), reduced thickness (20–300 mm), and high pressure operation [45]. One of the best ways to convert renewable energy sources into very pure hydrogen is through PEM water electrolysis. Indeed, this technology has many benefits such as a small footprint, compact design, high efficiency, fast response, high current density (e.g., over 2 A/cm^2), and lower temperature operation (e.g., 20–80°C). Additionally, the process produces ultra-pure hydrogen as well as oxygen as a byproduct [46].

From the chemical point of view, water is electrochemically split into hydrogen and oxygen at the respective electrodes in PEM water electrolysis, with hydrogen being produced at the cathode and oxygen at the anode. Process water feeds the anode where it splits into protons (H^+), electrons (e^-), and oxygen (O_2); subsequently, the proton conducting membrane transports these protons to the cathode side. Figure 12 depicts a schematic representation of the electrolysis process.

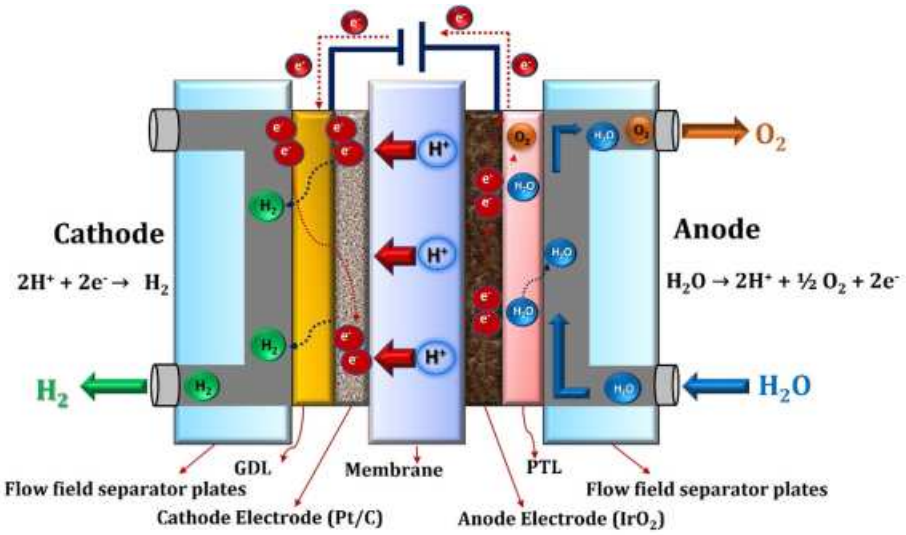

Figure 12: PEM electrolysis' reaction [41]

According to Xiang et al.[47], 2020 sees AEM and PEM starting at comparable capital cost levels, with SOE being much higher.

Another important point is the electricity consumption, which was 50 kWh/kg_{H_2} [48] in 2020 and should progressively drop down to $40kWh/kg_{H_2}$ by 2050 for both

AWE and PEM. With a lower initial electricity consumption of $40kWh/kg_{H_2}$ in 2020 and a further reduction down to $35kWh/kg_{H_2}$ by 2050, SOE may have an efficiency advantage as well.

PEM electrolyzer's Levelized Cost Of Hydrogen (LCOH) can be estimated between 40–60 €$/MWh$ as also reported by Bernuy-Lopez in [49]. This method also produces very pure hydrogen (99.999%).

Although the SOE's overall electricity consumption efficiency is higher and its operating and maintenance costs are significantly lower compared to the other analysed technologies so far, its initial costs are significantly higher. In terms of capital costs, AWE and PEM are more affordable and sustain competitive cost reductions over the long term in both capital and operating/maintenance costs [47].

Despite its high energy content in terms of kWh/kg (e.g., 33.3 kWh/kg for hydrogen versus 12.2 kWh/kg for gasoline [58]), which makes it a very interesting fuel, hydrogen's weakness lies in its low mass density in gas phase which results in a significant disadvantage in terms of energy density and storage (e.g., 2.22 kWh/l for hydrogen whereas gasoline has a density of 8.89 kWh/l). [50]); for this reason, high operating pressures are required. To obtain hydrogen at higher pressures, it is therefore needed to use compressors that raise the fluid pressure to facilitate storage and transportation, or systems that produce high pressure hydrogen directly.

The advantage offered by PEM electrolyzers lies in the solid structure that acts as an electrolyte (specifically $Nafion^{®}$) that allows maintaining its physical structure even at pressures higher than ambient pressures. This can be done either through mechanical compression (e.g., using screws to hold all parts of the cell at a preset pressure value) or through hydrodynamic compression with a fluid that keeps the system at set pressure (and temperature) values. This is made possible by a particular mechanism that consists of a flexible material pocket into which the membrane is put to enable uniform compression of the membrane.

When looking at a cell module similar to the one shown in Figure 13, two Porous Current Distributors (PCDs) and two corrosion-protected planar copper monopolar plates for current conduction, in and out of the pocket, are visible from the outside. The Catalyst Coated Membrane (CCM) layer, which is made of a thin layer of Nafion, is visible from the center of the structure. To get the process media to the active sites, plastic cell frames with built-in conduits for the media are used as proposed by Wirkert et al. [51].

Summing up, PEM electrolyzers provide an intriguing option for producing hydrogen both now and in the future.

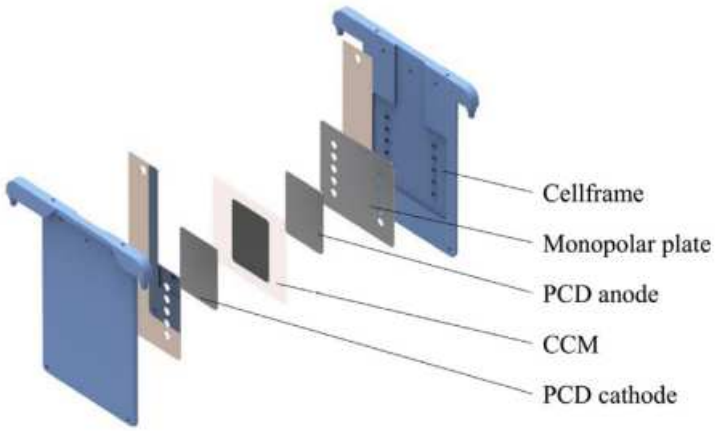

Figure 13: Simple model of a PEM electrolyzer cell [51]

4 Parameters used in the developed numerical model

To develop a mathematical model that can accurately resemble PEM electrolyzers' performance, it is imperative to establish the distinctive parameters of the electrolytic cells, namely those that use a solid membrane. In light of this, the following parameters are:

- Reference exchange current density (anodic and cathodic sides);
- Activation energy (anodic and cathodic sides);
- Charge transfer coefficients (anodic and cathodic sides);
- Reference conductivity of the membrane;
- Activation protonic energy;
- Variable parameters: operative pressure, operative temperature, water pressure, reference pressure, reference temperature, number of cells and active area;
- Constant parameters: gas constant, Faraday's constant, number of electrons, hydrogen's lower heating value, membrane thickness.

4.1 Reference exchange current density

The reference exchange current density is a critical parameter that describes the intrinsic electrochemical activity of the electrode material for a specific reaction at a given reference condition. It is a measure of the rate at which an electrochemical reaction occurs without any applied external voltage, and it is indicative of the catalytic activity of the electrode material. Both the electrolyzer and fuel cell operate better if the reference exchange current density is higher because this means that the electrode material is more efficient in catalyzing the reaction. Since it directly affects the efficiency and power output of such devices, this parameter is essential for their design and optimization. The type of membrane, the operating conditions, and the catalyst material have a substantial impact on the actual value of the reference exchange current density. The metric i_0 has been extensively used in technical applications to assess the suitability of catalysts, including water electrolyzers and fuel cells. Di-hydrogen is not very soluble in aqueous solutions and makes it challenging to experimentally determine the i_0 for catalysts that are highly reactive to the hydrogen reaction [52]. To compute the true current density passing through the electrolytic cell, the i_0 value has to be known a priori; indeed, considering the Arrhenius equation modified as proposed by Noyan et al. [53] [54], it can be computed as reported in Eq. 5 that refers to the current density circulating at the anode of the electrolytic cell, while eq. 6 occurs at the cathode side:

$$i_{0,\text{anode}} = i_{0,\text{ref,a}} \left(\frac{p_{O_2}}{P_{\text{ref}}}\right)^{0.25} \left(\frac{p_{H_2O}}{P_{\text{ref}}}\right) \exp\left[-\frac{E_{aa}}{R}\left(\frac{1}{T_{\text{cell}}} - \frac{1}{T_{\text{ref}}}\right)\right] \quad [A/cm^2] \tag{5}$$

$$i_{0,\text{cathode}} = i_{0,\text{ref,c}} \left(\frac{p_{H_2}}{P_{\text{ref}}}\right) \exp\left[-\frac{E_{ac}}{R}\left(\frac{1}{T_{\text{cell}}} - \frac{1}{T_{\text{ref}}}\right)\right] \quad [A/cm^2] \tag{6}$$

The anodic and cathodic current densities in electrolyzers can vary due to several reasons, including the used materials, the operating conditions, and the reactions that take place at each electrode. The anodic side of electrochemical systems, such as electrolyzers and fuel cells, frequently experiences harsher conditions than the cathodic side. Compared to the cathode reactions like the Hydrogen Evolution Reaction (HER), the anodic reactions—like the Oxygen Evolution Reaction (OER) in water electrolysis usually entail several electron transfer steps, which makes them intrinsically more complex and kinetically slower. Higher overpotentials are needed to drive the anodic reactions as a result of this complexity. The values selected for the exchange current densities, $i_{0,an}$ for the anode and $i_{0,cat}$ for the cathode, differ significantly one from another in the current available scientific literature as discussed also by Carmo et al. in [40]. In addition, challenging-to-quantify catalyst physical parameters affect the exchange current density, being an issue since the polarization curves that a model could predict rely significantly on the exchange current density that varies by more than seven orders of magnitude according to

Tijani et al. [55]. Indeed, this aspect is especially challenging for the anodic side [40].

4.2 Activation energy

The lowest energy needed to make the electrochemical reactions occur at the electrodes—the OER on the anodic side and the HER on the cathodic side is the activation energy in the context of an electrolyzer. Since the activation energy gives a picture of how quickly a reaction proceeds, it is an important factor. For an effective electrolysis, a lower activation energy is preferred because it allows the reaction to proceed more readily and at a lower applied potential. Indeed, the losses associated with the different working regimes must be considered to compute the cell voltage. At low current values, activation losses (overpotential) become significant and are calculated as follows:

$$V_{\text{act,anode}} = \left(\frac{RT_{\text{cell}}}{nF\alpha_{\text{anode}}}\right) \ln\left(\frac{i}{i_{0,\text{anode}}}\right) \quad [V] \tag{7}$$

$$V_{\text{act,cathode}} = \left(\frac{RT_{\text{cell}}}{nF\alpha_{\text{cathode}}}\right) \ln\left(\frac{i}{i_{0,\text{cathode}}}\right) \quad [V] \tag{8}$$

The anodic side is disadvantaged compared to the cathodic one in terms of activation energies' values, as it happens for current densities (see paragraph 4.1). The HER at the cathode is less complex than the OER at the anode. Whereas the HER uses one or two electrons, depending on the mechanism, the OER uses four electrons transfer to convert water into oxygen gas, protons, and electrons. When compared to the HER, the activation energy of the OER is usually higher due to its complexity which involves several steps and intermediates. The activation overpotential's value is strongly dependent on the current density i_0, which changes in response to changes in activation energy as reported in Eq. 5. In particular, when activation energy E_a increases, the current density i_0 decreases. This effect corresponds to a final growth of activation overpotential (see equation 7, where i_0 is the denominator of the logarithm) and consequently of the cell's electrical consumption.

4.3 Charge transfer coefficients

Often represented by the symbol α, the Charge Transfer Coefficient (CTC) is a dimensionless parameter that offers information about the kinetics of the electrochemical reactions, specifically on the energy barrier for electron transfer throughout the reaction. The Butler-Volmer equation, which expresses the rate of an electrochemical reaction about the applied potential, heavily relies on it. The charge transfer coefficient, which is a measure of how favorably an electron is transferred in a forward direction towards the product and in a backward direction towards the reactants, varies from 0 to 1. The activation overpotential and the CTC are closely linked. It has been observed that the previous overvoltage diminishes as the CTC increases from 0.1 to 1 at both the anode-cathode electrodes. Compared to the cathodic side, electrochemical reactions at the anodic one require more energy. Another explanation would be that more energy is needed at the anode to start the electro-kinetics process that breaks the connection between the oxygen and hydrogen atoms of a water molecule. On the other hand, since the two species react quickly to generate hydrogen molecules, the reaction between the hydrogen ion and the electron at the cathode side does not require more energy [56]. As a result, a lower CTC is obtained so that a less symmetric barrier is obtained. The Volmer-Heyrovsky or Volmer-Tafel mechanisms, conversely, are more commonly used in the HER and result in more symmetric energy barriers and higher CTCs. The temperature is the variable that has the biggest impact on this parameter, and in many works, such as in Niroula et al. [57], the relationship between CTC and temperature has been presented as a linear dependence.

4.4 Reference conductivity of the membrane

A PEM's reference conductivity is defined as its capacity to conduct either protons or hydrogen ions under particular operating conditions. In such a context, the conductivity is commonly expressed in terms of Siemens per meter (S/m). Due to their major effects on the membrane's conductivity, particular temperature and humidity levels are frequently included in the reference conditions. The conductivity is important for PEM membranes since it establishes the membrane's ability to transfer protons from one side to another with an efficiency that impacts the device's overall performance. The membrane's structure and material composition affect the value of the reference conductivity; for instance, under certain conditions, the reference conductivity of $Nafion^{®}$ usually ranges from 0.1 to 0.2 S/m. It is worth noting that a membrane's ability to transfer protons efficiently increases with the conductivity, which is advantageous for applications like electrolyzers and fuel cells. As Eq. 9 reports, a higher reference conductivity (σ_{ref} [58]) corresponds to a higher membrane conductivity (σ); hence, as the conductivity increases, ohmic losses decrease (V_{ohm}) as demonstrated through Eq. 10 (δ is membrane width) reported by Falcao et al. [59]. Higher conductivity results in greater proton transfer across the membrane

that reduces inefficiencies as previously described.

$$\sigma = \sigma_{\text{ref}} \cdot \exp\left[\frac{-E_{\text{pro}}}{R}\left(\frac{1}{T_{\text{ref}}} - \frac{1}{T_{\text{cell}}}\right)\right] \ [S/m] \tag{9}$$

$$V_{\text{ohm}} = \left(\frac{\delta}{\sigma}\right) \cdot \text{i} \ [V] \tag{10}$$

4.5 Activation protonic energy

The concept of the "activation protonic energy" refers to the energy needed to start the electrolysis process in a PEM electrolyzer. The energy barrier that needs to be broken for protons (H^+) to pass through the membrane from the anode to the cathode and to let the electrochemical reactions take place at both electrodes is referred to as the activation energy. Since the activation energy affects the electrolysis process's overall efficiency and energy requirements, its barrier is important. The electrolysis process can be more effective and use less electrical energy to produce a fixed amount of hydrogen if the activation energy is lower. One of the main research areas for creating more efficient and sustainable hydrogen production processes is to overcome this obstacle.

4.6 Variable parameters

- Operative pressure and temperature:
  Pressure and temperatures are instances of arbitrary parameters that can be used for characterising both the eletrolyser and fuel cells devices. Currently, the goal of this work is to develop a model that can forecast how a PEM electrolyzer will behave at different pressure and temperature conditions. The pressure has been specifically examined at the anode and cathode sides: the first one involves an oxygen reference pressure, while the second one considers a hydrogen one. Conversely, temperature refers to the "operative temperature" since it is thought to be stable across all the cells. Since these values may

be deemed arbitrary, they have been altered during the simulation to forecast how the cells would behave in various operating conditions.

- Water pressure:
  As the result of the varying temperature of the system, the water partial pressure at the cathode side changes as described by Antoine's equation [60]. The parameters needed to calculate the pressure value are presented in table 1, and the expression to calculate the exact value is presented in equation 11.

Table 1: Antoine's equation parameters

Parameter	Description
A_{ant}	5.203
B_{ant}	1733.926
C_{ant}	-39.485

$$p_{H_2O} = 10^{\left(A_{\text{ant}} - \frac{B_{\text{ant}}}{T_{\text{cell}} + C_{\text{ant}}}\right)} \cdot 133.322 \ [Pa] \tag{11}$$

- Reference pressure and temperature:
  The values of the reference temperature and pressure match the circumstances in which the PEM electrolyzer's parameters are determined. The model is built using these parameters. Reference temperature and pressure values are used to determine values for kinetics parameters, including reference exchange current density, activation energy, charge transfer coefficients, reference conductivity of the membrane, and activation protonic energy, depending on the operating circumstances provided by the experimental data.

- Number of cells and active area:
  In an electrolyzer, the number of cells refers to the total count of individual cells stacked together, while the active area is the surface area within each cell where the electrochemical reactions occur, directly impacting the efficiency and output of hydrogen and oxygen production. In this work, these two parameters change for the two different electrolyzers used to obtain the experimental data.

4.7 Constants parameters

After discussing the primary model parameters, it is crucial to consider additional parameters and constants that have been used to derive the mathematical model that characterizes the PEM electrolyzers' behaviour. Table 2 lists these values:

Table 2: Electrolyzer's constants

Parameter	Value
Gas constant [9], R (J/mol·K)	8.314
Faraday's constant [9], F (C/mol)	96485
Number of electrons [59] , n	2
Lower heating value of hydrogen [27], LHV (MJ/kg)	120
Nafion 115 membrane thickness, δ (cm)	0.0127

5 Cell voltage model

In this section, a numerical model that can accurately forecast the electrolyzer's behavior from the fundamental equation is presented. To do this, each term in the equation is expressed by taking into account its meaning; then, these terms are modified to produce a more versatile model that resembles the operation of PEM electrolysers at different operating conditions.

5.1 Basic cell model

Literature easily provides the fundamental equation that describes the progression of the cell voltage at ambient pressure (Carmo et al. [40], Falcao et al. [59], Lubello et al [61]), as presented in Eq. 12; this equation expresses the voltage value required for the electrolysis reaction to occur:

$$V = E + V_{\text{act}} + V_{\text{trans}} + V_{\text{ohm}} \ [V] \tag{12}$$

Since it is the theoretical voltage needed by the electrolyzer without accounting for losses, the first term E, which is known as the Open Circuit Voltage (OCV), is sometimes referred as the reversible cell voltage (E). In order to break through the molecular bonds, the activation overvoltage (V_{act}) is the voltage loss ascribed to accelerate the electrochemical reaction. Gas bubbles created by the reaction products and flow restriction to the catalyst sites, such as current collector and separator plate morphology, are the main causes of mass transfer losses (V_{trans}). Lastly, there are the ohmic losses (V_{ohm}) that are due to the resistance done towards the electron flow via separator plates and current collectors, as well as proton conduction through membranes [40]. Further details on this are reported below:

- **Open Circuit Voltage (OCV)**
  The open circuit voltage has been computed by using the Nernst's equation as follows:

$$E = E_{\text{rev}} + \left(\frac{R \cdot T_{\text{cell}}}{n \cdot F}\right) \cdot \ln\left(\frac{p_{\text{H}_2} \cdot (p_{\text{O}_2})^{0.5}}{p_{\text{H}_2O}}\right) \ [V] \tag{13}$$

  Here E_{rev} is calculated as follows:

$$E_{\text{rev}} = 1.229 - \left(0.9 \cdot 10^{-3}\right) \cdot (T_{\text{cell}} - 298) \ [V] \tag{14}$$

  The number of electrons involved in the reaction "n" is considered equal to 2 in this model (Falcao et al. [59]).

- **Activation overpotential**
  The energy needed to start a reaction is known as the activation overpotential

which is a loss of energy in a reaction. Utilization, loading, temperature, and catalyst material have a direct impact on this loss. The Butler-Volmer's equation describes the activation overpotential applicable to the anode (eq. 7) and cathode (eq. 8) separately (see paragraph 4.2). The accurate modeling of this phenomenon is challenging due to the influence of numerous parameters, including material processing, temperature, active catalyst areas, utilization, distribution, age, pressure, and morphology [62].

- **Mass transport overpotential**
  In PEM electrolyzers the mass transport overpotential, also referred to as the concentration overpotential, is mainly present at the cathode and is caused by restrictions in the transport of reactants to the reaction sites or the removal of products. When current densities are high, this phenomenon becomes important. This term has been neglected in this work as the focus is not on high current density operations.

- **Ohmic overpotential**
  The voltage loss connected to the resistance to ions flowing through the electrolyte and electrons flowing through the external circuit, which consists of the electrodes and any connecting materials, is known as the ohmic overpotential in PEM electrolyzers. This kind of overpotential, which is affected by factors like membrane conductivity, electrode and contact resistances, current density, temperature, and humidity is crucial to the overall effectiveness and performance of a PEM electrolyzer. The Ohmic overpotential is expressed by Eq. 10 (paragraph 4.4)

5.2 Parameters optimization

The parameters described in Section 4 are known only for a particular Membrane Electrode Assembly (MEA) at specific operating conditions. Currently, the ranges in which the previously explained parameters vary are known from the scientific literature, but at this stage, their exact values cannot be used since they are unknown.

Specifically, a model has been created to predict the behavior of PEM operating at two different conditions (e.g., fixed temperature and varying pressure, and vice versa) using experimental data from the hydrogen laboratory of the Westfalische Hochschule institute.

The developed model, which makes use of the following equations (Eqs. 15, 16, 17 model overpotentials, while equation 13 in paragraph 5.1 models the open circuit

voltage), is examined in detail in the following, and its reliability is assessed by comparing the numerical results with experiments.

$$V_{\text{act,anode}} = \left(\frac{RT_{\text{cell}}}{nF\alpha_{\text{anode}}}\right) \ln\left(\frac{i}{i_{0,\text{ref,a}}\left(\frac{p_{O_2}}{P_{\text{ref}}}\right)^{\text{a}}\left(\frac{p_{H_2O}}{P_{\text{ref}}}\right)^{\text{b}} e^{-\frac{E_{\text{aa}}}{R}\left(\frac{1}{T}-\frac{1}{T_{\text{ref}}}\right)}}\right) \ [V] \tag{15}$$

$$V_{\text{act,cathode}} = \left(\frac{RT_{\text{cell}}}{nF\alpha_{\text{cathode}}}\right) \ln\left(\frac{i}{i_{0,\text{ref,c}}\left(\frac{p_{H_2}}{P_{\text{ref}}}\right)^{\text{c}} e^{-\frac{E_{\text{ac}}}{R}\left(\frac{1}{T}-\frac{1}{T_{\text{ref}}}\right)}}\right) \ [V] \tag{16}$$

$$V_{\text{ohm}} = \frac{\delta}{\sigma_{\text{ref}}\, e^{-\frac{E_{\text{pro}}}{R}\left(\frac{1}{T_{\text{ref}}}-\frac{1}{T}\right)}} \cdot i \ [V] \tag{17}$$

- Variable pressure model:

  This workflow has been used to modify the general electrolyzer model to fit the variable pressure polarization curve found in the experimental test.

  1. **Identification of the kinetic parameters:** The initial step is the research of the kinetic parameters for the PEM cell membrane at specific pressure and temperature conditions, which are required by the developed model;
  2. **Gap in the scientific literature:** Upon reviewing the scientific literature, it is clear that data on these specific kinetic parameters at specific conditions of pressure and temperature are not available, thus leading to proceed with optimizing the parameters using a Python-based optimization process;
  3. **Parameter estimation through fitting:** Kinetic parameters (table 3) are obtained from an initial fitting process at a constant temperature of 40°C and pressure of 10 bar. Starting from this point onward, the parameters have been considered constants by assuming they do not depend on both the pressure and temperature;

4. **Optimization of pressure ratios:** Finally, exponents a, b, and c (Eqs. 15 and 16) for the pressure ratios are derived to optimize the polarization curves. The model is adjusted with experimental data provided at pressures of 20, 40, 60, and 100 bar with a constant temperature of 40°C. This step ensured that the model could accurately resemble the experimental results at different operating pressure conditions while maintaining the integrity of the temperature-dependent responses observed.

This workflow not only facilitates a precise characterization of the PEM but also enhances the predictability and applicability of the model at different operating conditions.

Parameters
Alpha anode (α_{anode})
Alpha cathode (α_{cathode})
Reference anode exchange current ($i_{0,\text{ref,a}}$)
Reference cathode exchange current ($i_{0,\text{ref,c}}$)
Activation energy anode (E_{aa}) [J/mol]
Activation energy cathode (E_{ac}) [J/mol]
Protonic energy (E_{pro}) [J/mol]
Reference conductivity (σ_{ref})

Table 3: Kinetic parameters

- Variable temperature model:

A similar strategy has been used for temperature variant polarization curves, just as it was for adapting the model to the variable pressure data.

1. **Literature review:** An exhaustive review of the existing scientific literature is carried out to search for kinetic parameters relevant to the PEM membrane at specified operational conditions. The scientific literature review revealed a lack of data for the membrane at particular pressure and temperature;
2. **Baseline parameter acquisition:** Kinetic parameters at atmospheric pressure are used and the temperature is fixed at 40°C. This step is fundamental for then parameterizing the PEM electrolyzer operations at different conditions;

3. **Coefficient values:** The model presented herein generally can be applied in a wide range of operations. Specifically, when operating at atmospheric pressure, the coefficients 'a', 'b', and 'c' are equal to zero. This simplification is justified because there is no need to adjust the reference current density values $i_{0,ref}$, at atmospheric pressure as it would be necessary at pressures exceeding this value as presented in Bove et al. work [53].
4. **Thermal optimization of alpha coefficients:** Subsequent steps involve the optimization of the alpha coefficients (Eqs. 15 and 16) at temperatures of 50°C, 60°C, and 70°C. This optimization is crucial to align the theoretical model with experimental data, ensuring that the increasing trend of alpha values with the temperature does not exceed the feasible operational range $0-1$. This constraint is fundamental to maintaining the validity and reliability of the model across a wide range of temperature spectra.

This methodology not only facilitates the accurate calibration of the model parameters at different thermal conditions but also ensures the predictability and applicability of the model at different operating conditions.

6 Experimental setup

The Westfälische Hochschule has kindly supplied all the data needed to develop the model.

A simplified scheme of how the electrolyzerworks is presented in figure 14.
The PEM (Proton Exchange Membrane) electrolyzer operates with water that must meet very high purity standards and be free of contaminants. At the anode, water undergoes oxidation, producing oxygen, protons (H^+), and electrons (e^-). These protons then migrate through the PEM. At the cathode, the protons (H^+) combine with electrons supplied by the external circuit to form hydrogen gas (H_2).
The recirculation of water is essential for managing the temperature and maintaining the hydration of the membrane, ensuring efficient operation. Analyzers are placed at the outlets of both the anode and cathode to monitor and ensure the quality and purity of the produced gases.
Additionally, nitrogen is used to control the pressure within the electrolytic cells, contributing to the stability and safety of the system. This setup ensures high efficiency and reliability in hydrogen production.

Thanks to specific technologies developed at the Westfälische Hochschule, two tests have been carried out at a fixed temperature and variable pressure (first setup described) and vice versa (second one) to get the polarization curve of the analysed PEM electrolyzers.

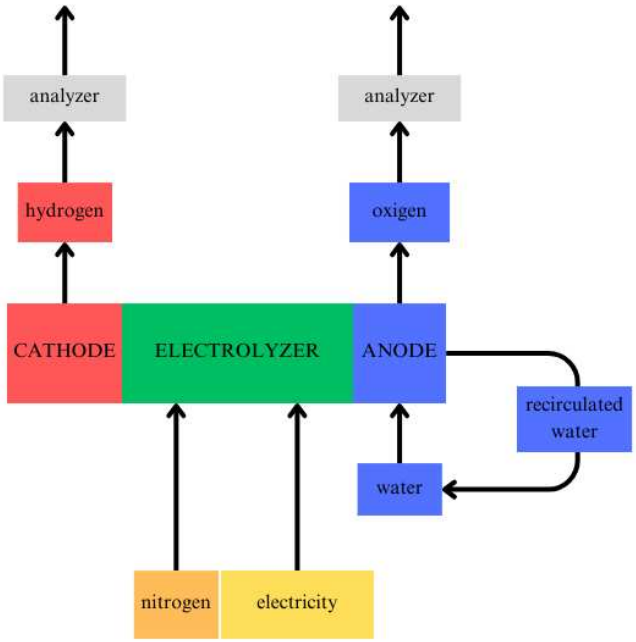

Figure 14: General layout of the electrolyzer test rig [63]

6.1 Variable pressure and fixed temperature setup

The work by Wirkert et al. [51] has been followed to obtain the polarization curves for fixed temperature and variable pressure.

The study emphasizes how crucial it is to maximize the electrical conductivity and flow media throughout the components of the electrolyzer, particularly at their interfaces, to guarantee the efficient operation of each cell in the stack. Additionally, all the cell's active area must have the same operating conditions. The degree of cell compression is the main factor affecting these conditions. Previous studies have shown that uneven cell compression hurts the effectiveness and long-term dependability of cells, indicating the necessity of concentrated development efforts directed toward attaining even compression.

Furthermore, the application of mechanical cell compression is contingent upon certain attributes, including the dimensions of the active cell area and the aggregate count of cells within a stack. Because of this specificity, any solutions created can only be used with specific cell or stack configurations.

Deviations from the ideal operating conditions may result from even small changes in component specifications or the number of cells in a stack, thus requiring additional engineering work and adjustments.

This work presents a modular system design (see Figure 15) that uses a hydraulic medium to compress each cell uniformly. This method ensures consistent cell compression regardless of variations in the active cell area or the number of cells in a stack, and it remains effective at any gas output pressure. Furthermore, by employing the hydraulic medium as a coolant, the process flow media is effectively separated from the heat management, thus allowing for an independent optimization of each.

Figure 15: Photograph of the PEMEL stack with a reinforced pressure housing [51].

The core components of this cell are monopolar plates made of copper foil, which are integrated into a plastic frame to form half of a flexible pocket. When assembled, these half-cells create a space between them, intended to house internal cell components such as Porous Current Distributors (PCD) and the Catalyst Coated Membrane (CCM). The entire cell assembly, shown in Figure 16, is subjected to homogeneous compression by a pressurized hydraulic medium surrounding the cell. The cell frame, made of an electrically insulating plastic material known as Polyether Ether Ketone (PEEK), is designed to withstand all process media and operating conditions. Additionally, process media transport channels are integrated into each of the four sides of the frame, connecting two opposing channels to the inner space for the media inlet and outlet via smaller channels evenly distributed along the sides of the active area.

Thanks to this system, which is shown in Figure 17, it is possible to carry on tests with various stacks that differed in the number of cells and dimensions, yielding significant results.

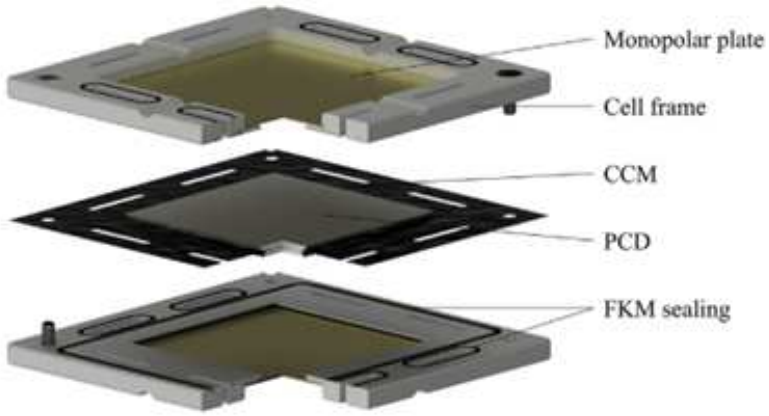

Figure 16: Two half cells consisting of plastic cell frames with integrated media channels comprising a monopolar plate[51]

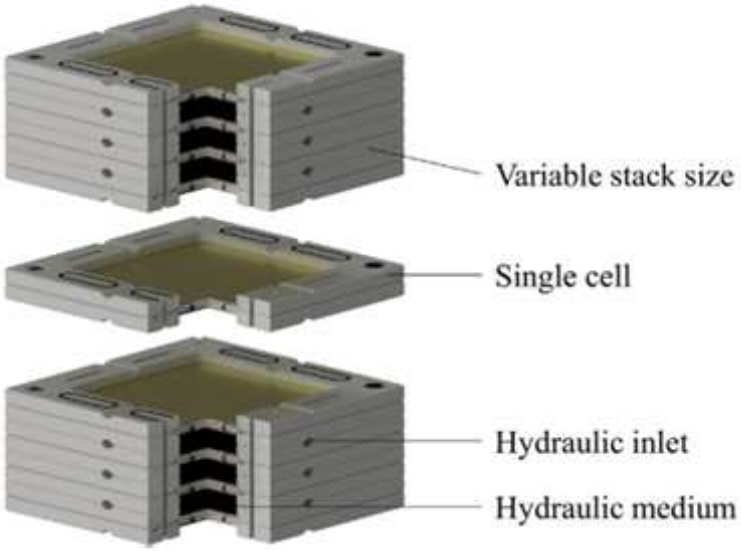

Figure 17: Modular PEM stack where the number of cells per stack can be easily varied [51]

This configuration allowed for the recording of the polarization curves shown in figure 19, and the tests were conducted as follows: a six-cell PEM electrolysis stack (see Figure 18) was set up in a pressure vessel for this investigation, which sealed the reactor against the environment up to 120 bar. It was successfully demonstrated that subsequent operation was possible up to a pressure level of 100 bar (hydrogen and oxygen).

Documenting the polarization curve is a crucial step in assessing an electrolysis stack's performance. The integrated power electronics, which can provide direct current up to 2800 A at a maximum of 16 V, were used for this purpose.

The "constant current" mode was used to record the polarization curve. The experiment involved increasing the current step-by-step until a current density of 1 A/cm^2 was achieved. To obtain more accurate information about the voltages in the stack, the resulting stack voltage was measured at the inverter's terminals.

The polarization curves at hydrogen outlet pressures of 10 bar, 20 bar, 40 bar, 60 bar, and 100 bar are displayed in Figure 19. The curves were recorded between 40 and $50C$, which is considered a moderate temperature.

Table 4 lists a detailed description of all the setup data.

Figure 18: Photograph of a prototype electrolyzer stack based on hydraulic compression [63]

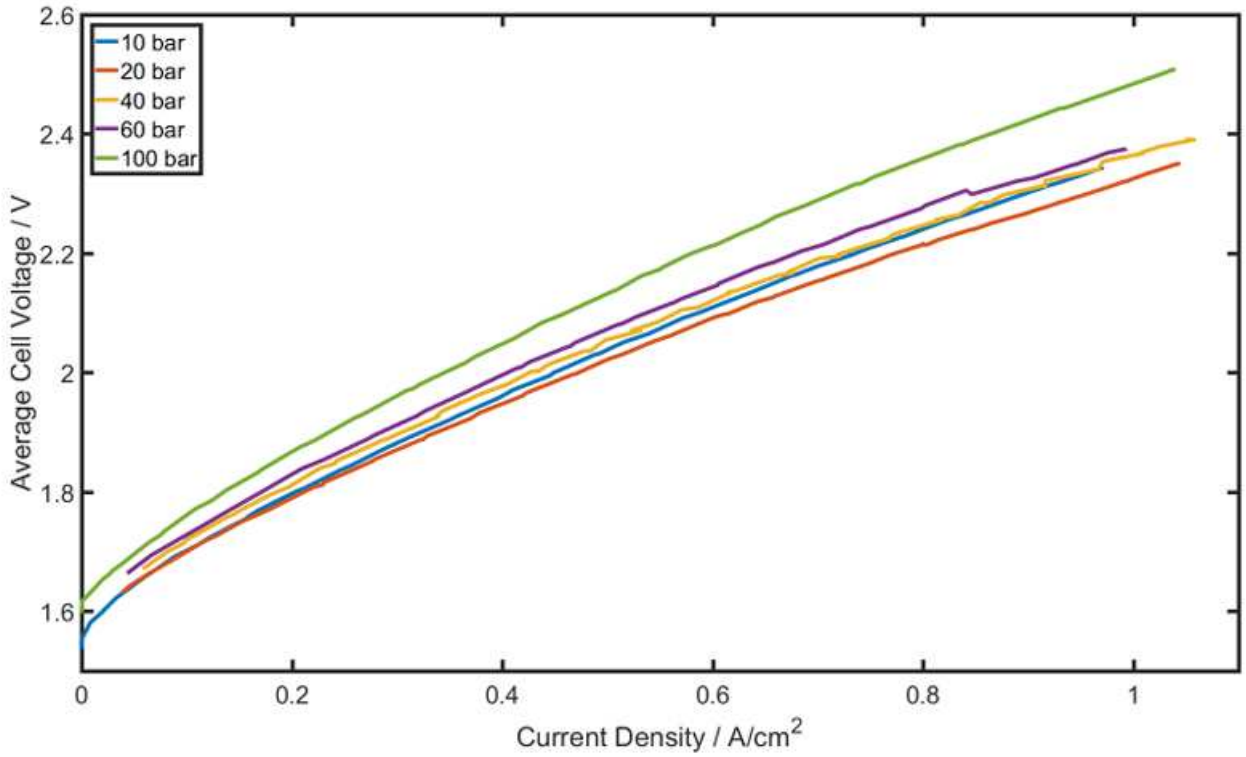

Figure 19: Polarization curves of a prototype PEM electrolysis stack based on hydraulic compression at various gas pressures [63]

Table 4: Variable pressure cell's setup

Parameter	Description
Number of cells, N_c	6
Active area [cm^2]	210
Pole plate anode	Au coated Cu
PTL anode	Titanium compound
Catalyst anode	Ir/IrOx
Membrane	Nafion 115
Catalyst cathode	Pt/C
PTL cathode	Carbon Paper
Pole plate cathode	Au coated Cu
Temperature	40 °C - 50 °C
Pressure	varying

6.2 Variable temperature and fixed pressure setup

The setup for this investigation, largely presented in Rost et al. [64] work, can be summed up as follows. The test cell was engineered based on research related to PEM fuel cell test systems with hydraulic single-cell compression, ensuring homogeneous current density distribution. A hydraulic medium (water or oil) surrounds the active cell components for temperature control, resulting in uniform temperature distribution. This principle was adapted for PEM water electrolysis, creating a single-cell test system for operation up to 80°C and 6.0 A/cm^2, with a maximum area of 25 cm^2 (150 A).

The PEM test system allows easy exchange of active cell components: Pole Plates (PPs), anodic Porous Transport Layers (PTLs), cathodic Gas Diffusion Layers (GDLs), and Catalyst Coated Membranes (CCMs). These components fit into a frame made of Polyether Ether Ketone (PEEK), chosen for its resistance to process water and gases. An integrated channel and gasket system guides process media and prevents leakage.

The test cell, loosely assembled initially, is inserted into a flexible Polyurethane (PU) pocket, and integrated into a pressure housing filled with silicone oil. Increasing hydraulic pressure compresses the cell uniformly. The housing, designed for up to 10 bar, includes a heat exchanger for precise temperature and pressure control, enabling reproducible conditions and flexibility in material testing.

An image of this setup is presented in figure 20.

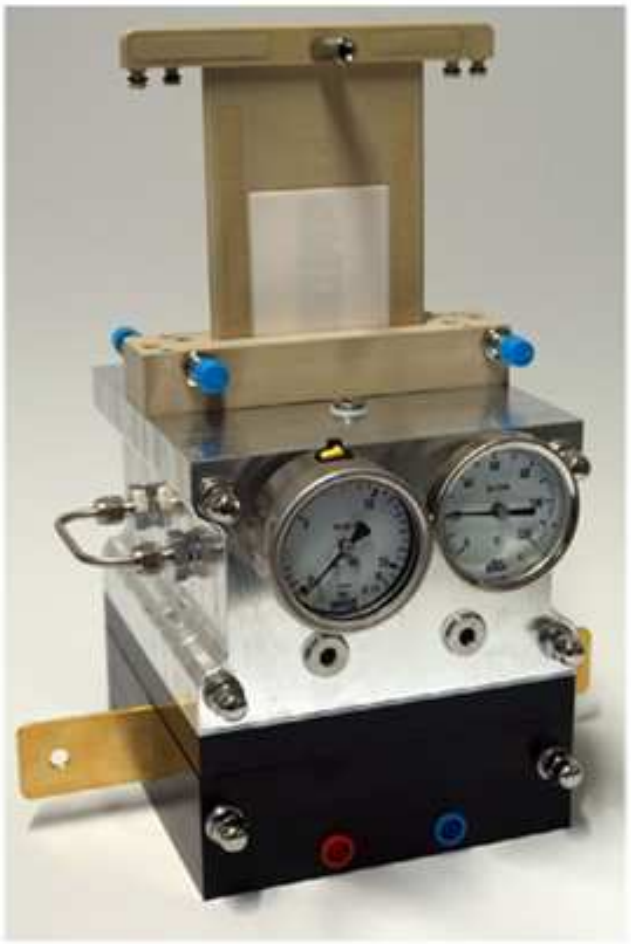

Figure 20: Photograph of the polymer electrolyte membrane water electrolyzer (PEM) test system [64]

With the help of this configuration, the polarization curves for a five-cell stack of 25 cm^2 each (see Figure 21) could be recorded. The tests were conducted in this manner: after the initial run-in procedure, which involved continuously loading the stack with 25 A for an hour, the test stack was subjected to defined steps of the current application, ranging from 0.0 to 50 A (equivalent to 2.0 A/cm^2) for 60 seconds each, before being gradually reduced by the protocol. The voltages of each test cell were measured and recorded simultaneously.

Polarization curves were also measured in additional experimental runs at various temperatures ($40C$, $50C$, $60C$, and $70C$) while maintaining the process water flow. The resulting curves are shown in Figure 21.
Finally, table 5 shows a detailed description of the cells' parameters.

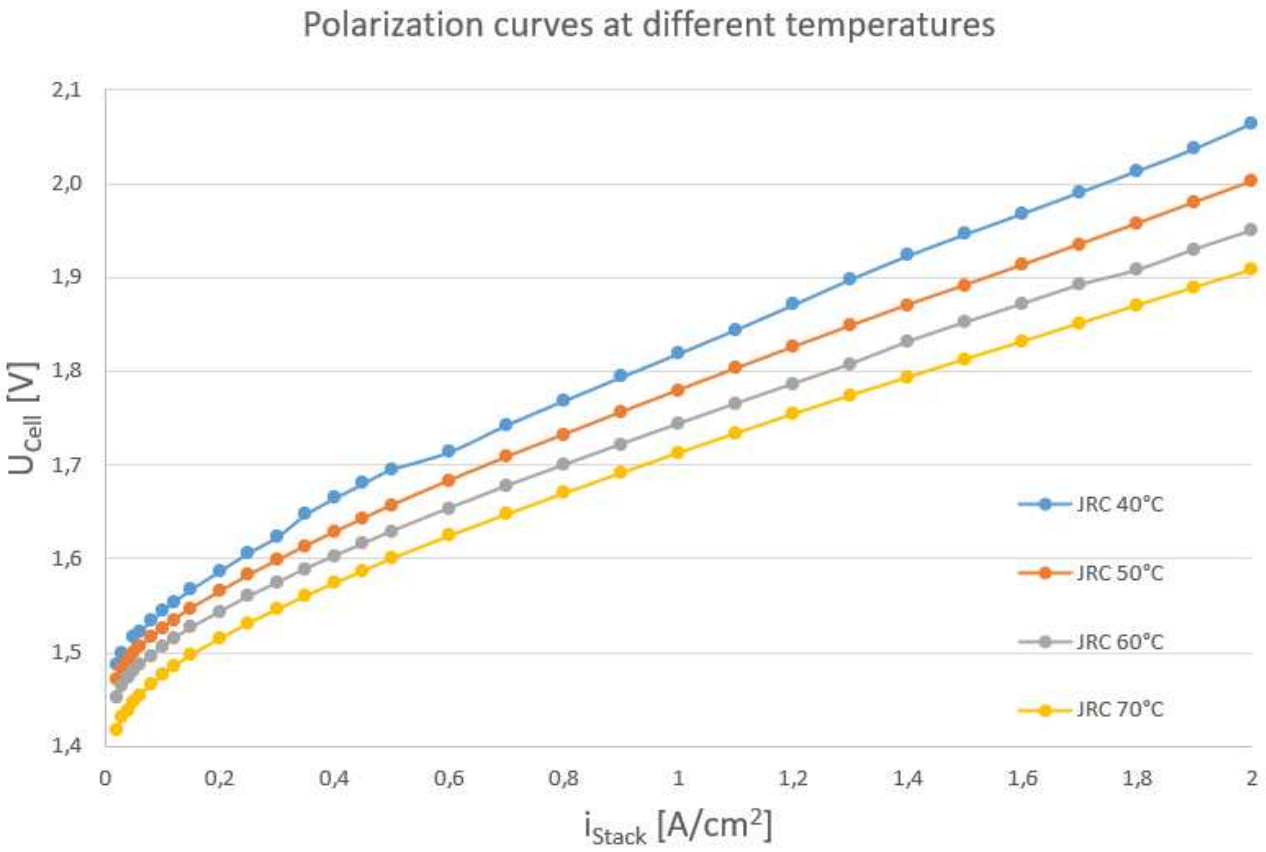

Figure 21: Experimental polarization curves for variable temperature setup [64]

Table 5: Variable temperature cell's setup

Parameter	Description
Number of cells, N_c	5
Active area [cm^2]	25
Pole plate anode	Coated Titanium sheet
PTL anode	Titanium compound
Catalyst anode	Ir/IrOx
Membrane	Nafion 115
Catalyst cathode	Pt/C
PTL cathode	Carbon Paper
Pole plate cathode	Coated Titanium sheet
Temperature	varying
Pressure	ambient

7 Results and comments

This section presents the comparison between the numerical results obtained through the model described in Section 5 and the experimental ones obtained from the electrolytic cell setup reported in Section 6. The main aim is to validate the mathematical model (see the entire code in the Appendix) to make it more accurate and reliable.

The comparison between numerical and experimental data is crucial for assessing the effectiveness of the model as a predictive tool in real-world testing, which is particularly significant in the context of hydrogen production as already discussed in Section 3.

Furthermore, this evaluation not only highlights the strengths and limitations of the current model but also provides valuable insights into possible improvements and refinements necessary for future applications of the model. The results of this comparison will lead to more accurate and efficient electrolytic cell designs in the ongoing efforts toward sustainable hydrogen production.

7.1 Variable pressure and fixed temperature

Firstly, the mathematical model has been used to predict the behavior of the electrolytic cell at different pressures while maintaining a constant temperature (see the code in the Appendix "Pressure Adaptation").

By keeping the temperature constant, the effects of pressure changes are isolated, thus allowing for a more precise analysis of its impacts on the cell's electrochemical processes.

Results from the setup presented in Section 6 are fundamental for validating the robustness and adaptability of the model at different pressure conditions, being a critical factor for designing scalable and flexible hydrogen production systems. The kinetic parameters (table 3) of the model are initially estimated through a fitting process using experimental data obtained at specific operating conditions, namely at a pressure of 10 bar and a temperature of 40°C.

The model provides several parameter combinations that allow for the minimization of the error between the model and the experimental data during the optimization process because of the use of Python. The algorithm found the combination of numerical values of the parameters that gave the lowest RMSE, and these values (table 6) are used in the following calculations.

This approach allowed to establish a reliable baseline for the model's parameters, as presented in Figure 22 and table 6 that are critical for performing accurate

simulations and predictions with other operating conditions.

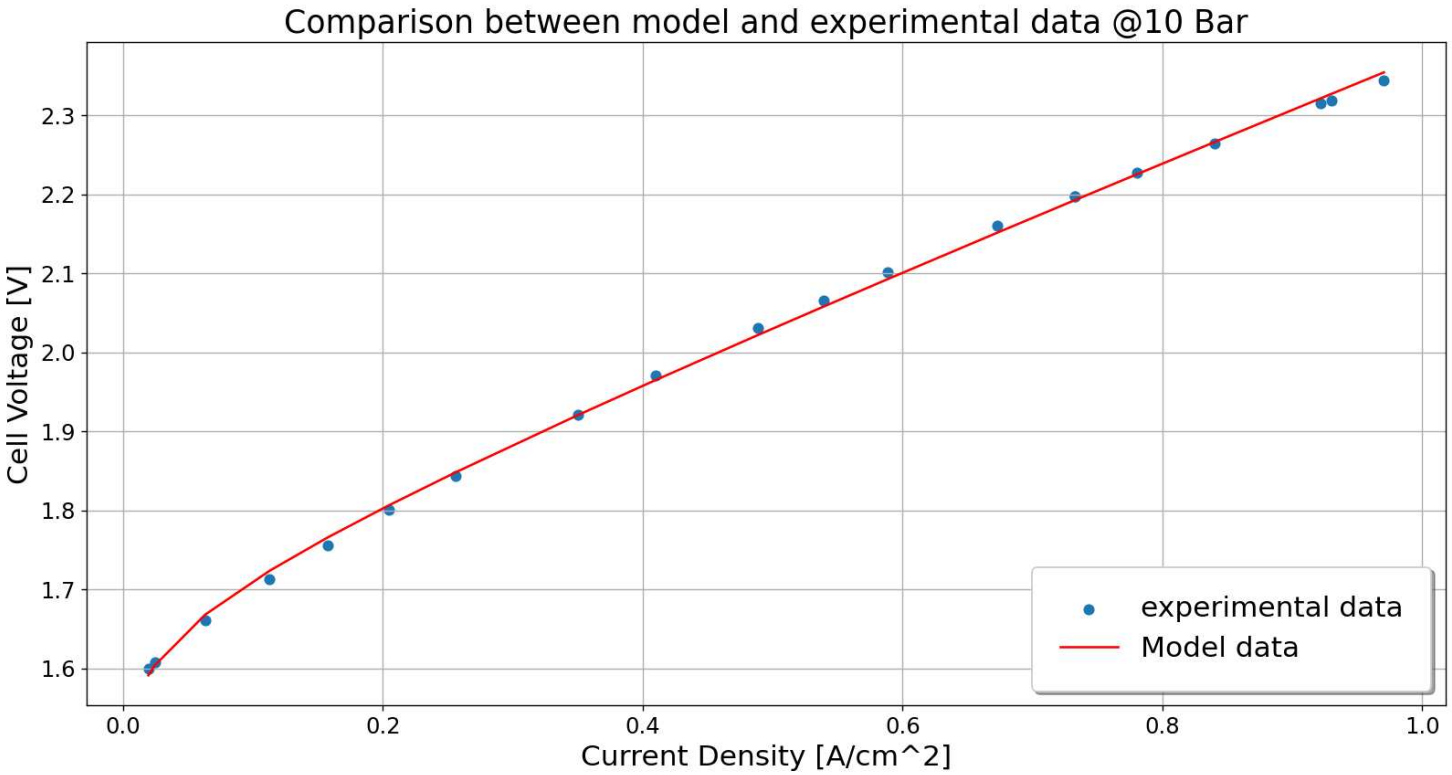

Figure 22: Model fitting @40°C and 10 bar

Table 6: Baseline kinetic parameters at 40°C and 10 bar

Parameter	**Value**
RMSE	0.0069
Alpha anode (α_{anode})	0.952
Alpha cathode (α_{cathode})	0.510
Reference anode exchange current ($i_{0,\text{ref,a}}$)	0.749
Reference cathode exchange current ($i_{0,\text{ref,c}}$)	0.755
Activation energy anode (E_{aa}) [J/mol]	7067.56
Activation energy cathode (E_{ac}) [J/mol]	5120.99
Protonic energy (E_{pro}) [J/mol]	98.64
Reference conductivity (σ_{ref})	0.0020
Exponent p_{O_2} (a)	0.25
Exponent p_{H_2O} (b)	0.44
Exponent p_{H_2} (c)	1.00

Table 7 provides a detailed comparison between the model and the experimental results obtained at a fixed pressure of 10 bar and temperature of $40C$ along with respective relative percentage error defined as Eq. 18

$$\text{relative error} = \left| \frac{\text{experimental voltage} - \text{model voltage}}{\text{experimental voltage}} \right| \times 100\,[\%] \tag{18}$$

Table 7: Comparison of model and experimental voltage values with respective relative percentage errors

Index	**Model voltage (V)**	**Experimental voltage (V)**	**Relative error (%)**
1	1.591	1.600	0.541
2	1.604	1.608	0.229
3	1.668	1.661	0.409
4	1.724	1.713	0.609
5	1.766	1.756	0.550
6	1.806	1.801	0.288
7	1.848	1.844	0.229
8	1.921	1.921	0.004
9	1.965	1.971	0.294
10	2.022	2.030	0.421
11	2.058	2.065	0.348
12	2.093	2.101	0.403
13	2.151	2.161	0.434
14	2.193	2.197	0.214
15	2.193	2.198	0.216
16	2.226	2.227	0.076
17	2.266	2.265	0.070
18	2.322	2.315	0.281
19	2.327	2.319	0.357
20	2.354	2.344	0.437

7.2 Higher pressure values

The application of the developed model to predict the behavior of the PEM electrolyzer at significantly higher pressures of 60 and 100 bar, while using the exponents determined at a baseline pressure of 10 bar, has revealed substantial discrepancies between the model and the experimental data. As shown in Figures 23 and 24), the voltage predicted by the model does not align well with the observed values at higher pressures.

These discrepancies, clearly listed in Tables 8 and 9, are primarily attributed to the model's reliance on kinetic exponents that are optimized at lower pressure. Knowing that the reaction kinetics can significantly change at different pressure regimes, the assumption that exponents remain constant across different pressure values may lead to inaccurate predictions.

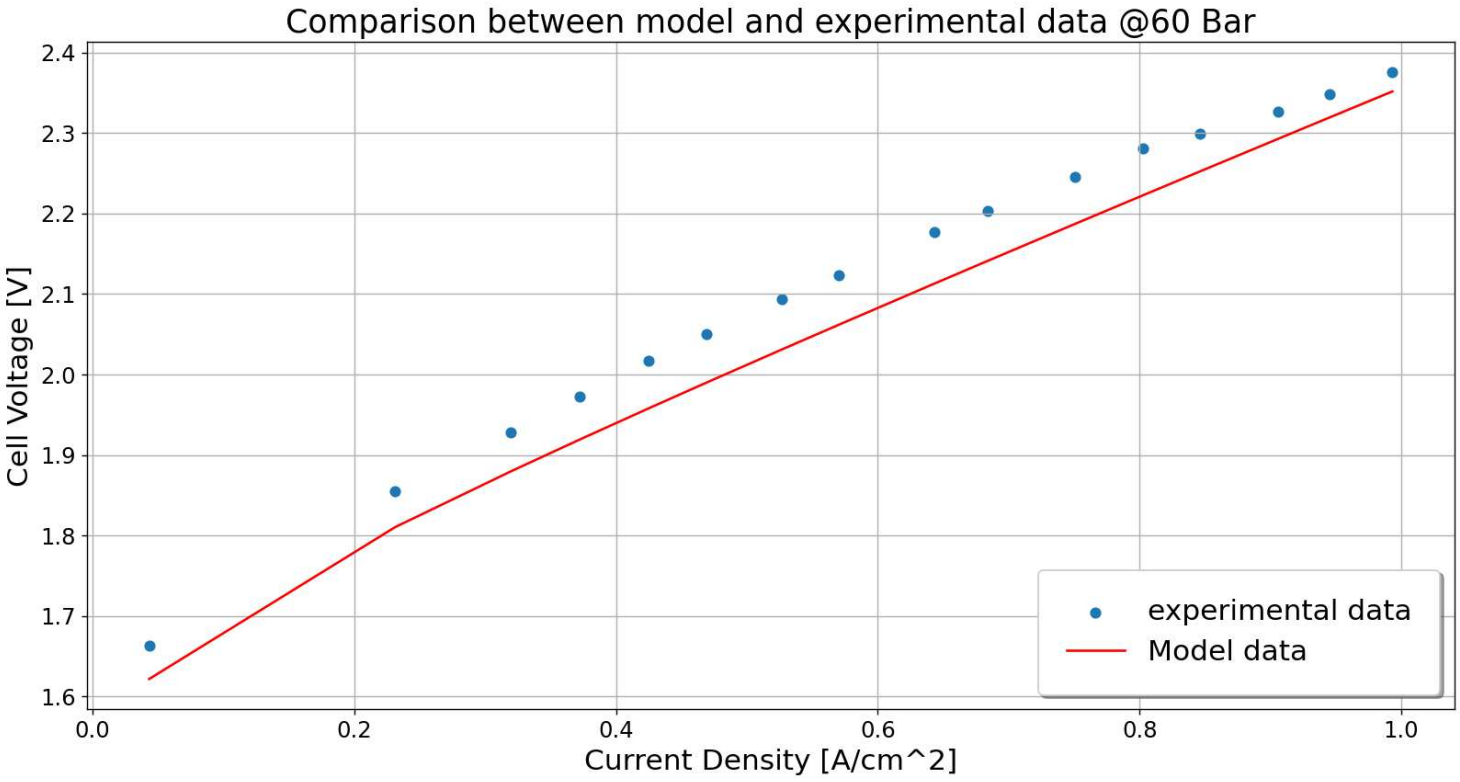

Figure 23: Comparison between the model and experimental polarization curve without exponents optimization @60 bar and 40°C

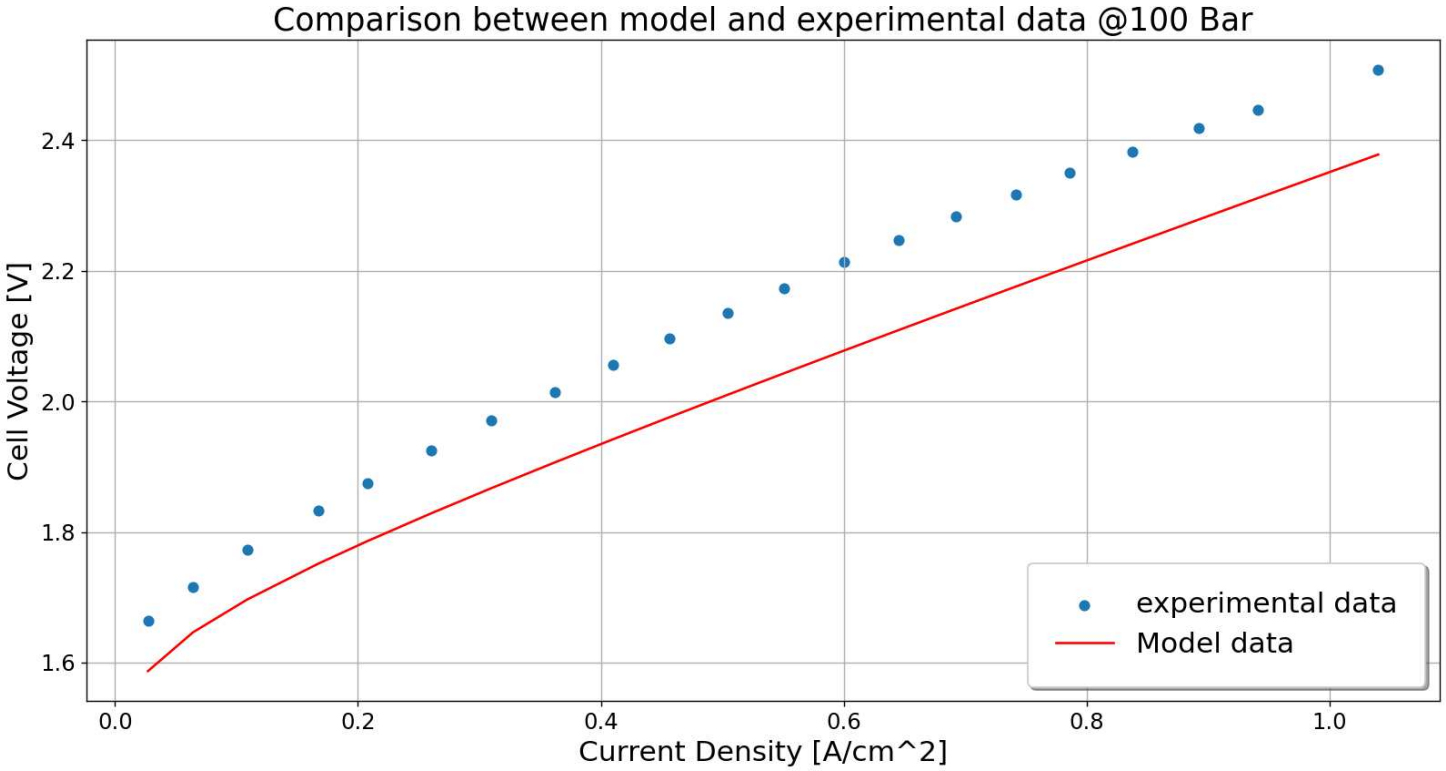

Figure 24: Comparison between the model and experimental polarization curve without exponents optimization @100 bar and 40°C

Table 8: Comparison of model predictions and experimental data at 60 bar with respective relative percentage errors

Index	**Model voltage (V)**	**Experimental voltage (V)**	**Relative error (%)**
1	1.622	1.663	2.514
2	1.810	1.855	2.396
3	1.879	1.928	2.513
4	1.919	1.973	2.728
5	1.958	2.017	2.928
6	1.990	2.050	2.940
7	2.031	2.093	2.955
8	2.062	2.124	2.912
9	2.113	2.177	2.935
10	2.141	2.203	2.820
11	2.187	2.245	2.592
12	2.223	2.280	2.531
13	2.253	2.299	2.019
14	2.293	2.327	1.456
15	2.319	2.349	1.257
16	2.352	2.376	1.002

Table 9: Comparison of model predictions and experimental data at 100 bar with respective relative percentage errors

Index	**Model voltage (V)**	**Experimental voltage (V)**	**Relative error (%)**
1	1.587	1.663	4.593
2	1.646	1.716	4.055
3	1.696	1.772	4.279
4	1.752	1.833	4.421
5	1.786	1.875	4.764
6	1.829	1.925	4.997
7	1.867	1.971	5.262
8	1.906	2.014	5.355
9	1.942	2.056	5.564
10	1.975	2.096	5.771
11	2.010	2.136	5.889
12	2.043	2.174	6.013
13	2.078	2.213	6.124
14	2.109	2.247	6.142
15	2.142	2.283	6.198
16	2.176	2.317	6.110
17	2.206	2.350	6.122
18	2.241	2.382	5.912
19	2.279	2.418	5.766
20	2.311	2.447	5.544
21	2.378	2.508	5.169

The deviations underscore the need for a second phase of model fitting focused specifically on optimizing the kinetic exponents for higher pressure conditions. By re-adjusting these exponents, the model's accuracy increases and thereby reduces the gap between the numerical and experimental values. This optimization process is crucial not only for improving the model's predictive capabilities but also for extending its applicability to a wider range of operating conditions.

In the optimization phase, the minimization of the Root Mean Square Error (RMSE) between the numerical and experimental data is obtained by adjusting the pressure dependency exponents in the model which influence the predicted cell voltages at different operating conditions. The objective function, which is defined to compute the RMSE, guided the optimization process using the experimental voltage values as a reference.

To optimize the exponents, a numerical optimization technique using the L-BFGS-B algorithm is employed, which is a well-suited method for problems with bound constraints as reported in the Appendix "Pressure Adaptation", namely in

module 1. This approach allowed for fine-tuning the exponents within a predefined range, ensuring realistic and physically plausible model adjustments. The specific details of the Python script used for this optimization, including the implementation of the objective function and the optimization routine, are detailed in the Appendix "Pressure Adaptation".

7.3 Optimization results

Following the optimization of the kinetic exponents as detailed in the Appendix "Pressure Adaptation", significant improvements are observed in the model's accuracy. The subsequent sections present both a qualitative and a quantitative analysis of these enhancements, highlighting the reduced discrepancies between the model and the experimental results.

As shown in Figures 25 and 26, the optimized model demonstrates a remarkable improvement in predicting the voltage across different operating conditions, which confirms the effectiveness of the parameter adjustments made in the optimization process.

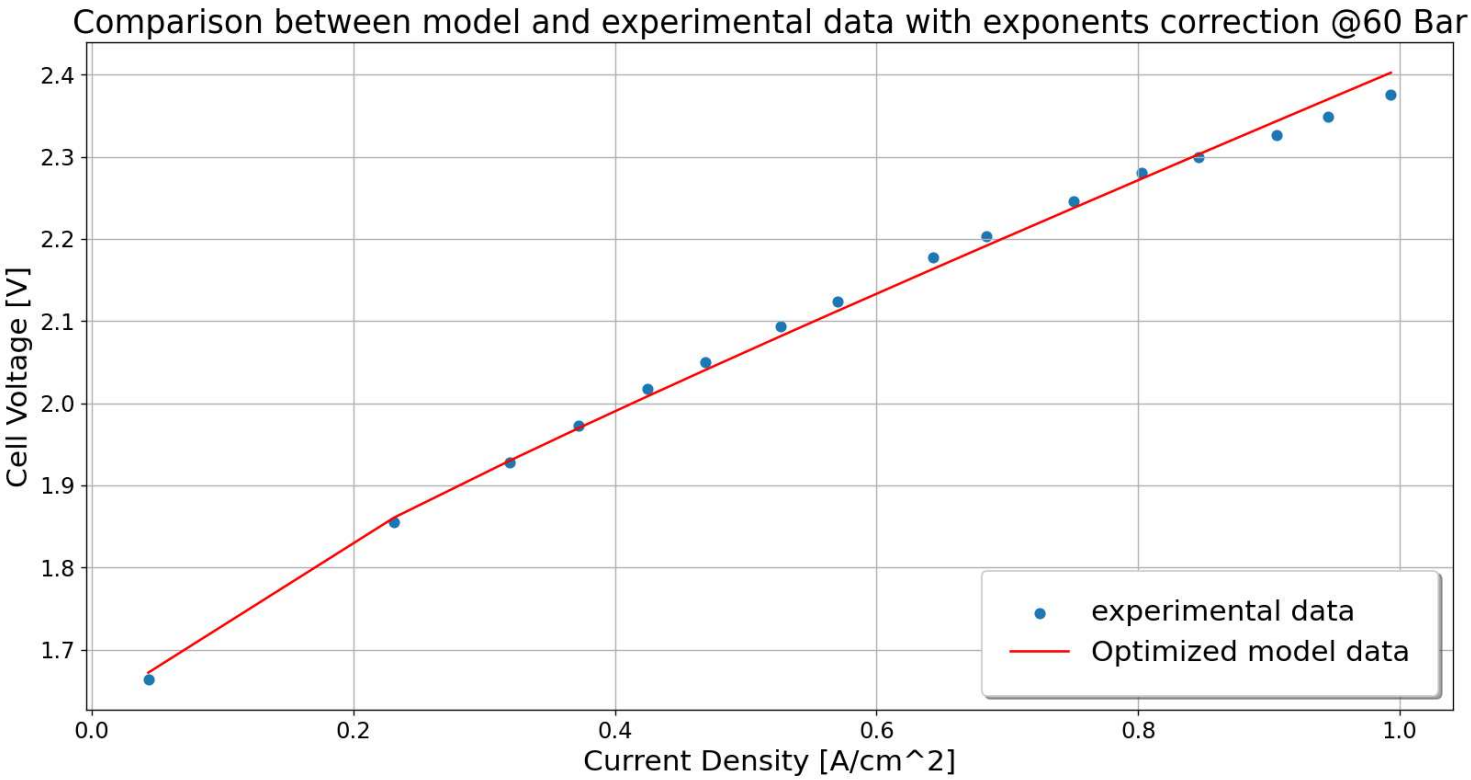

Figure 25: Comparison between the model and experimental polarization curve with exponents optimization @60bar and 40°C

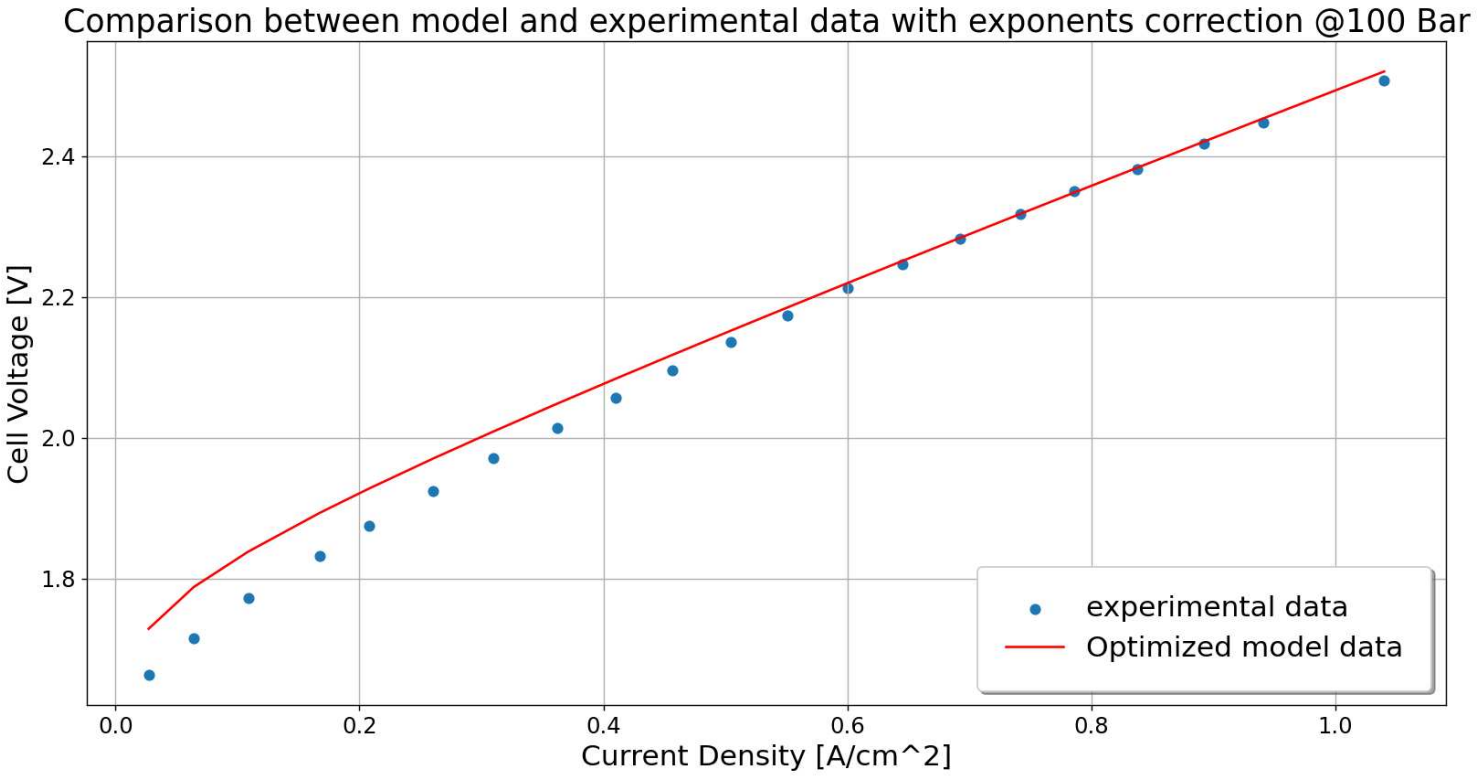

Figure 26: Comparison between the model and experimental polarization curve with exponents optimization @100bar and 40°C

Tables 10 and 11 report the effectiveness of optimizing the kinetic exponents in our model. By adjusting these exponents, the prediction capability of the model increased further. Tables compare the optimized model data against the experimental values, showing both the initial and optimized percentage errors. The remarkable reduction of the errors highlights the success of the optimization process in enhancing the model's accuracy.

Table 10: Comparison of model predictions and experimental data at 60 bar with respective relative percentage errors

Index	**Optimized model voltage (V)**	**Experimental voltage (V)**	**Relative error % (with optimization)**	**Relative error % (without optimization)**
1	1.672	1.663	0.52	2.51
2	1.861	1.855	0.32	2.40
3	1.930	1.928	0.10	2.51
4	1.970	1.973	0.17	2.73
5	2.008	2.017	0.43	2.93
6	2.041	2.050	0.48	2.94
7	2.082	2.093	0.55	2.96
8	2.112	2.124	0.54	2.91
9	2.163	2.177	0.62	2.94
10	2.192	2.203	0.53	2.82
11	2.237	2.245	0.34	2.59
12	2.273	2.280	0.32	2.53
13	2.303	2.299	0.18	2.02
14	2.343	2.327	0.71	1.46
15	2.370	2.349	0.89	1.26
16	2.402	2.376	1.12	1.00

Table 11: Comparison of model predictions and experimental data at 100 bar with respective relative percentage errors

Index	**Optimized model voltage (V)**	**Experimental voltage (V)**	**Relative error % (with optimization)**	**Relative error % (without optimization)**
1	1.729	1.663	3.95	4.59
2	1.788	1.716	4.23	4.05
3	1.839	1.772	3.74	4.28
4	1.894	1.833	3.33	4.42
5	1.928	1.875	2.81	4.76
6	1.971	1.925	2.39	5.00
7	2.009	1.971	1.95	5.26
8	2.048	2.014	1.70	5.35
9	2.084	2.056	1.35	5.56
10	2.118	2.096	1.01	5.77
11	2.152	2.136	0.76	5.89
12	2.185	2.174	0.53	6.01
13	2.220	2.213	0.30	6.12
14	2.251	2.247	0.18	6.14
15	2.284	2.283	0.03	6.20
16	2.318	2.317	0.02	6.11
17	2.348	2.350	0.07	6.12
18	2.383	2.382	0.05	5.91
19	2.421	2.418	0.11	5.77
20	2.454	2.447	0.26	5.54
21	2.520	2.508	0.50	5.17

By extending this technique to data at pressures of 20 and 40 bar, it is possible to obtain through the model the polarization curves at various pressures. With a small RMSE value for each curve, as listed in Table 12, the modelled curves fit the experimental data well as shown in Figure 27.

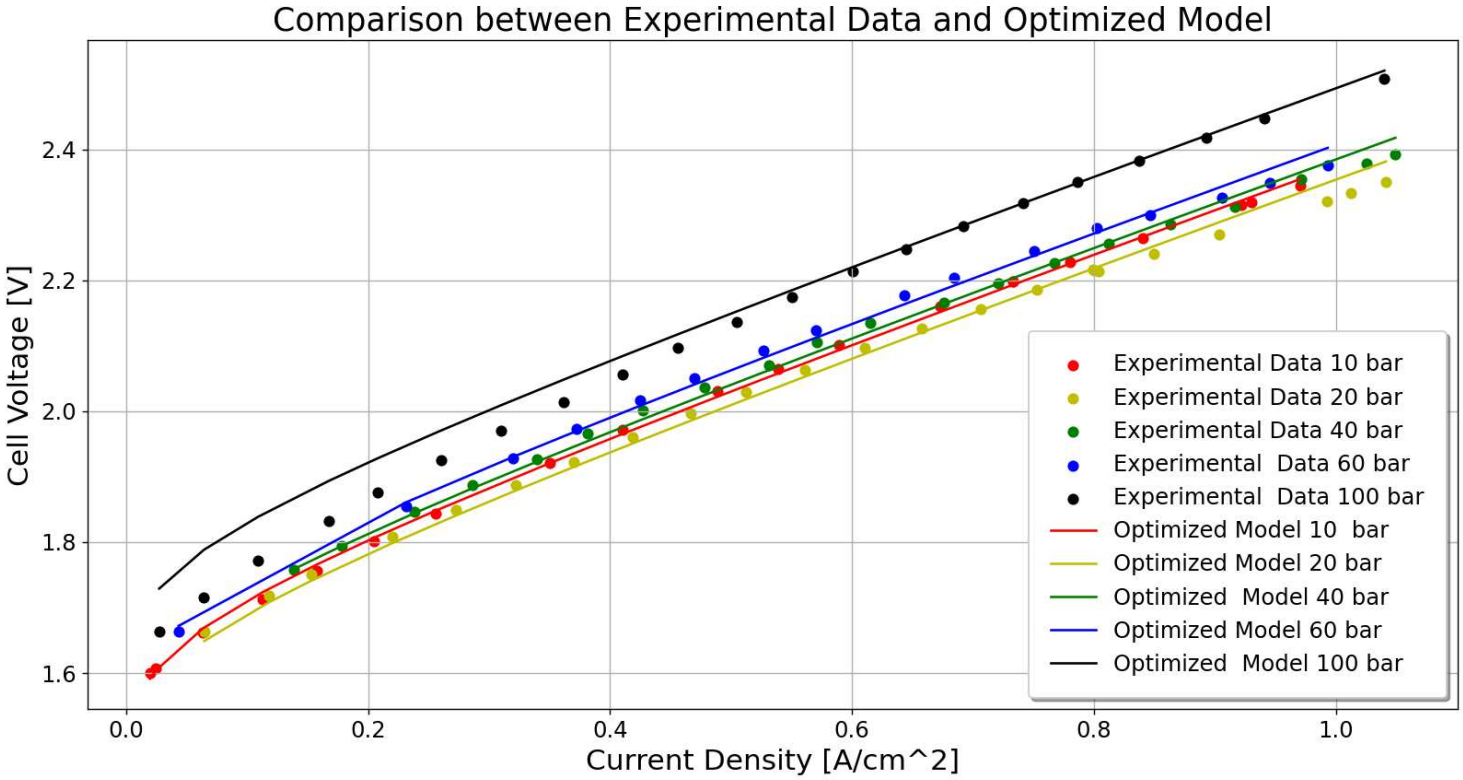

Figure 27: Comparison between the model and experimental polarization curve at different pressure values and 40°C

Table 12: RMSE values for different pressure levels used in experimental tests

Pressure	**RMSE**
10 bar	0.0069
20 bar	0.0139
40 bar	0.0113
60 bar	0.0123
100 bar	0.0359

Throughout the optimization process explained in this section, the kinetic exponents are adjusted to minimize the error between the numerical and experimental data. The results of this optimization provided valuable insights into how these exponents vary with increasing pressure levels. These data are crucial for enhancing the model's adaptability and precision across different operating conditions. To effectively illustrate these variations, Table 13 presents the optimized values of the exponents at different pressures. These findings are essential for documenting the model's behaviour under different conditions. A graphical representation is displayed in Figure 28.

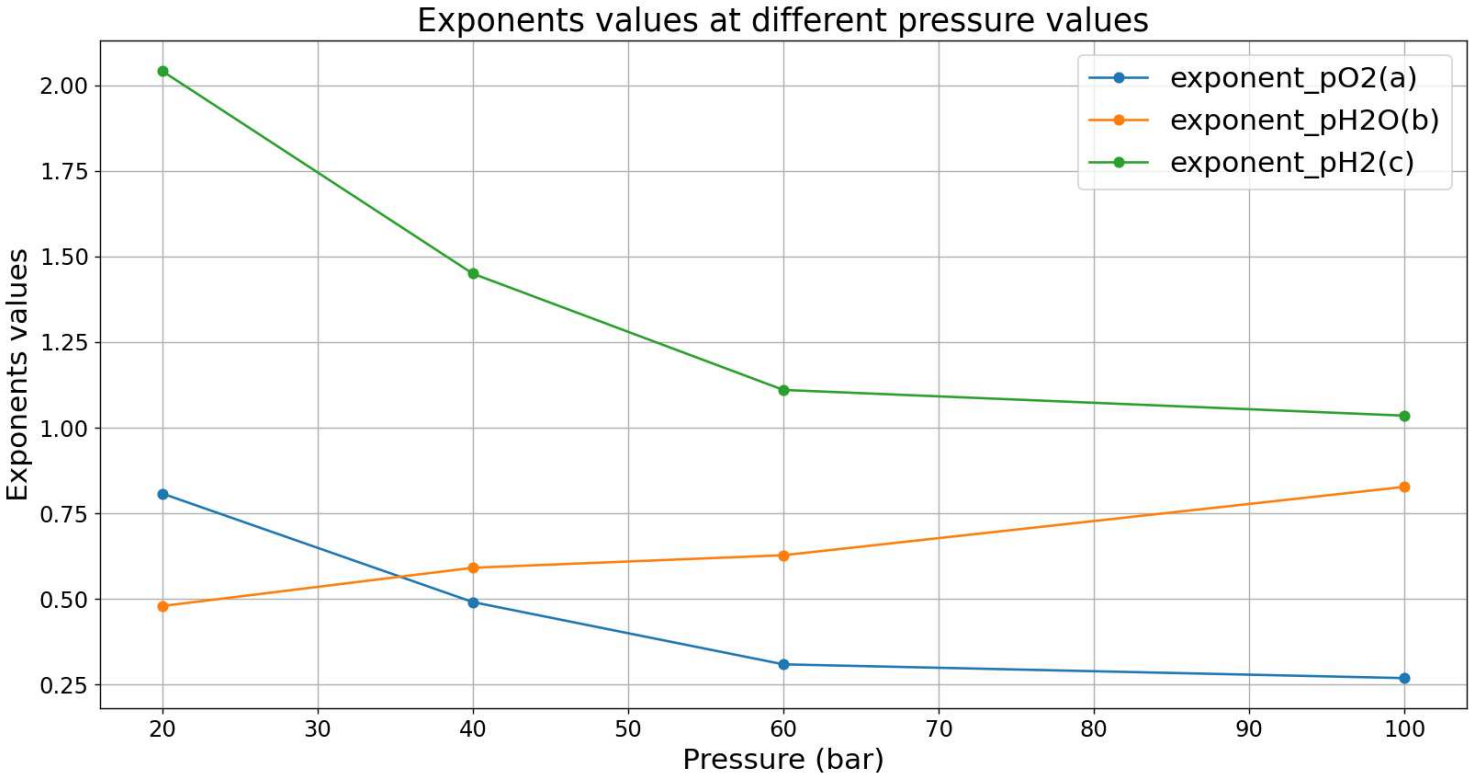

Figure 28: Optimized exponents at different pressures

Table 13: Optimized exponents values at different pressures

Pressure	**Exponent** a	**Exponent** b	**Exponent** c
20 bar	0.8079	0.4794	2.0417
40 bar	0.4910	0.5910	1.4499
60 bar	0.3091	0.6277	1.1103
100 bar	0.2689	0.8274	1.0352

The model's robustness and dependability have been demonstrated by the significant improvement in its ability to correctly predict the experimental data brought about by the optimization of kinetic exponents across different pressure levels. The model fits the tested conditions well, capturing the dynamics of the system at pressures up to 100 bar according to the results of these adjustments.

In the future, more experimental data at even higher pressures will be required to verify and further improve the model. More research will be essential to guarantee that the model can work dependably in harsher environments by increasing its applicability and practicality in real-world situations.

An electrolyzer's activation losses can be efficiently decreased by raising the pressure inside (see equations 15 and 16). This decrease is important because improved reaction kinetics and greater gas diffusion are made possible by increased pressure, which results in more effective operation. The activation energy needed for the electrochemical reactions drops with increasing pressure, which lowers overall energy losses. Because operating at greater pressures can considerably increase the efficiency of hydrogen production, this connection is essential for maximizing the performance of electrolyzers.

However, while the pressure rises, the exponents a and c decrease (see table 13): this brings to light a diminishing return on the benefits of increasing pressure. The initial increase in pressure has a substantial impact on reducing losses, but as the pressure continues to rise, the incremental benefit becomes smaller. This non-linear behavior suggests that the effectiveness of each subsequent increase in pressure diminishes progressively.

The analysis of losses in an electrolyzer, using a Python model with a fitting algorithm, further supports this observation. The results indicate that while higher pressure reduces activation losses, the decreasing exponents imply a progressively less significant impact on loss reduction with continued pressure increases.

This result is crucial for optimizing the efficiency of electrolyzers because it emphasizes the necessity of weighing the advantages of increased pressure against diminishing returns, potential expenses, and technical difficulties related to operating at extremely high pressures. By building more effective electrolyzer systems that can function well under a variety of pressures, the efficiency and viability of hydrogen generation technologies are eventually increased. This relationship is made easier by an understanding of this relationship. It is feasible to create a hydrogen generation process that is more economical and sustainable by carefully controlling operational pressures.

7.4 Variable temperature and fixed pressure

Following the analysis of variable pressure conditions, the mathematical model has also been applied to explore the behaviour of the PEM electrolyzer at variable temperatures while keeping the ambient pressure. This investigation focuses on how temperature fluctuations affect the electrochemical processes within the cell by providing interesting insights into the dynamics of hydrogen production.

By fixing the pressure at the atmospheric level, the effects of the temperature variations allow to get a detailed examination of their impacts on the efficiency and stability of the electrolytic process. The findings from this study are essential for assessing the temperature sensitivity of the cell, which is crucial for optimizing operational strategies.

Since alpha values are the only parameters that depend on the temperature, they are the main subject of this discussion as explained in Section 4. Following the findings of Bove et al. [53], which were previously discussed in Section 5, the proposed model has been modified by neglecting the reference current density correction. To achieve this, the pressure ratio exponents have been set equal to zero.

The kinetic parameters for this model setup are initially estimated through a fitting process using experimental data obtained at specific operating conditions, specifically at an ambient pressure of 1 bar and a temperature of $40C$. The parameter combination is executed to have the lowest RMSE as described in Section 7.1.

This method provides a solid foundation for the model's parameters as shown in Figure 29 and Table 14, thus facilitating the achievement of accurate simulations and predictions with new variable conditions.

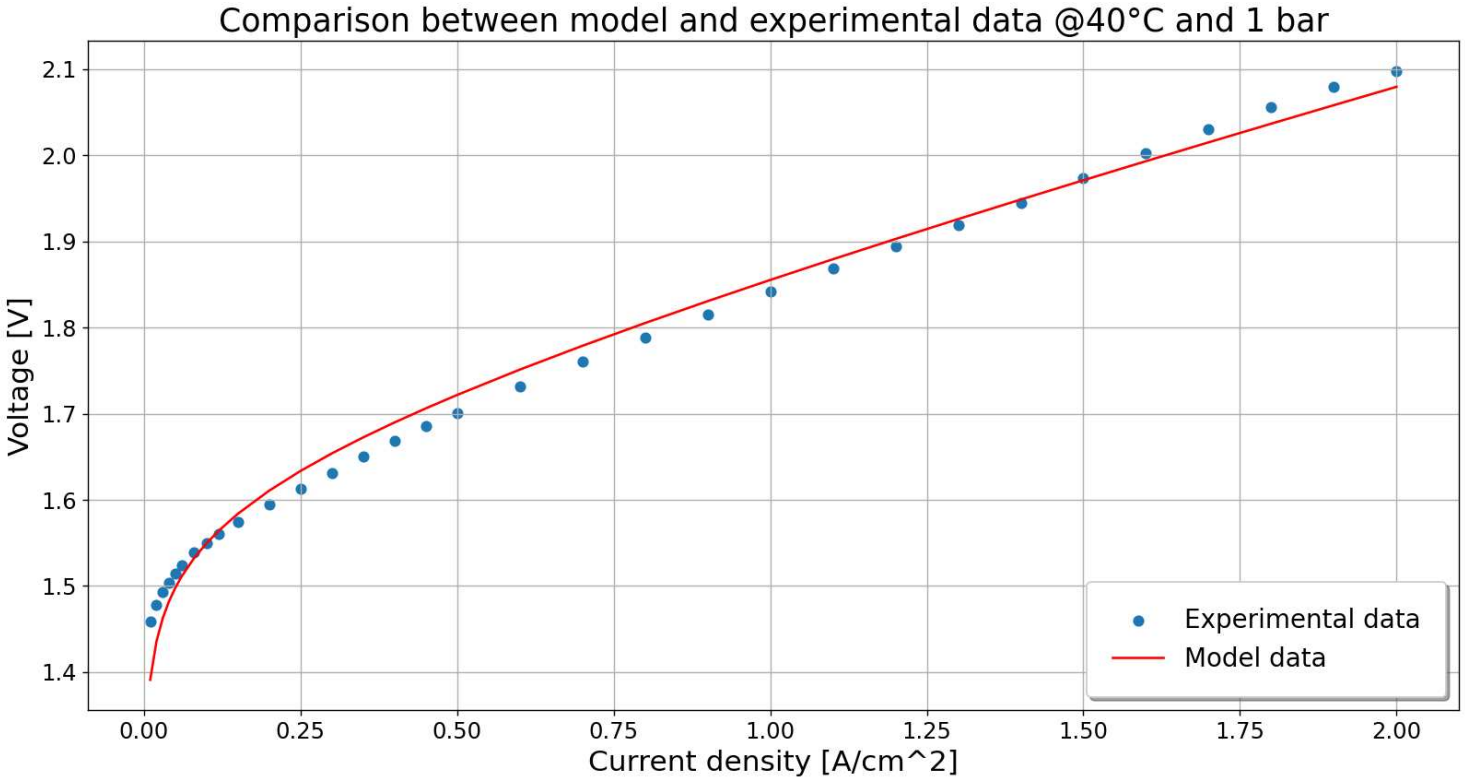

Figure 29: Model fitting @40°C and 1 bar

Table 14: Baseline kinetic parameters at 40°C and 1 bar

Parameter	**Value**
RMSE	0.0214
Alpha anode (α_{anode})	0.800
Alpha cathode (α_{cathode})	0.300
Reference anode exchange current ($i_{0,\text{ref,a}}$)	0.020
Reference cathode exchange current ($i_{0,\text{ref,c}}$)	0.225
Activation energy anode (E_{aa}) [J/mol]	38723.72
Activation energy cathode (E_{ac}) [J/mol]	4589.81
Protonic energy (E_{pro}) [J/mol]	3049.91
Reference conductivity (σ_{ref})	0.0070

7.5 Higher temperatures and optimization results

In the next phase of this study, while keeping all the parameters fixed except those related to alpha, the temperature is incrementally raised to 50°C, 60°C, and 70°C. This approach is fundamental to isolate the impact of temperature on the alpha coefficients, which play a critical role in the model's ability to accurately replicate the electrochemical processes under varying thermal conditions.

To align the model predictions more closely with the experimental data at higher temperatures, a curve fitting technique is used specifically focusing on optimizing the alpha values as reported in the Appendix "Temperature Adaptation" in module 1. This methodological choice is driven by the need to understand and quantify how these key parameters adapt to changes in temperature, ensuring that the model remains still robust and predictive across different scenarios.

Results of these optimizations are shown in the following figures, which depict the adjusted alpha values and their effectiveness in reducing the discrepancies between the model and experimental results. This enhanced model, with temperature-specific alpha values, provides a more accurate and reliable tool for predicting the performance of the PEM electrolyzer at different temperature conditions.

Figure 33 represent the variation of alpha with the temperature.

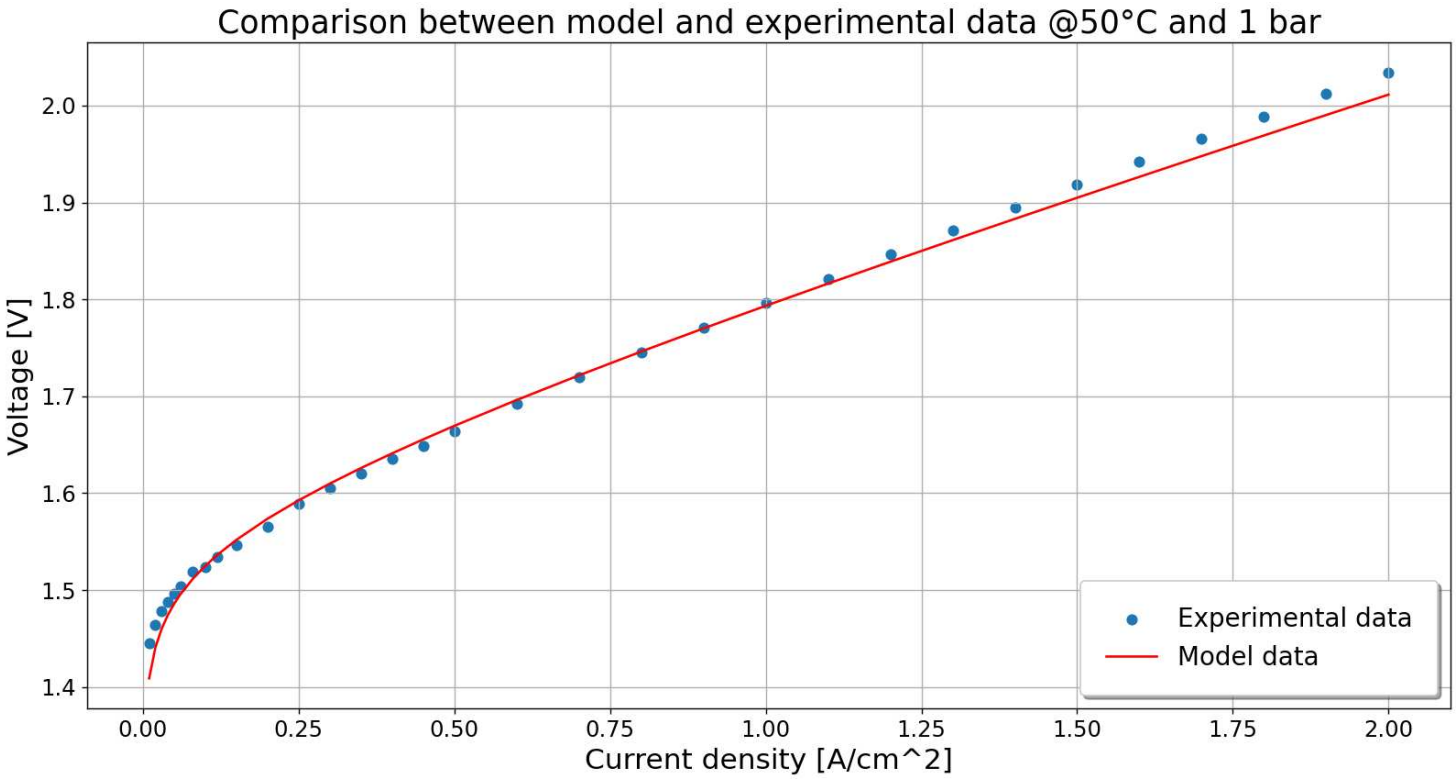

Figure 30: Comparison between the model and experimental polarization curve with alpha optimization @50°C and 1 bar

Table 15: RMSE and optimized alpha values at 50°C

Parameter	**Value**
RMSE	0.0129
Alpha anode (α_{anode})	0.800
Alpha cathode (α_{cathode})	0.543

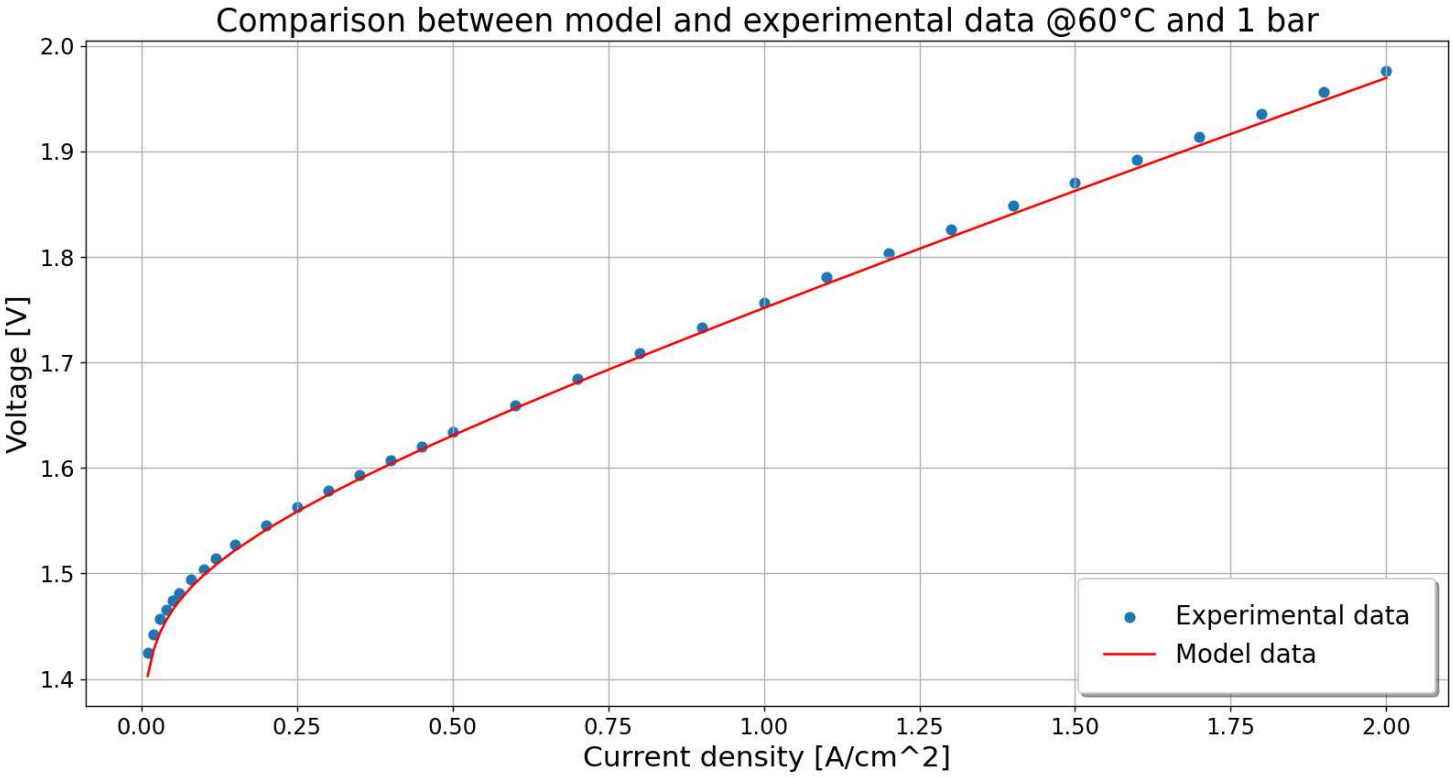

Figure 31: Comparison between the model and experimental polarization curve with alpha optimization @60°C and 1 bar

Table 16: RMSE and optimized alpha values at 60°C

Parameter	**Value**
RMSE	0.0079
Alpha anode (α_{anode})	0.800
Alpha cathode (α_{cathode})	0.900

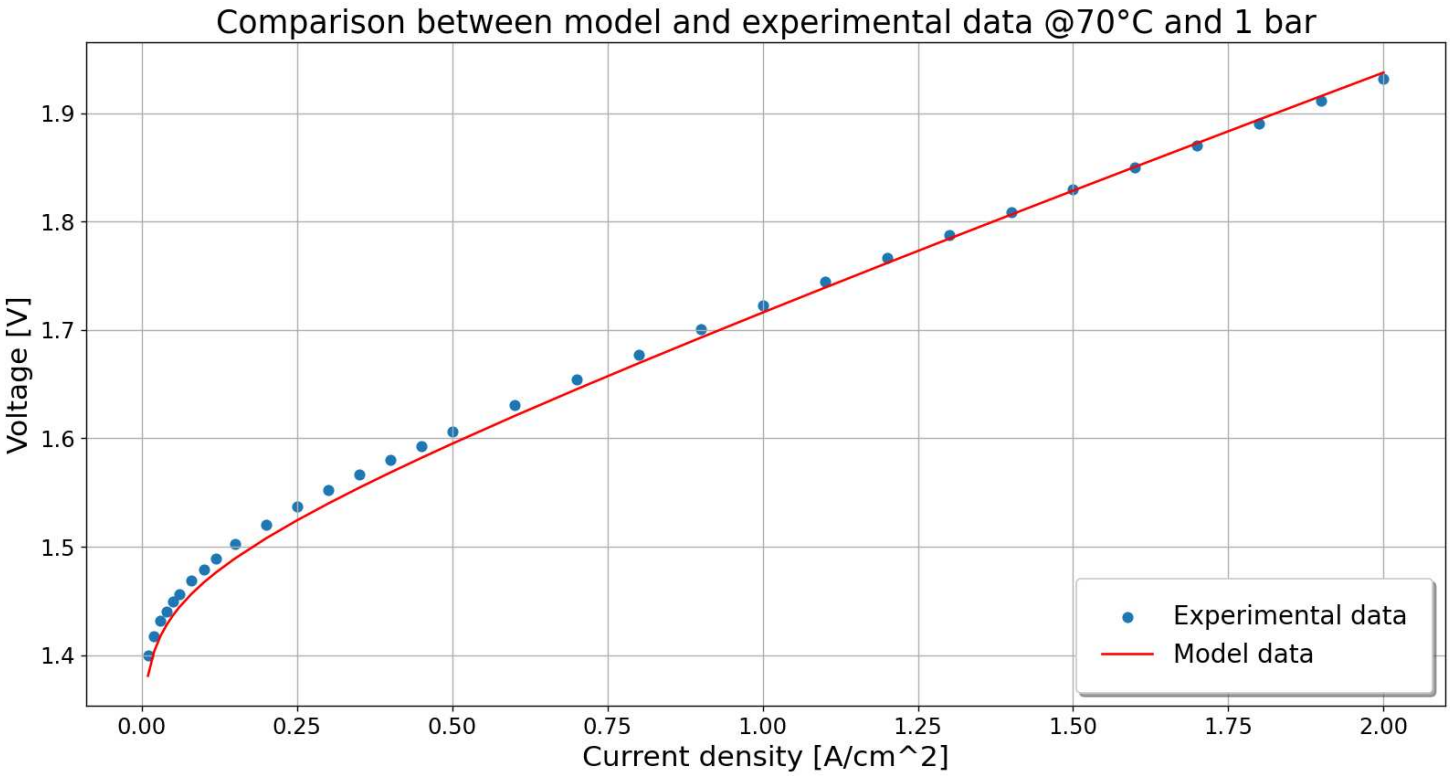

Figure 32: Comparison between the model and experimental polarization curves with alpha optimization @70°C and 1 bar

Table 17: RMSE and optimized alpha values at 70°C

Parameter	**Value**
RMSE	0.0103
Alpha anode (α_{anode})	1.000
Alpha cathode (α_{cathode})	1.000

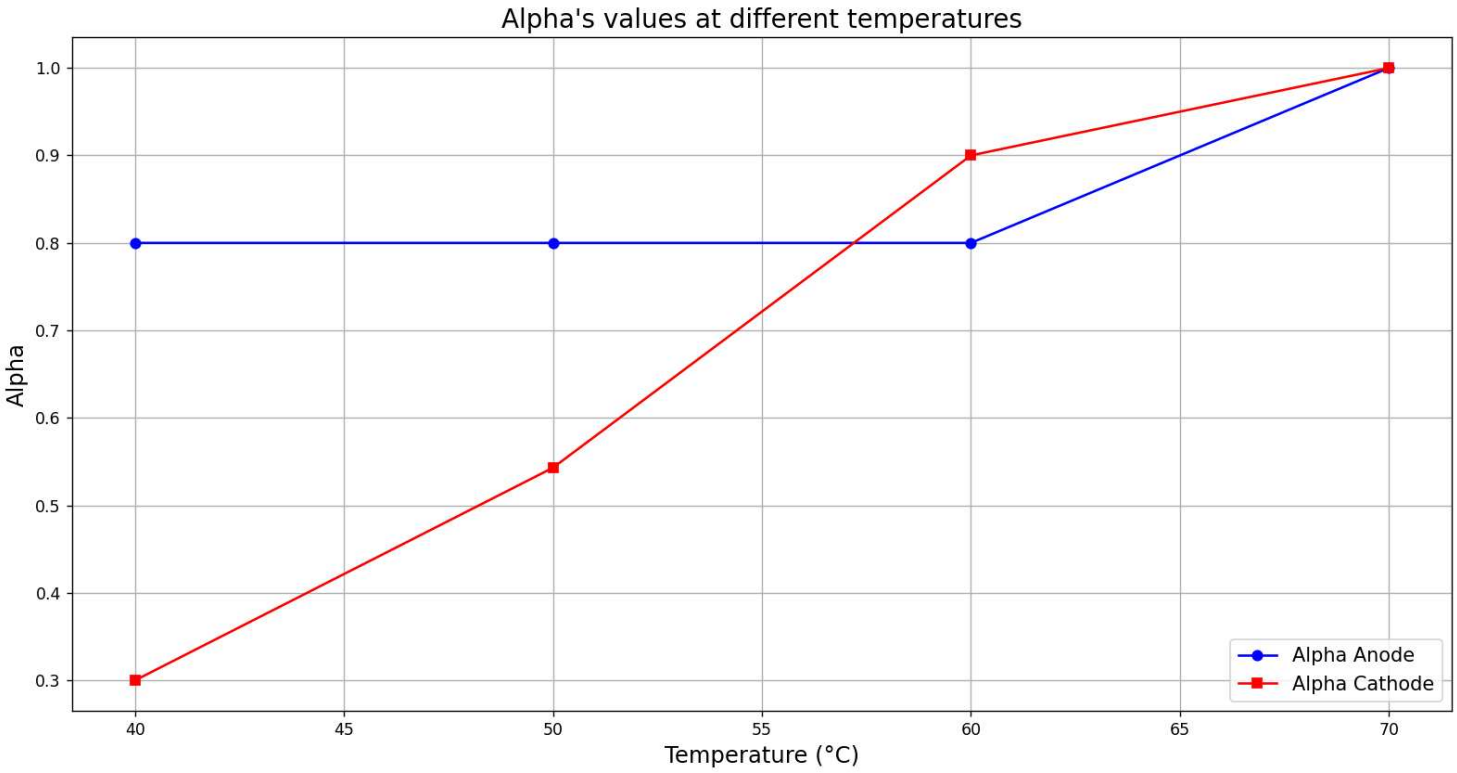

Figure 33: Alpha's values at different temperatures

Summing up, the developed model has demonstrated excellent agreement with the experimental data provided. The polarization curves at different temperatures, which are shown in Figure 34, clearly depict how well the optimized model fits the experimental data. This fitting procedure does not only validate the model's robustness but also its reliability in simulating the electrochemical processes of the electrolytic cell at different temperature conditions.

Working with this workflow has allowed to minimize the difference between the the model and experimental data by using empirically derived alpha values. Given the lack of specific scientific literature relations for the variation of alpha with temperature, such as the correlation presented in Section 4, the empirical approach is indispensable. By systematically adjusting the alpha values based on the fitting process, the model is effectively tailored to resemble the behaviour observed in experiments.

This methodology not only underscores the adaptability of the developed model to different operating conditions but also highlights the potential for further refinement and application in other similar systems where temperature plays a crucial role in system performance.

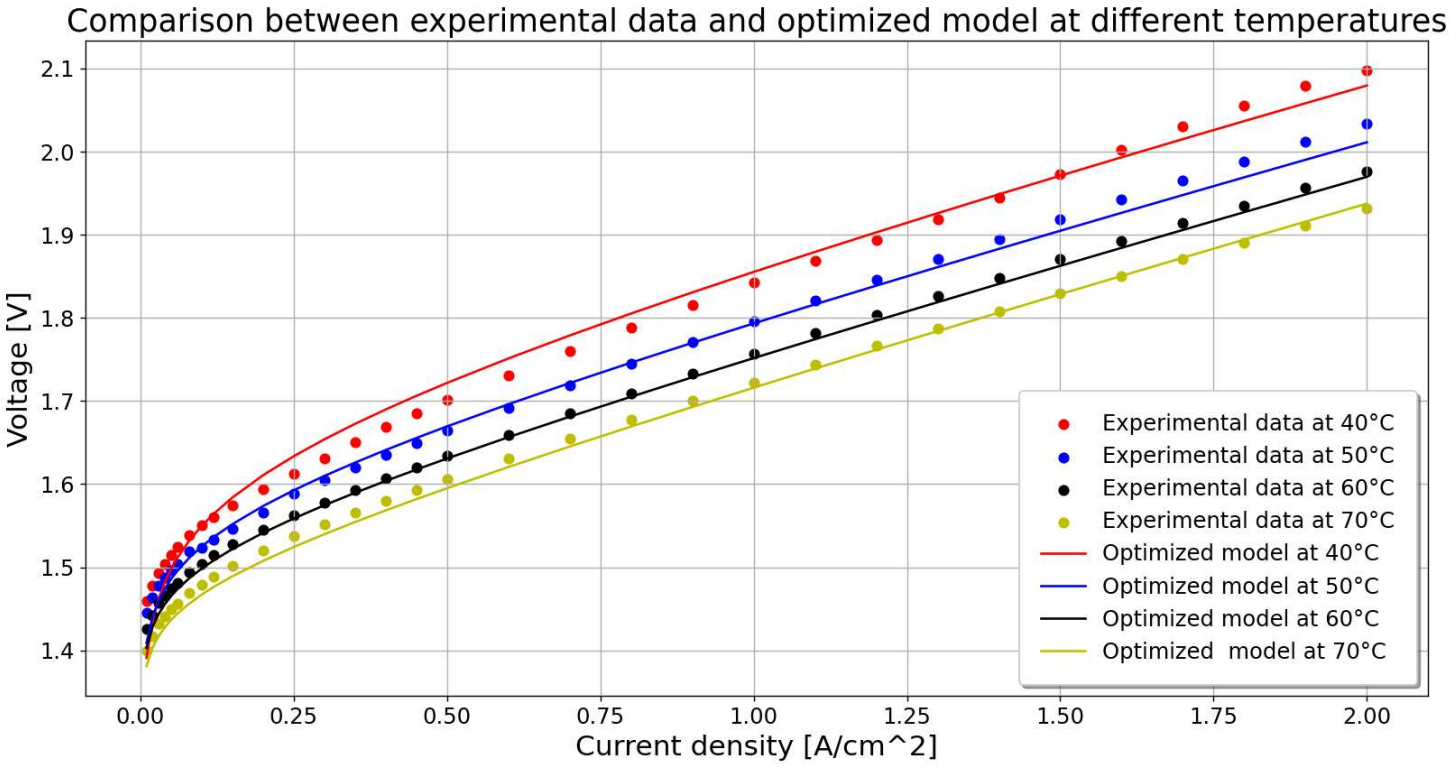

Figure 34: Comparison between the model and experimental polarization curve with alpha optimization

There are several reasons why the charge transfer coefficient values at the anode and cathode increase as the temperature rises (see Tables 15, 16 and 17). First of all, the higher temperature promotes ion mobility in the electrolyte material of the PEM cell, allowing for quicker ion transport to the electrodes.
Consequently, this quickens the pace at which charges are transferred across the electrode/electrolyte contact, raising the charge transfer coefficient. Higher temperatures also encourage quicker electrode reactions, which speed up the exchange of electrons between the electrode and electrolyte ions.

Moreover, better electrical contact is fostered by improved electrode/electrolyte interface conformation at higher temperatures, which allows for increased ion transfer rates and, in turn, raises the charge transfer coefficient. This phenomenon is consistent with observations made in the literature. In different publications, such as in Niroula et al. [57], a positively associated linear relationship has been established between temperature and charge transfer coefficient (see figure 33).

While creating an accurate quantitative relationship between charge transfer coefficient and temperature proves problematic for the model, the continual increase in these values highlights the role of temperature in impacting cell performance. Based on the experimental data collected, further analysis can disclose an exact relationship customized for the particular cell being studied.

Conclusions

Reducing greenhouse gas emissions to combat climate change and achieve sustainability is an important challenge. This entails switching to cleaner technologies and renewable energy sources instead of fossil fuels. In this shift, green hydrogen—which is created with renewable energy sources like solar and wind—is essential.

The use of green hydrogen has the potential to greatly lower the carbon footprint of industries like heavy industry and long-distance transportation that are difficult to electrify. It also ensures a steady supply by acting as a storage medium for excess renewable energy. Achieving a carbon-neutral economy and a sustainable future requires green hydrogen.

This study reports the insights of a numerical model developed in Python to resemble the performance of a PEM electrolyzer operating at different operating conditions in terms of both pressure and temperature. The model has been thoroughly validated with experimental data provided by Westfälische Hochschule (Section 6), showing excellent agreement and thereby proving its accuracy and reliability in simulating real-world operational scenarios (see Figures 27 and 34).

The flexibility of the developed model under investigation allows for a potential extension to higher pressures operation (see Section 7.1) and temperatures (see Section 7.4) beyond those specifically analyzed within this work. Such an extension remains feasible within reasonable proximity to the conditions already examined, suggesting that the model can be effectively scaled up to meet more demanding operational settings.

Furthermore, the benefits of letting electrolyzers operate at a pressure higher than the atmospheric one and high temperatures are considerable. Indeed, higher temperatures can lead to a reduction in electrical consumption, primarily due to the lowering of the OCV (see Eq. 14). Similarly, high pressure operation can drastically lower the system's overall energy consumption by possibly eliminating, or significantly reducing, the need for a subsequent hydrogen compression stage, although it is difficult to predict in advance whether the electrolyzer's energy consumption will increase as a result of an increase in the OCV (see Eq. 13) or decrease as a result of a decrease in activation losses (see Eqs. 15 and 16).

Generally, the need for external hydrogen compression can be reduced or deleted in low pressure applications like methane blending by incorporating such conditions into the system design. This increases also the efficiency and the financial sustainability of hydrogen production technologies in applications that require high pressures like hydrogen fuel for cars and trucks with 700 and 350 bar, respectively [65].

In conclusion, the results of this work not only demonstrate the effectiveness of the developed model but also highlight its applicability for future enhancements

and broader implementation. The gained insights lay a solid foundation for ongoing advancements in the field of electrolytic hydrogen production, steering towards more sustainable and efficient energy solutions.

Appendix

Pressure adaptation

Module 1:

```
    """Pressure adaptation model"""

import numpy as np
from scipy.optimize import curve_fit
import pandas as pd
import matplotlib.pyplot as plt
from exponents_optimization import optimize_exponents
from v_prediction_pressure import V_predicted_pressure


#data import:

df = pd.read_csv('pressure_data/ui_10_norm.csv', sep='\s+',\
                  header=None).iloc[::3, :]
x_10 = df[1].iloc[::-1].reset_index(drop=True).loc[1:]  \
    # Current density
x_10 = pd.to_numeric(x_10)
y = df[0].iloc[::-1].reset_index(drop=True).loc[1:]   \
    # Voltage
y = pd.to_numeric(y)
temperature = 50
pressure = 10


def fo(x, alphaanode, alphacathode, i0refa, i0refc, Eaa,\
 Eac, Epro, sigmaref, exponent_pO2, exponent_pH2O, exponent_pH2):
    # Constants
    R = 8.314  # Gas constant (J/mol*K)
    F = 96485  # Faraday constant (C/mol)
    n = 2  # Number of electrons involved in the \
    #electrochemical reaction

    # Temperature and pressure conversion
    T = temperature + 273.15  # Cell temperature (K)
    Pa = pressure * 100000  # Pressure on the anode side (Pa)
    Pc = pressure * 100000  # Pressure on the cathode side (Pa)
    TH2O = temperature  # Water temperature

    deltha = 0.00127  # Nafion 115 membrane thickness (cm)
    Tref = T  # Reference temperature
    Pref = pressure * 100000  # Reference pressure
```

```
    # Antoine equation for water pressure
    Aant = 5.20389
    Bant = 1733.926
    Cant = 39.485
    pH2O = (np.exp(Aant - (Bant / (TH2O + Cant)))) * 1000

    # Partial pressures
    pO2 = Pa - pH2O  # Partial pressure of oxygen (Pa)
    pH2 = Pc - pH2O  # Partial pressure of hydrogen (Pa)

    # Open circuit voltage (OCV)
    Erev = 1.229 - (0.9 * 10**-3 * (T - 298))
    # Reversible potential (V)
    E = Erev + ((R * T) / (n * F)) * (np.log((pH2 * \
                            (pO2**0.5)) / pH2O))

    # Overpotentials
    anode_overpotential = ((R * T) / (n * F * alphaanode)) \
    * np.log(x / (i0refa *((pO2 / Pref)**exponent_pO2) * \
    ((pH2O / Pref)**exponent_pH2O)* np.exp((-Eaa / R) * \
    ((1 / T) - (1 / Tref)))))
    cathode_overpotential = ((R * T) / (n * F * alphacathode))\
 * np.log(x / (i0refc* ((pH2 / Pref)**exponent_pH2) * np.exp\
        ((-Eac / R) * ((1 / T) - (1 / Tref)))))
    ohmic_loss = (deltha / (sigmaref * np.exp((-Epro / R) * \
                    ((1 / Tref) - (1 / T))))) * x

    return E + anode_overpotential + cathode_overpotential + \
    ohmic_loss


initial_guess = [0.8,0.23,0.006058, 0.006058, 1000,1000,100,\
                  0.0075,0.25, 1, 1]
param_bounds=([0,0,0,0,1000,1000,100,0,0.25,0.25,0.25],[1,1,\
            10**0,10**0,150000,150000,20000,0.02,4,4,4])
# alphaanode,alphacathode,i0refa, i0refc, Eaa,Eac,Epro,
#sigmaref,exponent_pO2,exponent_pH2O,exponent_pH2

#curve fitting:

popt, pcov = curve_fit(fo, x_10, y,p0=initial_guess,\
                    bounds=param_bounds)
```

```
y_pred = fo(x_10, *popt)
V_10 = V_predicted_pressure(x_10,temperature,temperature,\
pressure,pressure,popt[0],popt[1],popt[2],popt[3],popt[4],\
popt[5],popt[6],popt[7],popt[8],popt[9],popt[10])
percentual_error = abs((y-y_pred)/y)*100



rmse_10 = np.sqrt(np.mean((y - V_10)**2))

plt.figure(figsize=(10, 6))
plt.scatter(x_10, y, label='experimental data')
plt.plot(x_10, V_10, color='red', label='Model data')
plt.title('Comparison between model and experimental data \
          @10 Bar')
plt.xlabel('Current Density [A/cm^2]')
plt.ylabel('Cell Voltage [V]')
plt.grid(True)

legend_text = f'RMSE: {rmse_10:.4f}\n' \
             f'alphaanode: {popt[0]:.3f}\n' \
             f'alphacatode: {popt[1]:.3f}\n' \
             f'i0refa: {popt[2]:.3f}\n' \
             f'i0refc: {popt[3]:.3f}\n' \
             f'Eaa: {popt[4]:.2f}\n' \
             f'Eac: {popt[5]:.2f}\n' \
             f'Epro: {popt[6]:.2f}\n' \
             f'sigmaref: {popt[7]:.4f}\n'\
             f'exponent_pO2: {popt[8]:.2f}\n'\
             f'exponent_pH2O: {popt[9]:.2f}\n'\
             f'exponent_pH2: {popt[10]:.2f}'

plt.legend(loc='lower right', frameon=True, framealpha=1, \
           shadow=True, borderpad=1)
plt.show()

print(legend_text)



# Experimental data 60 Bar:

df_60 = pd.read_csv('pressure_data/ui_60_norm.csv',\
                sep='\s+', header=None).iloc[::3, :]
x_60 = df_60[1].iloc[::-1].reset_index(drop=True)
```

```
x_60= pd.to_numeric(x_60)
y_60 = df_60[0].iloc[::-1].reset_index(drop=True)
y_60 = pd.to_numeric(y_60)

V_60 = V_predicted_pressure(x_60,temperature,temperature,\
pressure,60,popt[0],popt[1],popt[2],popt[3],popt[4],popt[5],\
popt[6],popt[7],popt[8],popt[9],popt[10])

percentual_error_60 = abs((y_60-V_60)/y_60)*100


rmse_60 = np.sqrt(np.mean((y_60 - V_60)**2))

plt.figure(figsize=(10, 6))
plt.scatter(x_60, y_60, label='experimental data')
plt.plot(x_60, V_60, color='red', label='Model data')
plt.title('Comparison between model and experimental data \
          @60 Bar')
plt.xlabel('Current Density [A/cm^2]')
plt.ylabel('Cell Voltage [V]')
plt.grid(True)

legend_text = f'RMSE: {rmse_60:.4f}\n' \
            f'alphaanode: {popt[0]:.3f}\n' \
            f'alphacatode: {popt[1]:.3f}\n' \
            f'i0refa: {popt[2]:.3f}\n' \
            f'i0refc: {popt[3]:.3f}\n' \
            f'Eaa: {popt[4]:.2f}\n' \
            f'Eac: {popt[5]:.2f}\n' \
            f'Epro: {popt[6]:.2f}\n' \
            f'sigmaref: {popt[7]:.4f}\n'\
            f'exponent_pO2: {popt[8]:.2f}\n'\
            f'exponent_pH2O: {popt[9]:.2f}\n'\
            f'exponent_pH2: {popt[10]:.2f}'

plt.legend(loc='lower right', frameon=True, framealpha=1,\
            shadow=True, borderpad=1)
plt.show()




# Experimental data 100 Bar

df_100 = pd.read_csv('pressure_data/ui_100_norm.csv',\
                sep='\s+', header=None).iloc[::3, :]
```

```
x_100 = df_100[0].iloc[::-1].reset_index(drop=True)
x_100= pd.to_numeric(x_100).iloc[1:]
y_100 = df_100[1].iloc[::-1].reset_index(drop=True)
y_100 = pd.to_numeric(y_100).iloc[1:]

V_100 = V_predicted_pressure(x_100,temperature,temperature,\
pressure,100,popt[0],popt[1],popt[2],popt[3],popt[4],popt[5],\
popt[6],popt[7],popt[8],popt[9],popt[10])

percentual_error_100 = abs((y_100-V_100)/y_100)*100

rmse_100 = np.sqrt(np.mean((y_100 - V_100)**2))

plt.figure(figsize=(10, 6))
plt.scatter(x_100, y_100, label='experimental data')
plt.plot(x_100, V_100, color='red', label='Model data')
plt.title('Comparison between model and experimental data\
          @100 Bar')
plt.xlabel('Current Density [A/cm^2]')
plt.ylabel('Cell Voltage [V]')
plt.grid(True)

legend_text = f'RMSE: {rmse_100:.4f}\n' \
            f'alphaanode: {popt[0]:.3f}\n' \
            f'alphacatode: {popt[1]:.3f}\n' \
            f'i0refa: {popt[2]:.3f}\n' \
            f'i0refc: {popt[3]:.3f}\n' \
            f'Eaa: {popt[4]:.2f}\n' \
            f'Eac: {popt[5]:.2f}\n' \
            f'Epro: {popt[6]:.2f}\n' \
            f'sigmaref: {popt[7]:.4f}\n'\
            f'exponent_pO2: {popt[8]:.2f}\n'\
            f'exponent_pH2O: {popt[9]:.2f}\n'\
            f'exponent_pH2: {popt[10]:.2f}'

plt.legend(loc='lower right', frameon=True, framealpha=1,\
            shadow=True, borderpad=1)
plt.show()




# Experimental data 20 and 40 Bar:

df_20 = pd.read_csv('pressure_data/ui_20_norm.csv',\
```

```
            sep='\s+', header=None).iloc[::3, :]
x_20 = df_20[1].iloc[::-1].reset_index(drop=True)
x_20= pd.to_numeric(x_20).iloc[1:]
y_20 = df_20[0].iloc[::-1].reset_index(drop=True)
y_20 = pd.to_numeric(y_20).iloc[1:]

df_40 = pd.read_csv('pressure_data/ui_40_norm.csv',\
        sep='\s+', header=None).iloc[::3, :]
x_40 = df_40[1].iloc[::-1].reset_index(drop=True)
x_40= pd.to_numeric(x_40).iloc[1:]
y_40 = df_40[0].iloc[::-1].reset_index(drop=True)
y_40 = pd.to_numeric(y_40).iloc[1:]


# exponents optimization:

exponents_20 = optimize_exponents(x_20,y_20,temperature,\
temperature,pressure,20,popt[0],popt[1],popt[2],popt[3],\
popt[4],popt[5],popt[6],popt[7])
V_20_optimized = V_predicted_pressure(x_20,temperature,\
temperature,pressure,20,popt[0],popt[1],popt[2],popt[3],\
popt[4],popt[5],popt[6],popt[7],exponents_20[0],exponents_20[1],\
exponents_20[2])

exponents_40 = optimize_exponents(x_40,y_40,temperature,\
temperature,pressure,40,popt[0],popt[1],popt[2],popt[3],\
popt[4],popt[5],popt[6],popt[7])
V_40_optimized = V_predicted_pressure(x_40,temperature,\
temperature,pressure,40,popt[0],popt[1],popt[2],popt[3],\
popt[4],popt[5],popt[6],popt[7],exponents_40[0],exponents_40[1],\
exponents_40[2])

exponents_60 = optimize_exponents(x_60,y_60,temperature,\
temperature,pressure,60,popt[0],popt[1],popt[2],popt[3],\
popt[4],popt[5],popt[6],popt[7])
V_60_optimized = V_predicted_pressure(x_60,temperature,\
temperature,pressure,60,popt[0],popt[1],popt[2],popt[3],\
popt[4],popt[5],popt[6],popt[7],exponents_60[0],exponents_60[1],\
exponents_60[2])


exponents_100 = optimize_exponents(x_100,y_100,temperature,\
temperature,pressure,100,popt[0],popt[1],popt[2],popt[3],\
popt[4],popt[5],popt[6],popt[7])
V_100_optimized = V_predicted_pressure(x_100,temperature,\
temperature,pressure,10,popt[0],popt[1],popt[2],popt[3],popt[4],\
```

```
popt[5],popt[6],popt[7],exponents_100[0],exponents_100[1],\
exponents_100[2])


differenze = V_100_optimized-y_100
differenza_massima = differenze.abs().max()
indice_max = differenze.abs().idxmax()
valore_y_100 = y_100[indice_max]
differenza_percentuale = (differenza_massima / valore_y_100) * 100


rmse_60_optimized = np.sqrt(np.mean((y_60 - V_60_optimized)**2))

plt.figure(figsize=(10, 6))
plt.scatter(x_60, y_60, label='experimental data')
plt.plot(x_60, V_60_optimized, color='red', label='Optimized\
         model data')
plt.title('Comparison between model and experimental data \
    with exponents correction @60 Bar')
plt.xlabel('Current Density [A/cm^2]')
plt.ylabel('Cell Voltage [V]')
plt.grid(True)

legend_text = f'RMSE: {rmse_60_optimized:.4f}\n' \
            f'exponent_pO2: {exponents_60[0]:.2f}\n'\
            f'exponent_pH2O: {exponents_60[1]:.2f}\n'\
            f'exponent_pH2: {exponents_60[2]:.2f}'

plt.plot([], [], ' ', label=legend_text)
plt.legend(loc='lower right', frameon=True, framealpha=1, \
        shadow=True, borderpad=1)
plt.show()


rmse_100_optimized = np.sqrt(np.mean((y_100 - V_100_optimized)**2))

plt.figure(figsize=(10, 6))
plt.scatter(x_100, y_100, label='experimental data')
plt.plot(x_100, V_100_optimized, color='red', label='Optimized\
          model data')
plt.title('Comparison between model and experimental data with\
           exponents correction @100 Bar')
plt.xlabel('Current Density [A/cm^2]')
plt.ylabel('Cell Voltage [V]')
plt.grid(True)
```

```
legend_text = f'RMSE: {rmse_100_optimized:.4f}\n' \
            f'exponent_pO2: {exponents_100[0]:.2f}\n'\
            f'exponent_pH2O: {exponents_100[1]:.2f}\n'\
            f'exponent_pH2: {exponents_100[2]:.2f}'

plt.plot([], [], ' ', label=legend_text)
plt.legend(loc='lower right', frameon=True, framealpha=1, \
           shadow=True, borderpad=1)
plt.show()


percentual_error_60_optimized = abs((y_60-V_60_optimized)\
                                    /y_60)*100

percentual_error_100_optimized = abs((y_100-V_100_optimized)\
                                     /y_100)*100

print(f"Maximum different between data and model: \
      {differenza_massima:.3f} [V] ({differenza_percentuale:.1f}%)")

rmse_10 = np.sqrt(np.mean((y - V_10)**2))
rmse_20 = np.sqrt(np.mean((y_20 - V_20_optimized)**2))
rmse_40 = np.sqrt(np.mean((y_40 - V_40_optimized)**2))
rmse_60 = np.sqrt(np.mean((y_60 - V_60_optimized)**2))
rmse_100 = np.sqrt(np.mean((y_100 - V_100_optimized)**2))

plt.figure(figsize=(10, 6))
plt.scatter(x_10, y, color='red', label='Experimental Data \
            10 bar')
plt.scatter(x_20, y_20, color='y', label='Experimental Data \
            20 bar')
plt.scatter(x_40, y_40, color='green', label='Experimental\
             Data 40 bar')
plt.scatter(x_60, y_60, color='b', label='Experimental\
             Data 60 bar')
plt.scatter(x_100, y_100, color='black', label='Experimental\
             Data 100 bar')
plt.plot(x_10, V_10, color='red', label='Optimized Model 10\
          bar')
plt.plot(x_20, V_20_optimized, color='y', label='Optimized \
         Model 20 bar')
plt.plot(x_40, V_40_optimized, color='green', label='Optimized\
          Model 40 bar')
plt.plot(x_60, V_60_optimized, color='b', label='Optimized \
         Model 60 bar')
plt.plot(x_100, V_100_optimized, color='black', label='Optimized\
```

```
          Model 100 bar')
plt.title('Comparison between Experimental Data and \
          Optimized Model')
plt.xlabel('Current Density [A/cm^2]')
plt.ylabel('Cell Voltage [V]')
plt.grid(True)
legend_text = f'RMSE 10 bar: {rmse_10:.4f}\n' \
            f'RMSE 20 bar: {rmse_20:.4f}\n' \
            f'RMSE 40 bar: {rmse_40:.4f}\n' \
            f'RMSE 60 bar: {rmse_60:.4f}\n' \
            f'RMSE 100 bar: {rmse_100:.4f}'

plt.legend(loc='lower right', frameon=True, framealpha=1,\
            shadow=True, borderpad=1)
plt.show()

print(legend_text)

pressures = [20,40, 60, 100]

exponents_at_10 = [popt[8],popt[9],popt[10]]
exponents_at_20 = [exponents_20[0],exponents_20[1],\
                   exponents_20[2]]
exponents_at_40 = [exponents_40[0],exponents_40[1],\
                   exponents_40[2]]
exponents_at_60 = [exponents_60[0],exponents_60[1],\
                   exponents_60[2]]
exponents_at_100 = [exponents_100[0],exponents_100[1],\
                    exponents_100[2]]


exponents = np.array([
    [exponents_at_20[0], exponents_at_20[1],\
      exponents_at_20[2]],
    [exponents_at_40[0], exponents_at_40[1], \
     exponents_at_40[2]],
    [exponents_at_60[0], exponents_at_60[1],\
      exponents_at_60[2]],
    [exponents_at_100[0], exponents_at_100[1],\
      exponents_at_100[2]]
])

labels = ['exponent_pO2(a)', 'exponent_pH2O(b)', \
          'exponent_pH2(c)']

plt.figure(figsize=(10, 6))
```

```
for i in range(len(labels)):
    plt.plot(pressures, exponents[:, i], \
             label=labels[i], marker='o')

plt.title('Exponents values at different pressure values')
plt.xlabel('Pressure (bar)')
plt.ylabel('Exponents values')
plt.legend()
plt.grid(True)
plt.show()
```

Module 2:

```
    """exponents optimization script"""

import numpy as np
from scipy.optimize import minimize
from v_prediction_pressure import V_predicted_pressure

def optimize_exponents(currents, voltages, T_ref, \
temperature, P_ref, pressure,alphaanode, alphacathode,\
 i0refa, i0refc, Eaa, Eac, Epro, sigmaref):
    def objective_function(exponents):
        exponent_pO2, exponent_pH2O, exponent_pH2 = exponents
        predicted_voltages = []
        for current in currents:
            voltage = V_predicted_pressure(current, T_ref,\
 temperature, P_ref, pressure,alphaanode, alphacathode, i0refa,\
 i0refc, Eaa, Eac, Epro, sigmaref, exponent_pO2, exponent_pH2O, \
exponent_pH2)
            predicted_voltages.append(voltage)
        rmse = np.sqrt(np.mean((predicted_voltages - voltages)\
                               **2))

        return rmse

    initial_exponents = [0.25, 1, 1]
    result = minimize(objective_function, initial_exponents,\
 method='L-BFGS-B', bounds=[(0.25, 4), (0.25, 4), (0.25, 4)])
    return result.x
```

Module 3:

```
    """Calculation of polarization curve given\
kinetics parameters"""
import numpy as np

def V_predicted_pressure(x, T_ref, temperature,\
 P_ref, pressure, alphaanode, alphacathode, i0refa,\
 i0refc, Eaa, Eac, Epro, sigmaref, exponent_pO2, \
exponent_pH2O, exponent_pH2):
    # Constants
    R = 8.314  # Gas constant (J/mol*K)
    F = 96485  # Faraday constant (C/mol)
    n = 2  # Number of electrons involved in
    #the electrochemical reaction

    # Temperature and pressure conversion
    T = temperature + 273.15  # Cell temperature (K)
    Pa = pressure * 100000  # Pressure on the anode side (Pa)
    Pc = pressure * 100000  # Pressure on the cathode side (Pa)
    TH2O = temperature  # Temperature of the water
    # Material and reaction parameters
    deltha = 0.00127  # Nafion 115 membrane thickness (cm)
    Tref = T_ref + 273.15  # Reference temperature
    Pref = P_ref * 100000  # Reference pressure


    # Antoine equation for water pressure
    Aant = 5.20389
    Bant = 1733.926
    Cant = 39.485
    pH2O = (np.exp(Aant - (Bant / (TH2O + Cant)))) * 1000

    # Partial pressures
    pO2 = Pa - pH2O  # Partial pressure of oxygen (Pa)
    pH2 = Pc - pH2O  # Partial pressure of hydrogen (Pa)

    # Open circuit voltage (OCV)
    Erev = 1.229 - (0.9 * 10**-3 * (T - 298))
    # Reversible potential (V)
    E = Erev + ((R * T) / (n * F)) * (np.log((pH2 *\
    (pO2**0.5)) / pH2O))

    # Overpotentials
    anode_overpotential = ((R * T) / (n * F * alphaanode))\
     * np.log(x / (i0refa *((pO2 / Pref)**exponent_pO2) * \
    ((pH2O / Pref)**exponent_pH2O)* np.exp((-Eaa / R) *\
```

```
                        ((1 / T) - (1 / Tref)))))
    cathode_overpotential = ((R * T) / (n * F * alphacathode)) \
* np.log(x / (i0refc* ((pH2 / Pref)**exponent_pH2) *\
         np.exp((-Eac / R) * ((1 / T) - (1 / Tref)))))
    ohmic_loss = (deltha / (sigmaref * np.exp((-Epro / R)\
                        * ((1 / Tref) - (1 / T))))) * x

    return E + anode_overpotential + cathode_overpotential \
    + ohmic_loss
```

Temperature adaptation

Module 1:

```
"""Temperature adaptation model"""

import numpy as np
from scipy.optimize import curve_fit
import pandas as pd
import matplotlib.pyplot as plt
from scipy.optimize import differential_evolution
from v_prediction import V_predicted


file_path = 'Polarization_curves_40_to_70_degrees.xlsx'
data = pd.read_excel(file_path, decimal=',',skiprows=2)

max_index = data['Current density 40'].idxmax()
data_until_max = data.loc[max_index:]

x_40 = data_until_max['Current density 40']
y_40 = data_until_max['Cell1 40']

temperature = 40
pressure = 1.01325
exponent_pO2 = 0
exponent_pH2O = 0
exponent_pH2 = 0


def model(x, params):
    alphaanode, alphacathode, i0refa, i0refc, Eaa,\
          Eac, Epro, sigmaref = params
    # Costants
    R = 8.314  # gas constant (J/mol*K)
    F = 96485  # Faraday constant (C/mol)
    n = 2  # electrons involved in the reaction

    T = temperature + 273.15  # Cell temperature (K)
    Pa = pressure * 100000  # anode pressure (Pa)
    Pc = pressure * 100000  # cathode pressure (Pa)
    TH2O = 40 # water temperature

    # Parametri materiali e reazione
    deltha = 0.00127  # Nafion 115 thickness (cm)
    Tref = temperature + 273.15  # reference temperature
    Pref = pressure * 100000 # reference pressure
```

```
    # Antoine's equation for water pressure
    Aant = 8.07131
    Bant = 1733.926
    Cant = 39.485
    pH2O = (np.exp(Aant - (Bant / (TH2O + Cant)))) * 1000

    # Partial pressures
    pO2 = Pa - pH2O # oxygen Partial pressure (Pa)
    pH2 = Pc - pH2O # hydroge Partial pressure (Pa)

    # Open circuit voltage (OCV)
    Erev = 1.229 - (0.9 * 10**-3 * (T - 298))\
    # reversible voltage (V)
    E = Erev + ((R * T) / (n * F))*np.log(((pO2)**0.5)*pH2/pH2O)

    # overpotentials
    anode_overpotential = ((R * T) / (n * F * alphaanode)) * \
    np.log(x / (i0refa *((pO2 / Pref)**exponent_pO2) * \
    ((pH2O / Pref) **exponent_pH2O)* np.exp((-Eaa / R) * \
                                ((1 / T) - (1 / Tref)))))
    cathode_overpotential = ((R * T) / (n * F * alphacathode)) \
    * np.log(x / (i0refc *((pH2 / Pref)**exponent_pH2)*\
    np.exp((-Eac / R) * ((1 / T) - (1 / Tref)))))
    ohmic_loss = (deltha / (sigmaref * np.exp((-Epro / R) * \
    ((1 / Tref) - (1 / T))))) * x

    return E + anode_overpotential +\
    cathode_overpotential + ohmic_loss


def cost_function(params):
    predicted = model(x_40, params)
    return np.sum((y_40 - predicted) ** 2)


bounds = [(0, 0.8), (0, 0.30), (0, 0.1), (0, 10), (0, 40000), \
        (0, 10000), (0, 4000), (0.0055, 0.0070)]

result = differential_evolution(cost_function, bounds)


popt = result.x

#parameters for minimum RMSE:
```

```
parameters =  [0.800, 0.300, 0.020, 0.225, 38723.72, 4589.81, \
               3049.91, 0.0070]

y_pred_40 = model(x_40, parameters)


rmse_40 = np.sqrt(np.mean((y_40 - y_pred_40)**2))

plt.figure(figsize=(10, 6))
plt.scatter(x_40, y_40, label='Experimental data')
plt.plot(x_40, y_pred_40, color='red', label='Model data')
plt.title('Comparison between model and experimental data @40°C \
          and 1 bar')
plt.xlabel('Current density [A/cm^2]')
plt.ylabel('Voltage [V]')
plt.grid(True)

legend_text = f'RMSE: {rmse_40:.4f}\n' \
            f'alphaanode: {parameters[0]:.3f}\n' \
            f'alphacathode: {parameters[1]:.3f}\n' \
            f'i0refa: {parameters[2]:.3f}\n' \
            f'i0refc: {parameters[3]:.3f}\n' \
            f'Eaa: {parameters[4]:.2f}\n' \
            f'Eac: {parameters[5]:.2f}\n' \
            f'Epro: {parameters[6]:.2f}\n' \
            f'sigmaref: {parameters[7]:.4f}'

plt.legend(loc='lower right', frameon=True, framealpha=1, \
           shadow=True, borderpad=1)
plt.show()




# experimental data @ 50°C

def model_50C(x, alphaanode, alphacathode):
    return V_predicted(x, temperature, 50, pressure, pressure, \
alphaanode, alphacathode, parameters[2], parameters[3], \
parameters[4], parameters[5], parameters[6], parameters[7])

x_50 = data_until_max['Current density 50']
y_50 = data_until_max['Cell1 50']

initial_alpha_50 = [popt[0], popt[1]]
```

```
alpha_bounds = ([popt[0],popt[1]],[1,1])
alpha_opt_50, _ = curve_fit(model_50C, x_50, y_50, \
                p0=initial_alpha_50, bounds=alpha_bounds)
y_pred_50 = model_50C(x_50, *alpha_opt_50)



rmse_50 = np.sqrt(np.mean((y_50 - y_pred_50)**2))

plt.figure(figsize=(10, 6))
plt.scatter(x_50, y_50, label='Experimental data')
plt.plot(x_50, y_pred_50, color='red', label='Model data')
plt.title('Comparison between model and experimental data @50°C \
          and 1 bar')
plt.xlabel('Current density [A/cm^2]')
plt.ylabel('Voltage [V]')
plt.grid(True)
legend_text = f'RMSE: {rmse_50:.4f}\n' \
            f'alphaanode: {alpha_opt_50[0]:.3f}\n' \
            f'alphacathode: {alpha_opt_50[1]:.3f}\n' \


plt.legend(loc='lower right', frameon=True, framealpha=1, \
           shadow=True, borderpad=1)
plt.show()


# experimental data @ 60°C

def model_60C(x, alphaanode, alphacathode):
    return V_predicted(x, temperature, 60, pressure, pressure,\
 alphaanode, alphacathode, parameters[2], parameters[3],\
 parameters[4], parameters[5], parameters[6], parameters[7])

x_60 = data_until_max['Current density 60']
y_60 = data_until_max['Cell1 60']

initial_alpha_60 = [alpha_opt_50[0],alpha_opt_50[1]]
alpha_bounds = ([alpha_opt_50[0],alpha_opt_50[1]],[1,0.9])
alpha_opt_60, _ = curve_fit(model_60C, x_60, y_60, \
                p0=initial_alpha_60, bounds=alpha_bounds)
y_pred_60 = model_60C(x_60, *alpha_opt_60)



rmse_60 = np.sqrt(np.mean((y_60 - y_pred_60)**2))
```

```
plt.figure(figsize=(10, 6))
plt.scatter(x_60, y_60, label='Experimental data')
plt.plot(x_60, y_pred_60, color='red', label='Model data')
plt.title('Comparison between model and experimental data @60°C \
          and 1 bar')
plt.xlabel('Current density [A/cm^2]')
plt.ylabel('Voltage [V]')
plt.grid(True)
legend_text = f'RMSE: {rmse_60:.4f}\n' \
            f'alphaanode: {alpha_opt_60[0]:.3f}\n' \
            f'alphacathode: {alpha_opt_60[1]:.3f}\n' \


plt.legend(loc='lower right', frameon=True, framealpha=1,\
          shadow=True, borderpad=1)
plt.show()

print(legend_text)



# experimental data @ 70°C

def model_70C(x, alphaanode, alphacathode):
    return V_predicted(x, temperature, 70, pressure, pressure,\
 alphaanode, alphacathode, parameters[2], parameters[3], \
parameters[4], parameters[5], parameters[6], parameters[7])

x_70 = data_until_max['Current density 70']
y_70 = data_until_max['Cell1 70']

initial_alpha_70 = [alpha_opt_60[0],alpha_opt_60[1]]
alpha_bounds = ([alpha_opt_60[0],alpha_opt_60[1]],[1.0,1.0])
alpha_opt_70, _ = curve_fit(model_60C, x_70, y_70,\
                 p0=initial_alpha_70, bounds=alpha_bounds)
y_pred_70 = model_70C(x_70, *alpha_opt_70)


rmse_70 = np.sqrt(np.mean((y_70 - y_pred_70)**2))

plt.figure(figsize=(10, 6))

plt.figure(figsize=(10, 6))
plt.scatter(x_70, y_70, label='Experimental data')
plt.plot(x_70, y_pred_70, color='red', label='Model data')
```

```
plt.title('Comparison between model and experimental data @70°C \
          and 1 bar')
plt.xlabel('Current density [A/cm^2]')
plt.ylabel('Voltage [V]')
plt.grid(True)
legend_text = f'RMSE: {rmse_70:.4f}\n' \
            f'alphaanode: {alpha_opt_70[0]:.3f}\n' \
            f'alphacathode: {alpha_opt_70[1]:.3f}\n' \


plt.legend(loc='lower right', frameon=True, framealpha=1, \
           shadow=True, borderpad=1)
plt.show()

print(legend_text)



plt.figure(figsize=(10, 6))
plt.scatter(x_40, y_40,color='red', label='Experimental \
            data at 40°C')
plt.scatter(x_50, y_50,color='b', label='Experimental data\
             at 50°C')
plt.scatter(x_60, y_60, color='black', label='Experimental\
             data at 60°C')
plt.scatter(x_70, y_70, color='y', label='Experimental data\
             at 70°C')
plt.plot(x_40, y_pred_40, color='red', label='Optimized\
          model at 40°C')
plt.plot(x_50, y_pred_50, color='b', label='Optimized\
          model at 50°C')
plt.plot(x_60, y_pred_60, color='black', label='Optimized\
          model at 60°C')
plt.plot(x_70, y_pred_70, color='y', label='Optimized \
         model at 70°C')
plt.title('Comparison between experimental data and \
          optimized model at different temperatures')
plt.xlabel('Current density [A/cm^2]')
plt.ylabel('Voltage [V]')
plt.grid(True)
plt.plot([], [], ' ')
plt.legend(loc='lower right', frameon=True, framealpha=1,\
            shadow=True, borderpad=1)
plt.show()
```

Module 2:

```
    """Calculation of polarization curve\
given kinetics parameters"""
import numpy as np

def V_predicted(x,T_ref,temperature,P_ref,pressure,\
 alphaanode,alphacathode,i0refa, i0refc, Eaa,Eac,\
    Epro, sigmaref):

    # Costants
    R = 8.314  # gas constant (J/mol*K)
    F = 96485  # Faraday constant (C/mol)
    n = 2  # electrons involved in the reaction

    T = temperature + 273.15  # Cell temperature (K)
    Pa = pressure * 100000  # anode pressure (Pa)
    Pc = pressure * 100000  # cathode pressure (Pa)
    TH2O = temperature # water temperature

    deltha = 0.00127  #  Nafion 115 thickness (cm)
    Tref = T_ref + 273.15  # reference temperature
    Pref = P_ref* 100000 # reference pressure
    exponent_pO2 = 0 # exponent a
    exponent_pH2O = 0 # exponent b
    exponent_pH2 = 0 # exponent c

    # Antoine's equation for water pressure
    Aant = 8.07131
    Bant = 1733.926
    Cant = 39.485
    pH2O = (np.exp(Aant - (Bant / (Cant+TH2O)))) * 1000

   # Partial pressures
    pO2 = Pa - pH2O # oxygen Partial pressure (Pa)
    pH2 = Pc - pH2O # hydroge Partial pressure (Pa)

    # Open circuit voltage (OCV)
    Erev = 1.229 - (0.9 * 10**-3 * (T - 298))
    # reversible voltage (V)
    E = Erev + ((R * T) / (n * F))*np.log(((pO2)**0.5)*pH2/pH2O)

    # overpotentials
    anode_overpotential = ((R * T) / (n * F * alphaanode)) * np.log\
    (x / (i0refa *((pO2 / Pref)**exponent_pO2) * ((pH2O / Pref)\
    **exponent_pH2O)* np.exp((-Eaa / R) * ((1 / T) - (1 / Tref)))))
    cathode_overpotential = ((R * T) / (n * F * alphacathode)) *\
```

```
 np.log(x / (i0refc *((pH2 / Pref)**exponent_pH2)* np.exp\
((-Eac / R) * ((1 / T) - (1 / Tref)))))
ohmic_loss = (deltha / (sigmaref * np.exp((-Epro / R) *\
     ((1 / Tref) - (1 / T))))) * x

return E + anode_overpotential + \
    cathode_overpotential + ohmic_loss
```

Bibliography

[1] International Energy Agency. *Global Share of Total Energy Supply by Source, 2018*. Accessed 2 April 2024. 2018. URL: https://www.iea.org/data-and-statistics/charts/global-share-of-total-energy-supply-by-source-2018.

[2] International Energy Agency. *Energy Statistics Data Browser*. Accessed 2 April 2024. 2024. URL: https://www.iea.org/data-and-statistics/data-tools/energy-statistics-data-browser?country=WORLD&fuel=Energy%20supply&indicator=TESbySource.

[3] International Energy Agency. *Net Zero by 2050*. Accessed 2 April 2024. 2024. URL: https://www.iea.org/reports/net-zero-by-2050.

[4] Massachusetts Institute of Technology Energy Initiative. *Future of Energy Storage*. Accessed: 2023-04-03. 2023. URL: https://energy.mit.edu/research/future-of-energy-storage/.

[5] *The long-term energy storage challenge*. Accessed: 2023-04-03. Apr. 2023. URL: https://www.chemistryworld.com/features/the-long-term-energy-storage-challenge/4017303.article.

[6] *The $2.5 trillion reason we can't rely on batteries to clean up the grid*. Accessed: 2023-04-03. July 2018. URL: https://www.technologyreview.com/2018/07/27/141282/the-25-trillion-reason-we-cant-rely-on-batteries-to-clean-up-the-grid/.

[7] Qusay Hassan et al. "Hydrogen energy future: Advancements in storage technologies and implications for sustainability". In: *Journal of Energy Storage* 72 (2023), p. 108404. ISSN: 2352-152X. DOI: https://doi.org/10.1016/j.est.2023.108404. URL: https://www.sciencedirect.com/science/article/pii/S2352152X23018017.

[8] Nan Ma et al. "Large scale of green hydrogen storage: Opportunities and challenges". In: *International Journal of Hydrogen Energy* 50 (2024), pp. 379–396. ISSN: 0360-3199. DOI: https://doi.org/10.1016/j.ijhydene.2023.09.021. URL: https://www.sciencedirect.com/science/article/pii/S0360319923045883.

[9] Zainul Abdin et al. "Hydrogen as an energy vector". In: *Renewable and Sustainable Energy Reviews* 120 (2020), p. 109620. ISSN: 1364-0321. DOI: https://doi.org/10.1016/j.rser.2019.109620. URL: https://www.sciencedirect.com/science/article/pii/S1364032119308275.

[10] Abd El-Shafy A. Nafeh. "Hydrogen production from a PV/PEM electrolyzer system using a neural-network-based MPPT algorithm". In: *International Journal of Numerical Modelling: Electronic Networks, Devices and Fields* 24.3 (2011), pp. 282–297. DOI: https://doi.org/10.1002/jnm.778. eprint: https://onlinelibrary.wiley.com/doi/pdf/10.1002/jnm.778. URL: https://onlinelibrary.wiley.com/doi/abs/10.1002/jnm.778.

[11] N.V. Dale, M.D. Mann, and H. Salehfar. "Semiempirical model based on thermodynamic principles for determining 6kW proton exchange membrane electrolyzer stack characteristics". In: *Journal of Power Sources* 185.2 (2008), pp. 1348–1353. ISSN: 0378-7753. DOI: https://doi.org/10.1016/j.jpowsour.2008.08.054. URL: https://www.sciencedirect.com/science/article/pii/S0378775308016686.

[12] Timothy D. Myles et al. "Species transport in a high-pressure oxygen-generating proton-exchange membrane electrolyzer". In: *International Journal of Hydrogen Energy* 37.17 (2012). 12th CHEC, pp. 12451–12463. ISSN: 0360-3199. DOI: https://doi.org/10.1016/j.ijhydene.2012.05.123. URL: https://www.sciencedirect.com/science/article/pii/S0360319912012669.

[13] European Commission. *The European Green Deal*. 2023. URL: https://commission.europa.eu/strategy-and-policy/priorities-2019-2024/european-green-deal_en (visited on 04/03/2023).

[14] Manfred Hafner and Pier Paolo Raimondi. "Priorities and challenges of the EU energy transition: From the European Green Package to the new Green Deal". In: *Russian Journal of Economics* 6.4 (2020), pp. 374–389. ISSN: 2618-7213. DOI: 10.32609/j.ruje.6.55375. eprint: https://doi.org/10.32609/j.ruje.6.55375. URL: https://doi.org/10.32609/j.ruje.6.55375.

[15] Eurostat. *EU energy mix and import dependency Statistics Explained*. Data extracted on March 4, 2022. Planned article update: May 31, 2023. 2022. URL: https://ec.europa.eu/eurostat/statistics-explained/SEP/104551.pdf (visited on 03/04/2022).

[16] International Energy Agency. *Energy Statistics Data Browser for Europe*. Accessed 2 April 2024. 2024. URL: https://www.iea.org/data-and-statistics/data-tools/energy-statistics-data-browser?country=WEOEUR&fuel=Energy%20supply&indicator=TESbySource.

[17] International Energy Agency. *Energy Statistics Data Browser for Italy*. Accessed 2 April 2024. 2024. URL: https://www.iea.org/data-and-statistics/data-tools/energy-statistics-data-browser?country=ITALY&fuel=Energy%20supply&indicator=TESbySource.

[18] Jasmine Ramsebner et al. "The sector coupling concept: A critical review". In: *WIREs Energy and Environment* 10.4 (2021), e396. DOI: https://doi.org/10.1002/wene.396. eprint: https://wires.onlinelibrary.wiley.com/doi/pdf/10.1002/wene.396. URL: https://wires.onlinelibrary.wiley.com/doi/abs/10.1002/wene.396.

[19] Manuel Götz et al. "Renewable Power-to-Gas: A technological and economic review". In: *Renewable Energy* 85 (2016), pp. 1371–1390. ISSN: 0960-1481. DOI: https://doi.org/10.1016/j.renene.2015.07.066. URL: https://www.sciencedirect.com/science/article/pii/S0960148115301610.

[20] Peter D. Lund et al. “Review of energy system flexibility measures to enable high levels of variable renewable electricity”. In: *Renewable and Sustainable Energy Reviews* 45 (2015), pp. 785–807. ISSN: 1364-0321. DOI: https://doi.org/10.1016/j.rser.2015.01.057. URL: https://www.sciencedirect.com/science/article/pii/S1364032115000672.

[21] Herib Blanco and André Faaij. “A review at the role of storage in energy systems with a focus on Power to Gas and long-term storage”. In: *Renewable and Sustainable Energy Reviews* 81 (2018), pp. 1049–1086. ISSN: 1364-0321. DOI: https://doi.org/10.1016/j.rser.2017.07.062. URL: https://www.sciencedirect.com/science/article/pii/S1364032117311310.

[22] Ram Ramachandran and Raghu K. Menon. “An overview of industrial uses of hydrogen”. In: *International Journal of Hydrogen Energy* 23.7 (1998), pp. 593–598. ISSN: 0360-3199. DOI: https://doi.org/10.1016/S0360-3199(97)00112-2. URL: https://www.sciencedirect.com/science/article/pii/S0360319997001122.

[23] Meiling Yue et al. “Hydrogen energy systems: A critical review of technologies, applications, trends and challenges”. In: *Renewable and Sustainable Energy Reviews* 146 (2021), p. 111180. ISSN: 1364-0321. DOI: https://doi.org/10.1016/j.rser.2021.111180. URL: https://www.sciencedirect.com/science/article/pii/S1364032121004688.

[24] Agenzia Italiana per l’Energia Nuova e le Tecnologie (ENEA). *Tecnologie e Prospettive del Power to Gas*. Accessed 2 April 2024. 2024. URL: https://www.eai.enea.it/archivio/energia-e-green-new-deal-sommario/tecnologie-e-prospettive-del-power-to-gas.html.

[25] Yun Teng et al. “Multi-energy storage system model based on electricity heat and hydrogen coordinated optimization for power grid flexibility”. In: *CSEE Journal of Power and Energy Systems* 5.2 (2019), pp. 266–274. DOI: 10.17775/CSEEJPES.2019.00190.

[26] KPMG. *Long Duration Energy Storage & ESG*. Accessed 2 April 2024. 2023. URL: https://kpmg.com/ie/en/home/insights/2023/11/long-duration-energy-storage-esg.html.

[27] Kasper T. Møller et al. “Hydrogen - A sustainable energy carrier”. In: *Progress in Natural Science: Materials International* 27.1 (2017). SI-HYDROGEN STORAGE MATERIALS, pp. 34–40. ISSN: 1002-0071. DOI: https://doi.org/10.1016/j.pnsc.2016.12.014. URL: https://www.sciencedirect.com/science/article/pii/S1002007116303240.

[28] Royal Society of Chemistry. *Hydrogen - Element information, properties and uses — Periodic Table*. Accessed: 2023-04-04.

[29] National Institute of Standards and Technology (NIST). *NIST Chemistry WebBook, NIST Standard Reference Database*. Accessed 2 April 2024. URL: https://webbook.nist.gov/chemistry/fluid/.

[30] National Institute for Occupational Safety and Health. *NIOSH Pocket Guide to Chemical Hazards - Hydrogen*. Accessed: 2024-06-06. 2024. URL: https://www.cdc.gov/niosh/npg/npgd0333.html.

[31] W. Lucus and S. Chakrabarti. *Properties of Hydrogen - National Renewable Energy Laboratory*. Accessed: 2024-06-06. 2004. URL: https://www.nrel.gov/docs/fy04osti/34380.pdf.

[32] J.D. Holladay et al. "An overview of hydrogen production technologies". In: *Catalysis Today* 139.4 (2009). Hydrogen Production - Selected papers from the Hydrogen Production Symposium at the American Chemical Society 234th National Meeting Exposition, August 19-23, 2007, Boston, MA, USA, pp. 244–260. ISSN: 0920-5861. DOI: https://doi.org/10.1016/j.cattod.2008.08.039. URL: https://www.sciencedirect.com/science/article/pii/S0920586108004100.

[33] International Energy Agency. *Global Hydrogen Review 2023. Executive Summary*. 2023. URL: https://www.iea.org/reports/global-hydrogen-review-2023/executive-summary (visited on 05/03/2024).

[34] International Energy Agency. *Global Hydrogen Review 2022. Executive Summary*. 2022. URL: https://www.iea.org/reports/global-hydrogen-review-2022/executive-summary (visited on 05/03/2024).

[35] S. Shiva Kumar and V. Himabindu. "Hydrogen production by PEM water electrolysis – A review". In: *Materials Science for Energy Technologies* 2.3 (2019), pp. 442–454. ISSN: 2589-2991. DOI: https://doi.org/10.1016/j.mset.2019.03.002. URL: https://www.sciencedirect.com/science/article/pii/S2589299119300035.

[36] Kleinman Center for Energy Policy. *Renewable Hydrogen: The Future of Storage and Fuel of the Future*. Accessed 2 April 2024. 2023. URL: https://kleinmanenergy.upenn.edu/news-insights/renewable-hydrogen-the-future-of-storage-and-fuel-of-the-future/.

[37] ANSYS. *The Future of Energy is Turquoise*. Accessed 2 April 2024. 2021. URL: https://www.ansys.com/blog/future-of-energy-is-turquoise.

[38] S. Seetharaman et al. "Graphene oxide modified non-noble metal electrode for alkaline anion exchange membrane water electrolyzers". In: *International Journal of Hydrogen Energy* 38.35 (2013), pp. 14934–14942. ISSN: 0360-3199. DOI: https://doi.org/10.1016/j.ijhydene.2013.09.033. URL: https://www.sciencedirect.com/science/article/pii/S0360319913022246.

[39] S Trasatti. "Water electrolysis: who first?" In: *Journal of Electroanalytical Chemistry* 476.1 (1999), pp. 90–91. ISSN: 1572-6657. DOI: https://doi.org/10.1016/S0022-0728(99)00364-2. URL: https://www.sciencedirect.com/science/article/pii/S0022072899003642.

[40] Marcelo Carmo et al. “A comprehensive review on PEM water electrolysis”. In: *International Journal of Hydrogen Energy* 38.12 (2013), pp. 4901–4934. ISSN: 0360-3199. DOI: https://doi.org/10.1016/j.ijhydene.2013.01.151. URL: https://www.sciencedirect.com/science/article/pii/S0360319913002607.

[41] S. Shiva Kumar and Hankwon Lim. “An overview of water electrolysis technologies for green hydrogen production”. In: *Energy Reports* 8 (2022), pp. 13793–13813. ISSN: 2352-4847. DOI: https://doi.org/10.1016/j.egyr.2022.10.127. URL: https://www.sciencedirect.com/science/article/pii/S2352484722020625.

[42] W. Dönitz and E. Erdle. “High-temperature electrolysis of water vapor—status of development and perspectives for application”. In: *International Journal of Hydrogen Energy* 10.5 (1985), pp. 291–295. ISSN: 0360-3199. DOI: https://doi.org/10.1016/0360-3199(85)90181-8. URL: https://www.sciencedirect.com/science/article/pii/0360319985901818.

[43] Ruth Knibbe et al. “Solid Oxide Electrolysis Cells: Degradation at High Current Densities”. In: *Journal of The Electrochemical Society* 157.8 (June 2010), B1209. DOI: 10.1149/1.3447752. URL: https://dx.doi.org/10.1149/1.3447752.

[44] W. T. Grubb. “Batteries with Solid Ion Exchange Electrolytes: I . Secondary Cells Employing Metal Electrodes”. In: *Journal of The Electrochemical Society* 106.4 (Apr. 1959), p. 275. DOI: 10.1149/1.2427329. URL: https://dx.doi.org/10.1149/1.2427329.

[45] Wu Xu and Keith Scott. “The effects of ionomer content on PEM water electrolyser membrane electrode assembly performance”. In: *International Journal of Hydrogen Energy* 35.21 (2010). VIII symposium of the Mexican Hydrogen Society, pp. 12029–12037. ISSN: 0360-3199. DOI: https://doi.org/10.1016/j.ijhydene.2010.08.055. URL: https://www.sciencedirect.com/science/article/pii/S0360319910016940.

[46] Pavlos Nikolaidis and Andreas Poullikkas. “A comparative overview of hydrogen production processes”. In: *Renewable and Sustainable Energy Reviews* 67 (2017), pp. 597–611. ISSN: 1364-0321. DOI: https://doi.org/10.1016/j.rser.2016.09.044. URL: https://www.sciencedirect.com/science/article/pii/S1364032116305366.

[47] Pianpian Xiang et al. “Evaluation of LCOH of conventional technology, energy storage coupled solar PV electrolysis, and HTGR in China”. In: *Applied Energy* 353 (2024), p. 122086. ISSN: 0306-2619. DOI: https://doi.org/10.1016/j.apenergy.2023.122086. URL: https://www.sciencedirect.com/science/article/pii/S0306261923014502.

[48] Olga Kanz et al. “Review and Harmonization of the Life-Cycle Global Warming Impact of PV-Powered Hydrogen Production by Electrolysis”. In: *Frontiers in Electronics* 2 (2021). ISSN: 2673-5857. DOI: 10.3389/felec.2021.711103. URL: https://www.frontiersin.org/articles/10.3389/felec.2021.711103.

[49] Carlos Bernuy-Lopez. *Electrolysis Technologies and LCOH: Current State and Prospects for 2030*. Accessed: 2023-04-03. 2023. URL: https://hydrogentechworld.com/electrolysis-technologies-and-lcoh-current-state-and-prospects-for-2030.

[50] U.S. Department of Energy. *Hydrogen Storage*. Office of Energy Efficiency & Renewable Energy. 2024. URL: https://www.energy.gov/eere/fuelcells/hydrogen-storage (visited on 05/03/2024).

[51] F.J. Wirkert et al. "A modular design approach for PEM electrolyser systems with homogeneous operation conditions and highly efficient heat management". In: *International Journal of Hydrogen Energy* 45.2 (2020). International Hydrogen and Fuel Cell Conference 2018, Trondheim, Norway, pp. 1226–1235. ISSN: 0360-3199. DOI: https://doi.org/10.1016/j.ijhydene.2019.03.185. URL: https://www.sciencedirect.com/science/article/pii/S0360319919312145.

[52] Daoping Tang et al. "Calculations of the exchange current density for hydrogen electrode reactions: A short review and a new equation". In: *Journal of Electroanalytical Chemistry* 644.2 (2010). Electrochemistry and the Energy Landscape, pp. 144–149. ISSN: 1572-6657. DOI: https://doi.org/10.1016/j.jelechem.2009.11.031. URL: https://www.sciencedirect.com/science/article/pii/S1572665709004573.

[53] R. Bove and S. Ubertini. *Modeling Solid Oxide Fuel Cells: Methods, Procedures and Techniques*. Springer, 2008. ISBN: 978-1-4020-6994-9.

[54] I.C. Noyan and J.B. Cohen. "An X-ray diffraction study of the residual stress-strain distributions in shot-peened two-phase brass". In: *Materials Science and Engineering* 75.1 (1985), pp. 179–193. ISSN: 0025-5416. DOI: https://doi.org/10.1016/0025-5416(85)90188-0. URL: https://www.sciencedirect.com/science/article/pii/0025541685901880.

[55] Alhassan Salami Tijani et al. "Electrochemical characteristics of (PEM) electrolyzer under influence of charge transfer coefficient". In: *International Journal of Hydrogen Energy* 44.50 (2019), pp. 27177–27189. ISSN: 0360-3199. DOI: https://doi.org/10.1016/j.ijhydene.2019.08.188. URL: https://www.sciencedirect.com/science/article/pii/S0360319919332070.

[56] Alhassan Salami Tijani, Nur Afiqah Binti Kamarudin, and Fatin Athirah Binti Mazlan. "Investigation of the effect of charge transfer coefficient (CTC) on the operating voltage of polymer electrolyte membrane (PEM) electrolyzer". In: *International Journal of Hydrogen Energy* 43.19 (2018), pp. 9119–9132. ISSN: 0360-3199. DOI: https://doi.org/10.1016/j.ijhydene.2018.03.111. URL: https://www.sciencedirect.com/science/article/pii/S0360319918309017.

[57] S Niroula et al. "Parametric Modelling and Optimization of Alkaline Electrolyzer for the Production of Green Hydrogen". In: *IOP Conference Series: Materials Science and Engineering* 1279.1 (Mar. 2023), p. 12. ISSN: 1757-8981.

[58] R. García-Valverde et al. “Optimized photovoltaic generator–water electrolyser coupling through a controlled DC–DC converter”. In: *International Journal of Hydrogen Energy* 33.20 (2008), pp. 5352–5362. ISSN: 0360-3199. DOI: 10.1016/j.ijhydene.2008.06.015. URL: https://www.sciencedirect.com/science/article/pii/S036031990800712X.

[59] D.S. Falcão and A.M.F.R. Pinto. “A review on PEM electrolyzer modelling: Guidelines for beginners”. In: *Journal of Cleaner Production* 261 (2020), p. 121184. ISSN: 0959-6526. DOI: https://doi.org/10.1016/j.jclepro.2020.121184. URL: https://www.sciencedirect.com/science/article/pii/S0959652620312312.

[60] National Institute of Standards and Technology. *Hydrogen - NIST Chemistry WebBook*. Accessed: [2024-05-03].

[61] Pietro Lubello et al. “Assessment of hydrogen-based long term electrical energy storage in residential energy systems”. In: *Smart Energy* 8 (2022), p. 100088. ISSN: 2666-9552. DOI: https://doi.org/10.1016/j.segy.2022.100088. URL: https://www.sciencedirect.com/science/article/pii/S2666955222000260.

[62] R. García-Valverde, N. Espinosa, and A. Urbina. “Simple PEM water electrolyser model and experimental validation”. In: *International Journal of Hydrogen Energy* 37.2 (2012). 10th International Conference on Clean Energy 2010, pp. 1927–1938. ISSN: 0360-3199. DOI: https://doi.org/10.1016/j.ijhydene.2011.09.027. URL: https://www.sciencedirect.com/science/article/pii/S0360319911021380.

[63] Michael Brodmann. “Final Report on the Implementation of the Project ”FHInvest2016: Characterization and Qualification of PEM High-Pressure Electrolyzer Components in High-Pressure Operation up to 100 bar””. In: 03FH012IN6 (2016). Project Short Title: HiPresPEM.

[64] Ulrich Rost et al. “A novel advanced test system for polymer electrolyte membrane water electrolysis based on hydraulic cell compression”. In: *Fuel Cells* 22.6 (2022), pp. 284–289. DOI: https://doi.org/10.1002/fuce.202200068. eprint: https://onlinelibrary.wiley.com/doi/pdf/10.1002/fuce.202200068. URL: https://onlinelibrary.wiley.com/doi/abs/10.1002/fuce.202200068.

[65] H2 Südtirol. *FAQ*. Accessed: 2023-05-10. H2 Südtirol. 2023. URL: https://www.h2-suedtirol.com/it/faq (visited on 05/10/2023).